

浙 江 大 学



Dissertation Title: Ziv-Zakai Bound for Target
Non-linear Parameters Estimation

Submitted to: Graduate School of Zhejiang University

Author: Zongyu Zhang

Advisor: Prof. Zhiguo Shi

Diploma Date: Dec. 2023

Dissertation Defense Committee Members:

Prof. Guisheng Liao, Advisory Chair, Xidian University

Prof. Hai Lin, Zhejiang University

Prof. Lingling Sun, Hangzhou Dianzi University

Prof. Jianlong Li, Zhejiang University

Prof. Junwei Li, Zhejiang University

©

Copyright

2023

by

Zongyu Zhang

All Rights Reserved

Abstract

Nonlinear parameter estimation for targets is one of the fundamental problem in statistical signal processing, and has attracted a lot of research interest in the past few decades, where higher estimation accuracy is one of the key objectives. Since there is no general closed-form expression on minimum mean-squared error (MSE), the lower bounds on MSE becomes the benchmark on performance evaluation for estimation algorithms. In the past half century, researches are devoted to find a lower bound with global tightness, strong physical interpretability, and ease of use in specific estimation scenarios. Therein, Ziv-Zakai bound (ZZB) has been proven as one of the globally tightest lower bounds. It establishes the intuitive relationship between the estimation error and the probability of error of a hypothesis testing problem, which provides better physical interpretability compared with other lower bounds. However, it still remains challenging for ZZB in specific estimation scenarios with respect to the ease of use.

To this end, this dissertation provides a detailed literature review on the lower bounds on MSE for target nonlinear parameter estimation, focuses on the research on the ZZB for typical target nonlinear parameter estimation problems (e.g., distance and angle), and derives the explicit/closed-form and easy-to-use ZZB expressions for specific parameter estimation problems. The main contents of this dissertation are shown as follows:

1. An explicit ZZB for compressive time delay estimation is derived. This dissertation incorporates the ZZB derivation into the general compressive time delay estimation model, and breaks through the restriction of white Gaussian noise and specific random sensing kernel on the ZZB derivation, from which the derived ZZB is appropriate for arbitrary compressive sensing (CS) kernel and the arbitrary Gaussian colored noises. Thus, compared with the previous work, the derived ZZB shows better applicability to actual estimation scenario. According to the commonly used model such as deterministic model and Gaussian stochastic model, the derived ZZB is formulated as the function of CS kernel and the noise covariance matrix. The derived ZZB provides the global tight bound

and accurately predicts the threshold signal-to-noise ratio (SNR) entering the asymptotic region for the minimum mean squared error estimator

2. The closed-form ZZB for one-dimensional (1D) multi-source direction-of-arrival (DOA) estimation is derived, which reveals the relationship between the MSE convergence in the *a priori* performance region and the number of sources. According to the coherence/incoherence hybrid multi-source signal model, this dissertation formulates the ZZB as the function of the coherence coefficients among different sources, and introduces the order statistics to analyze the effect brought by the ordering process on the MSE convergence in the *a priori* performance region. The derived ZZB provides a unified expression for both the underdetermined and overdetermined multi-source DOA estimation.
3. The closed-form ZZB for two-dimensional (2D) multi-source DOA estimation is derived. This dissertation considers the partially correlated signal model and incorporates the correlated coefficient matrix into the ZZB derivation, such that the derived ZZB is formulated as the function of the correlated coefficient matrix. This dissertation discusses the substantial difference of the matching process between the estimated and the true DOAs in 2D multi-source DOA estimation and that in 1D multi-source DOA estimation, and demonstrate that, in 2D multi-source DOA estimation, the minimum Euclidean distance criterion is required to realize the matching process rather than an ordering process only along azimuth or elevation, which need the stochastic Euclidean bipartite matching problem to analyze the effect of the minimum Euclidean distance criterion on the MSE convergence in the *a priori* performance region. Meanwhile, this dissertation also provides the closed-form ZZB for azimuth/elevation estimation under 2D DOA signal model.

To all my lovers.

ACKNOWLEDGEMENTS

Starting from September 2018, I have spent five years pursuing my PhD at Zhejiang University. During these years, I have met many people and encountered many events. Through all the ups and downs, joys and sorrows, I was never alone. I must first thank all the old and new friends I have met over the past five years. It is you who have collectively shaped who I am today.

Among them, I want to sincerely thank my advisor, Professor Zhiguo Shi. It was his engaging introductory courses in my freshman year that guided me onto the path of professional study. During my PhD, he has helped, cared for, and guided me in various aspects, including academics, life, and career development. This will become an invaluable asset in my life. Over these five years, he has not only provided me with academic guidance but also taught me a lot through your actions in dealing with people and matters. No matter where I am in the future, Prof. Shi will always be my role model.

Then, I would like to express my heartfelt gratitude to Dr. Yujie Gu from Aptiv Corporation in the United States. I am thankful for his rigorous and meticulous research guidance, which he provided during his spare time despite his busy schedule. I appreciate him sacrificing weekends and various holidays, time that could have been spent with his family, to meticulously revise my thesis, from the overall logic to the smallest punctuation marks. Dr. Gu's detailed feedback has helped me improve my research skills and thinking abilities. Working with him has been a great fortune in my life. If I pursue a career in teaching in the future, I aspire to be a patient and responsible teacher like him.

Next, I would like to thank Professor Jiming Chen from the College of Control Science and Engineering at Zhejiang University. His earnest advice to 'be a good person first, then do things' has become a guiding principle for me throughout my PhD. He inspired me to understand problems from different perspectives and interpret them with various ways of thinking.

Particularly, I would like to thank Senior Brother Dr. Chengwei Zhou for his selfless guidance during the early stages of my PhD. As one of the mentors who introduced me to research

life, he led me through many aspects, including thesis and patent writing, helping me become a PhD student with a research mindset. I will remember this selfless help and dedication for the rest of my life.

I would like to thank Professor Maria S. Greco and Professor Fulvio Gini from the University of Pisa, Italy, for their guidance and assistance with my research work. During my one-year exchange visit at the University of Pisa, I am grateful for the many constructive suggestions they provided for my work, the new insights they offered during our discussions, and the care and help they extended to me when I was in a foreign country.

Also, I would like to thank Dr. Cunqi Shao from our research group for his valuable opinions and suggestions on the work involved in this thesis during his spare time. I am grateful for Dr. Shao's significant contributions to the key core derivations in this thesis. I also thank my Lab mates Ying Liu, Hang Zheng, Luning Lin, Chengyuan He for their inspiration and help with my research content in daily work. I appreciate Sihan Wen's meticulous proofreading of this dissertation. Additionally, I am grateful to Dr. Xiangtian Meng from Harbin Institute of Technology, Xiang Li from Harbin Institute of Technology, Xueyin Geng from Beihang University, Biao Xue from Nanjing University of Aeronautics and Astronautics, and Hang Yuan from Nanjing University of Aeronautics and Astronautics for their support and assistance with my research and life during my visit to the University of Pisa in Italy.

Finally, I want to sincerely thank my parents for their selfless dedication throughout my journey. Although they did not directly provide guidance or assistance with my research work, they have offered me the most solid safe harbor in this unprecedented era of change. The strong support they have built has given me the confidence and freedom to pursue my dreams, allowing me to face challenges without fear.

List of Abbreviations

Abbreviation	Full Name
1D	One-dimensional
2D	Two-dimensional
A/D	Analog-to-digital
APB	A priori bound
BAB	Bayesian Abel bound
BCRB	Bayesian Cramér-Rao bound
BZB	Bobrovsky-Zakai bound
BZZB	Bell-Ziv-Zakai bound
CDF	Cumulative distribution function
CR	Compression ratio
CRB	Cramér-Rao bound
CS	Compressive sensing
D/A	Digital-to-analog
DOA	Direction-of-arrival
EBMP	Euclidean bipartite matching problem
ESPRIT	Estimation of signal parameters via rotational invariant technique
FIM	Fisher information matrix
GLRT	Generalized likelihood ratio test
HCRB	Hybrid Cramér-Rao bound
IoT	Internet of things
LFM	Linear frequency modulated
LRT	Likelihood ratio test
MAP	Maximum a posteriori

Abbreviation	Full Name
MGF	Moment generating function
ML	Maximum likelihood
MLE	maximum likelihood estimation
MMSE	Minimum mean square error
MSE	Mean-squared error
MUSIC	MUltiple signal classification
PDF	Probability density function
RMB	Reuven-Messer bound
RMSE	Root mean-squared error
SNR	Signal-to-noise ratio
ULA	Uniform linear array
URA	Uniform rectangular array
w.r.t.	with respect to
WWB	Weiss-Weinstein bound
ZZB	Ziv-Zakai bound

List of Notations

Notations	Description
\mathbb{R}	Set of real numbers
\mathbb{C}	Set of complex numbers
$\Re[\cdot]$	Real part of a complex number
$[\cdot]^T$	Transpose
$[\cdot]^H$	Hermitian transpose
$[\cdot]^*$	Conjugate
$\text{Tr}\{\cdot\}$	Trace of a matrix
$ \cdot $	Determinant of a matrix
$\mathbf{0}_M$	M -dimensional all-zero vector
$\mathbf{1}_M$	M -dimensional all-one vector
\mathbf{I}_M	M -dimensional identity matrix
$\mathbb{E}\{\cdot\}$	Statistical expectation
$\mathbb{E}_\tau\{\cdot\}$	Statistical expectation with respect to τ
$\mathbb{V}\{\cdot\}$	Variance
$\mathcal{Q}(\cdot)$	Tail distribution function of the standard normal distribution
$\mathcal{U}\{\cdot\}$	Uniform distribution
$\mathcal{N}\{\cdot\}$	Gaussian distribution
$\mathcal{CN}\{\cdot\}$	Complex Gaussian distribution
$\text{vec}(\cdot)$	Vectorization
\otimes	Kronecker product
$\text{diag}[\cdot]$	Diagonal matrix
block diag $[\cdot]$	Block diagonal matrix
$\ \cdot\ _2$	ℓ_2 norm

Notations	Notations
------------------	------------------

$\Pr(\cdot)$	Probability
--------------	-------------

$K!$	Factorial of positive integer K
------	-----------------------------------

$\mathbf{a} \preceq \mathbf{b}$	All elements in vector $\mathbf{a} - \mathbf{b}$ are non-positive
---------------------------------	---

List of Contents

Abstract	I
ACKNOWLEDGEMENTS	IV
List of Abbreviations.....	VI
List of Notations	VIII
Content	X
List of Figures	XIII
List of Tables.....	XV
Chapter 1. Introduction	1
1.1 Literature review.....	3
1.1.1 Non-Bayesian bounds	4
1.1.2 Bayesian bounds.....	7
1.2 Motivation and Contributions	11
1.3 Publications	12
1.3.1 Book Chapter	12
1.3.2 Journal Papers	12
1.3.3 Conference Papers.....	13
1.3.4 Issued Patents.....	14
Chapter 2. Preliminaries	16
2.1 Basic ZZB derivation framework for scalar parameter estimation	16
2.2 Basic ZZB derivation framework for scalar parameter estimation	18
2.3 Summary.....	20
Chapter 3. ZZB for Compressive Time Delay Estimation	21
3.1 Introduction	21
3.2 Signal Model and CRB.....	24
3.3 ZZB Derivation	27
3.3.1 Minimum Probability of Error for Deterministic Model	27
3.3.2 Minimum Probability of Error for Stochastic Model	30

3.4 Simulation	35
3.4.1 Deterministic Model	36
3.4.2 Stochastic Model	43
3.5 Summary.....	44
Chapter 4. ZZB for Compressive Time Delay Estimation with Zero-Mean Gaussian Sig-	
nals	46
4.1 Introduction	46
4.2 Signal Model.....	48
4.3 ZZB Derivation	49
4.4 Simulation	52
4.5 Summary.....	54
Chapter 5. ZZB for 1D DOAs Estimation	55
5.1 Introduction	55
5.2 Signal Model, MSE and CRB	58
5.3 Derivation of ZZB for DOAs Estimation	60
5.3.1 Generalized ZZB for Multiple Sources DOA Estimation.....	61
5.3.2 ZZB for Estimation with Permutation Ambiguity	71
5.4 Simulations.....	77
5.5 Summary.....	82
Chapter 6. ZZB for 2D DOAs Estimation	83
6.1 Introduction	83
6.2 Signal Model, MSE and CRB	86
6.3 ZZB Derivation for 2D DOAs Estimation.....	89
6.3.1 ZZB derivation for independent DOAs	91
6.3.2 ZZB for estimation after matching process according to minimum Eu-	
clidean distance criterion.....	100
6.4 Numerical Analysis	108
6.5 Summary.....	112
Chapter 7. Conclusions and Future work.....	114

7.1 Conclusions	114
7.2 Future work	115
References	117

List of Figures

Figure 3.1	Radar receiver block diagram. (a) Traditional radar receiver; (b) CS radar receiver. The solid arrows denote the signal processed in analog domain, and the dashed arrows denote the signal processed in digital domain. The hollow arrows denote M parallel processing chains.	26
Figure 3.2	The influence of different compressive sensing kernels on the minimum probability of error. (a) Deterministic model; (b) Stochastic model.	34
Figure 3.3	RMSE comparison of deterministic ZZB, BCRB, and MMSE estimator with random Gaussian CS kernel. (a) $\tau \sim \mathcal{U}[0, \frac{80}{B}]$; (b) $\tau \sim \mathcal{N}(\frac{40}{B}, (\frac{10}{B})^2)$	36
Figure 3.4	Intersection points of ZZBs with different CRs.	38
Figure 3.5	Influence of time-bandwidth product on the derived ZZB.	38
Figure 3.6	RMSE comparison of deterministic ZZB, HCRB, and MMSE estimator considering nuisance unknown α with random Gaussian CS kernel. (a) $\tau \sim \mathcal{U}[0, \frac{80}{B}]$; (b) $\tau \sim \mathcal{N}(\frac{40}{B}, (\frac{10}{B})^2)$	39
Figure 3.7	RMSE comparison of deterministic ZZB, BCRB, and MMSE estimator with information-theoretic CS kernel proposed in [101]. (a) $\tau \sim \mathcal{U}[0, \frac{80}{B}]$; (b) $\tau \sim \mathcal{N}(\frac{40}{B}, (\frac{10}{B})^2)$	40
Figure 3.8	Performance comparison of deterministic ZZB and BCRB under different colored Gaussian noises with CR = 10. (a) 1 GHz waveform bandwidth; (b) 10 MHz waveform bandwidth.	41
Figure 3.9	Sensitivity analysis of the deterministic ZZB. (a) PDFs of time delay τ ; (b) The corresponding ZZBs and BCRBs.	42
Figure 3.10	RMSE comparison of stochastic ZZB and stochastic BCRB with random Gaussian CS kernel. (a) $\tau \sim \mathcal{U}[0, \frac{80}{B}]$; (b) $\tau \sim \mathcal{N}(\frac{40}{B}, (\frac{10}{B})^2)$	43
Figure 3.11	Asymptotic region threshold comparison of stochastic ZZB.	44
Figure 4.1	RMSE comparison of BCRB, Gaussian-approximated ZZB, ZZB, and the MMSE estimator with single CS kernel ($K = 1$).	53

Figure 4.2 RMSE comparison of BCRB, ZZB, and the MMSE estimator with different number of CS kernels.	53
Figure 5.1 Combination coefficients versus the SNR for single source.	76
Figure 5.2 Combination coefficients versus the SNR for two sources with different coherent coefficients.	76
Figure 5.3 Comparison of bounds for single source case ($K = 1$).	78
Figure 5.4 Comparison of bounds for multiple sources case ($K = 5$).	78
Figure 5.5 Effect of the number of snapshots on ZZB.	79
Figure 5.6 Effect of the number of sources on ZZB.	79
Figure 5.7 Effect of the mutual coherence on ZZB.	81
Figure 5.8 Effect of the <i>a priori</i> distribution of DOAs on ZZB.	81
Figure 5.9 ZZB for underdetermined DOA estimation.	81
Figure 6.1 Illustration of the reason why we need to adopt minimum Euclidean distance criterion for 2D matching between the estimated and the true DOAs.	101
Figure 6.2 Illustration of EBMP. (a) A complete bipartite graph \mathcal{G} between the sets of the true and the estimated DOAs. (b) The weighted matrix with the elements denoting the Euclidean distance. (c) One of the perfect matchings of the complete bipartite graph. (d) The elements in the weighted matrix corresponding to the perfect matching.	103
Figure 6.3 Effectiveness of the relaxation.	106
Figure 6.4 Comparison of bounds for single source 2D DOA estimation.	109
Figure 6.5 Comparison of bounds for multi-source estimation ($K = 3$).	109
Figure 6.6 Comparison of bounds for multi-source azimuth estimation ($K = 3$).	110
Figure 6.7 Comparison of coherent, correlated and uncorrelated bounds.	112

List of Tables

Table 3.1	Threshold points of ZZBs with different CRs.	37
-----------	---	----



Chapter 1. Introduction

Nonlinear parameter estimation has broad and important applications in many fields, such as communication, radar, sonar, remote sensing, IoT, autonomous driving, etc. For example, in wireless communication systems, communication base stations and user terminals ensure high-quality, low-latency communication with accurate localization. In radar systems, accurate estimation for target parameters, such as distance, angle, and speed, enables precise positioning and tracking. In sonar systems, target distance is determined by estimating the echo delay, facilitating underwater environment detection. In IoT systems, target positioning is achieved by estimating the time of arrival/time difference of arrival of signals, enabling real-time target states sensing. In autonomous driving systems, various methods such as LiDAR and millimeter-wave radar are used to scan road conditions, surrounding vehicles, and the road environment, and to estimate and perceive environmental parameters, thereby ensuring driving safety. Therefore, accurate nonlinear parameter estimation is critical for precise sensing in the real world. Over the past few decades, there are extensive studies on nonlinear parameter estimation in different scenarios, where higher estimation accuracy is always an important goal in theoretical algorithm design.

Mathematically, there is a fundamental difference between linear parameter estimation and nonlinear estimation. Specifically, based on a linear model between the parameters to be estimated and the received signals, the derivative of the received signal w.r.t. the parameters is independent of the parameters. Therefore, it is convenient to find the global optimal solution to minimize the estimation error. However, in nonlinear parameter estimation, the derivative of the received signal w.r.t. the parameters is still a function of the parameters due to the nonlinear model. Therefore, it is difficult to obtain the global optimal solution to minimize the estimation error in general[1]. In other words, in nonlinear parameter estimation, it is difficult to prove that an estimator always has the minimum estimation error in general. Obviously, this phenomenon also makes it difficult for estimator designers to understand the potential accuracy improvement of the proposed estimator under various conditions, thereby hindering how to further enhance



the estimator for better accuracy.

In the face of these challenges, performance bounds on estimation errors provide a powerful tool for performance evaluation [2], [3]. The performance bounds on estimation errors theoretically provide the accuracy limits for nonlinear parameter estimation problems, independent of specific algorithms. These bounds serve as a “yardstick” for evaluating the accuracy of nonlinear parameter estimation algorithms. For a given nonlinear parameter estimation problem, specifying its performance bounds on estimation errors means that the estimation accuracy of any algorithm cannot be better than the results given by the performance bounds. Therefore, the performance bounds on estimation errors for a given nonlinear parameter estimation problem are algorithm-independent and general.

Over the past half-century, extensive and in-depth research has been conducted on the performance bounds on estimation errors for nonlinear parameter estimation problems. However, the bounds derived through different methods exhibit significant differences in terms of the bound trends, effective ranges, computational burdens, and tightness. The concept of tightness of these bounds can be compared to the concepts of lower bounds and infimum in mathematics. For example, for the set of numbers $\{0, 1, 2, 3\}$, 2 is a lower bound, 1 is a tighter lower bound compared to 2, and 0 is the infimum (i.e., the tightest lower bound). Obviously, there are infinitely many lower bounds, but an overly loose lower bound cannot provide valuable assistance to algorithm researchers and may even mislead the performance evaluation. Additionally, as a performance evaluation tool, the simplicity and ease of use of the bound expression are crucial for algorithm researchers.

Therefore, for a given nonlinear parameter estimation problem, a “good” performance bound on estimation errors typically means:

- It provides tight estimation error bound for parameter estimation for as many scenarios as possible, such as under non-ideal observation conditions like low SNR and limited number of snapshots.
- It has explicit expression or even closed-form solution for specific parameter estimation problem, such that it is easy-to-use in performance evaluation.



However, these two requirements are somewhat conflicting. On one hand, providing tight performance bound means getting closer to the global optimal solution of the theoretical estimation error minimization problem, making it more difficult to derive. On the other hand, a easy-to-use and closed-form bound implies approximation and relaxation, which affects the tightness of the bound. Among the various performance bounds, the ZZB offers a tight performance bound derivation framework across the entire SNR range. The ZZB intuitively explains the actual parameter estimation behavior of the system, making it possible to achieve a closed-form expression of tight performance bounds across the entire SNR range.

Currently, although the basic ZZB derivation framework has been established, deriving explicit expressions or closed-form solutions for specific nonlinear parameter estimation problems remains challenging. Examples include deriving the ZZB under complex scenarios such as non-Gaussian noise, obtaining closed-form expressions of the ZZB for vector parameter estimation under multiple sources, and deriving closed-form expressions of the ZZB for joint estimation of multi-dimensional parameters under multiple sources. Therefore, it is of great significance to conduct research on explicit/closed-form ZZB expression for typical nonlinear parameter estimation problems such as distance and angle estimation, addressing the aforementioned challenges.

1.1 Literature review

Common estimation errors include the mean absolute error and the MSE. Compared to the mean absolute error, cost functions defined by the MSE are smooth and differentiable everywhere, making them more widely applicable in nonlinear parameter estimation problems. Consequently, since the 1940s, research on the performance bounds on MSE in nonlinear parameter estimation has been abundant.

Early research on the performance bounds on MSE primarily focused on fundamental mathematical theories. Generally, depending on the type of parameters to be estimated, the performance bounds on MSE can be divided into non-Bayesian performance bounds and Bayesian performance bounds.



1.1.1 Non-Bayesian bounds

In non-Bayesian bounds, the parameters to be estimated are considered as deterministic but unknown quantities. Therefore, these resulting bounds are related to the specific values of the parameters, effectively reflecting estimation performance on specific parameter values. Non-Bayesian bounds mainly include the CRB, the Bhattacharyya bound, and the Barankin bound (including its generalized forms).

1.1.1.1 CRB

As early as the 1940s, the CRB presented in [4], [5] evaluated the MSE lower bound for any unbiased estimator. It constructs the performance bound by solving the inverse of Fisher information and has been proven to asymptotically converge with the ML estimation under ideal observation conditions, thereby achieving a tight bound expression in the asymptotic region. Due to its straightforward derivation, CRB has been the most widely used bound over the past few decades. For example, in the 1980s and 1990s, [6], [7] first provided closed-form expressions of the CRB for DOA estimation problem for both deterministic and stochastic signal models. [6] has been cited thousands of times by researchers in the field over the past thirty years and received the IEEE Signal Processing Society Sustained Impact Paper Award in 2023. Subsequently, [8], [9] also provided expressions of the CRB for the underdetermined DOA estimation problem, successfully addressing the challenge where the rank deficiency of the FIM prevented the derivation of the CRB.

In practical applications, there are often mismatches between the assumed signal model and the actual received signal, even the actual received signal cannot be accurately modeled using analytical expressions. To address this issue, [10] first considered the problem of model mismatch, and provided a modified CRB for scalar parameter estimation problems. Subsequently, [11] extended the modified CRB for scalar parameter estimation to vector parameter estimation. Then, Fortunati *et al* further discussed the specific applications of the modified CRB in different parameter estimation problems under noise model mismatches [12]–[14]. [15] first considered the issue of non-analytical modeling of signal models in data-driven parameter estimation prob-



lems, and proposed a generative CRB as an approximate lower bound expression.

In recent years, the CRB has also been applied in research related to integrated radar and communication systems. In [16], a beamformer design method for integrated radar and communication systems was proposed with the minimization of the CRB as the objective function, providing a new perspective on the application of the CRB in the field of optimizer design. In [17], a joint design method for waveforms and discrete phase shifts in intelligent reflecting surface-assisted integrated sensing and communication systems was discussed, using the CRB for DOA estimation as a constraint.

Although the CRB is widely applied in various fields, its asymptotic optimality also indicates that under non-ideal observation conditions (e.g., low SNR, limited number of samples, etc.), the sporadic large estimation errors make the CRB unable to meet the conditions for asymptotic optimality. Hence, CRB becomes relaxed or even invalid in such scenario, which is so-called local performance bound for evaluating small estimation errors [3]. Specifically, the local performance bound refers to an estimation error performance bound that can only effectively reflect the performance limits of small estimation errors under ideal observation conditions. In contrast, a global performance bound refers to an estimation error performance bound that can effectively reflect the performance limits of both small estimation errors and large estimation errors.

1.1.1.2 Bhattacharyya bound

In the 1940s, Bhattacharyya first introduced the Bhattacharyya bound [18], which achieves better tightness compared to the CRB under low SNR conditions by utilizing the Bhattacharyya inequality [19]. Subsequently, [20] provided a convergence analysis of the Bhattacharyya bound. In [21], Tanaka *et al* theoretically discussed a series of signal statistical distribution families that can achieve the Bhattacharyya bound. [22] reviewed related research on the Bhattacharyya bound under the inverse Gaussian distribution and presented a series of results.

Similarly, in the context of model mismatch, [23] first provided a generalized expression of the Bhattacharyya bound. Subsequently, [24] derived the Bhattacharyya bound for time delay estimation problems. Compared to the traditional CRB, the Bhattacharyya bound can maintain



good tightness under low SNR conditions, but it still cannot effectively evaluate performance in scenarios with large estimation errors and also relies on the regularity conditions of the likelihood function. Additionally, the derivation of the Bhattacharyya bound depends on higher-order derivatives of the likelihood function and the function of the parameters to be estimated [19], such that it suffers from heavy computational burden and makes it difficult to be applied in specific nonlinear parameter estimation problems.

1.1.1.3 Barankin bound

Similarly, in the 1940s, Barankin introduced the Barankin bound based on the assumption of uniform unbiasedness in the parameter space [25]. Compared to the CRB and the Bhattacharyya bound, the Barankin bound is currently the tightest non-Bayesian performance bound for evaluating the MSE of uniformly unbiased estimators [19]. However, its theoretically tight characteristic makes it computationally infeasible in many practical scenarios, existing only as a theoretical expression. Consequently, numerous approximate expressions based on the Barankin bound have been proposed, such as the Hammersley-Chapman-Robbins bound [26], the McAulay-Seidman bound [27], the McAulay-Hofstetter bound [28], and the Abel bound [29]. [30] identified common features among the CRB, the Bhattacharyya bound, and the aforementioned Barankin bound, namely that these performance bounds are all based on the Taylor expansion of the likelihood function and the function of the parameters to be estimated, thereby achieving unification of these performance bounds. Based on this, [30] proposed a more computationally feasible and tighter expression of the Barankin bound. Marzetta *et al* proposed a method for computing the Barankin bound based on solving an unconstrained quadratic optimization problem [31].

Then, the Barankin bound has been applied in specific parameter estimation problems. [32] discussed the Barankin bound for variance estimation in generalized Gaussian random processes. [33] applied the Barankin bound to source localization parameter estimation in shallow water environments. Later, [34] further explored the application of the Barankin bound in source localization parameter estimation problems in uncertain ocean environments. [35] first provided the Barankin bound for target localization parameter estimation in multi-input multi-



output (MIMO) radar systems. In the same year, [36] presented the Barankin bound for target range and Doppler shift parameter estimation based on orthogonal transmission signals. Li *et al* in [37] provided the Barankin bound for target localization and direction finding in acoustic array systems.

From the existing work, although non-Bayesian performance bounds have made some progress in pursuing globally tight expressions, they treat the parameters to be estimated as deterministic but unknown quantities. Therefore, they cannot directly utilize the information provided by the *a priori* distribution of the parameters to be estimated. It presents limitations in further pursuing globally tight expressions for non-Bayesian performance bounds. The reason is that, under low SNR or limited observations, the behavior of the estimator tends to converge according to the *a priori* variance (covariance) of the parameters, and this *a priori* information is not considered by non-Bayesian performance bounds.

1.1.2 Bayesian bounds

In Bayesian bounds, the parameters to be estimated are treated as random variables with a certain *a priori* distribution. As such, under low SNR conditions, Bayesian bounds can effectively reflect the convergence characteristics of the estimator based on the *a priori* distribution of the parameters, thereby providing a tighter estimation error performance bound even in low SNR *a priori* regions. Bayesian performance bounds are mainly divided into two categories: the WWB and the ZZB.

1.1.2.1 WWB

The WWB was initially proposed by Weiss and Weinstein in [38]. In recent years, Renaux and Todros *et al* pointed out in [39], [40] that, some Bayesian performance bounds derived from non-Bayesian performance bounds all belong to the generalized WWB based on covariance inequalities, such as the BCRB [41], the Bayesian Bhattacharyya bound [41], and the BAB [42], the Borovsky-Mayer-Wolf-Zakai bound [43], the BZB [44], and the RMB (i.e., the Barankin bound extended under the Bayesian framework) [45],



In specific parameter estimation problems, [46] provided the WWB for target direction estimation using a 2D antenna array. Subsequently, Xu *et al* derived the WWB for matched field parameter estimation problems [47]. Vu *et al* presented the WWB for three-dimensional source localization parameter estimation under deterministic signal models [48] and the WWB for DOA estimation using polarized arrays [49], along with threshold SNR predictions. Then, [50] discussed the application of the WWB in array signal processing for both deterministic and non-deterministic models and provided relevant results. [51] derived the WWB for carrier frequency estimation problems with data assistance. [52] discussed the application of the WWB in colocated linear array MIMO radar structure parameter estimation and predicted the threshold SNR. [53] provided the WWB for multiple change-point estimation problems in non-stationary signals.

However, the WWB and its extensions are mostly derived based on various covariance inequalities. Although WWB can achieve tight expressions theoretically, it has the following issues:

- The tightness of the WWB is related to the order of derivatives involved. Specifically, pursuing tighter bounds requires higher-order derivative operations.
- The derivation of the WWB requires to solve non-convex optimization problems related to the dimension of the parameter space and relies on empirical rules for selecting test points, which makes the resulted WWB difficult to be analyzable [3]¹.
- The covariance inequalities relied upon by the WWB makes it difficult to establish an intuitive connection with the actual behavior of system parameter estimation [39]. Thus, the WWB cannot directly reflect the behavior of system estimation.

1.1.2.2 ZZB

Unlike the WWB, the ZZB establishes an intuitive connection between the lower bound on MSE and the minimum error probability of a binary hypothesis testing problem through the

¹The selection method of different test points can affect the final result of the WWB. Therefore, the reliance on empirical rules for test point selection directly impacts the reliability of the WWB results.



MSE identity. Therefore, compared to the WWB, the ZZB can intuitively explain the behavior of system parameter estimation. For example, at extremely low SNR, the binary hypothesis testing problem tends to make random decisions between the two hypotheses based on the *a priori* distribution of the parameters, with this decision process being almost unaffected by the observed data. Consequently, the MSE value indicated by the ZZB converges based on the *a priori* variance (covariance) of the parameters, which well explains the behavior of actual systems making random estimates based on the *a priori* distribution at extremely low SNR. Additionally, the derivation of the ZZB does not involve the empirical selection of test points, thus providing better solid results. Furthermore, the global tightness of the ZZB does not rely on higher-order derivative, making it potentially applicable to a wider range of signal models.

ZZB was first proposed and refined in the 1960s and 1970s [54]–[56]. Unlike other performance bounds that start from abstract mathematical derivations, the ZZB originated from the specific problem of single-target signal time delay parameter estimation. In the 1990s, Bell *et al* in [57] first extended the ZZB from scalar parameter estimation problems to vector parameter estimation problems, i.e., BZZB. In [58], they provided a closed-form solution for the ZZB in the single-source 2D DOA estimation problem.

In the problem of time delay estimation, Sadler *et al* conducted a series of studies on the ZZB in scenarios such as ultra-wideband signals [59], frequency-selective fading channel chirp signals [60], and unknown convolutional random channel signals [61]. Decarli *et al* first introduced the generalized LRT to study the ZZB for time delay estimation of unknown deterministic signals [62]. Ramasamy *et al* discussed the ZZB for time delay estimation under the framework of CS, considering random CS kernels and Gaussian white noise constraints [63]. Subsequently, [64], [65] extended the ZZB for the problem of compressed sensing time delay estimation to arbitrary compressed sensing kernels and arbitrary colored Gaussian noise (Chapter 3 of this dissertation), and further discussed the exact solution of the ZZB for time delay estimation under the zero-mean Gaussian random signal model [66] (Chapter 4 of this dissertation). [67] combined the ZZB with cognitive radar, providing an expression for the ZZB for time delay estimation in cognitive radar.

In DOA estimation, Gu *et al* proposed an improved ZZB in the 1990s and explored its



applications in DOA estimation and other related problems [68]. [69] provided the ZZB for single-source DOA estimation using sparse linear arrays. [70] derived the ZZB for wideband signal DOA estimation considering mutual coupling between array elements. In [71], the ZZB was applied to the effective aperture design of sparse subarray millimeter-wave systems, highlighting the limitation that previous ZZBs for DOA estimation were only applicable to single source scenarios. Subsequently, [72] provided a closed-form ZZB expression for multi-source DOA estimation based on linear arrays and revealed the relationship between the ZZB and the number of sources in the *a priori* performance region (Chapter 5 of this dissertation).

In other nonlinear parameter estimation problems for target localization, Dardari *et al* provided the ZZB expression for time-of-arrival (TOA) estimation under the condition that the ultra-wideband receiver has known channel statistics [73]. Gifford *et al* used the ZZB to discuss the impact of multipath information on TOA estimation performance. Wang *et al* analyzed the impact of inter-cell interference on localization accuracy in cellular network applications using the ZZB [74]. [75] analyzed the ZZB for TOA estimation in Orthogonal Frequency-Division Multiplexing (OFDM) systems.

Additionally, the ZZB is also applied in fields such as quantum, optics, and image processing. [76]–[78] discusses the ZZB in quantum parameter estimation problems and its performance analysis. [79] applied the ZZB to synchronous visible light positioning systems, providing the corresponding performance bounds. [80] applied the ZZB in image processing to evaluate the alignment accuracy between images.

In other analyses and applications of the ZZB, [81] used the ZZB to evaluate the trade-off between localization performance and communication performance in millimeter-wave communication and sensing systems. [82] optimized the ZZB to achieve SNR adaptive ranging waveform design. [83] analyzed the convergence performance of the ZZB in the *a priori* performance region.



1.2 Motivation and Contributions

Based on the literature review, it is evident that compared to non-Bayesian performance bounds, Bayesian performance bounds are much more easier to characterize the performance trend of parameter estimators under low SNR by utilizing the *a priori* distribution of parameters. Compared to the WWB, the ZZB has the advantage of intuitively explaining the behavior of system parameter estimation and does not rely on factors such as empirical test point selection that affect the reliability of the bound. In summary, among the various parameter estimation performance bounds, the ZZB has the following advantages:

- As a Bayesian performance bound, the ZZB effectively utilizes *a priori* information about parameters, making it easier to achieve globally tight expression.
- The fundamental principles and basic analytical framework of the ZZB can intuitively reflect the behavior of system parameter estimation, providing good interpretability.
- The fundamental principles of the ZZB exhibit good completeness and reliability.

Therefore, this dissertation selects the ZZB as the main research subject and conducts research on its application in nonlinear parameter estimation problems for target localization.

Most existing work is based on ideal assumptions such as single target parameters and Gaussian white noise. However, the ZZB in more complex parameter estimation scenarios still requires further research. Therefore, this dissertation focuses on typical parameter estimation problems in target localization, such as distance (time delay) and angle (DOA), and conducts studies on ZZB in complex scenarios involving non-white noise and multi-target estimation.

The dissertation is divided into eight chapters, with the arrangement and specific research content as follows:

Chapter 1 is the introduction. This chapter introduces the research background and significance of performance bounds for nonlinear parameter estimation errors in target localization. It also provides an overall review of the current research status of performance bounds for nonlinear parameter estimation errors. Additionally, this chapter highlights the advantages and



potential of the ZZB compared to other estimation error performance bounds and focuses on the challenges it faces in existing nonlinear parameter estimation problems for target localization. Chapter 2 covers the preliminaries. This chapter introduces the basic derivation framework of the ZZB in scalar parameter estimation problems and vector parameter estimation problems. Chapters 3 and 4 investigate the ZZB for time delay estimation based on CS. These chapters apply the analytical framework of the ZZB for scalar parameter estimation to compressive time delay estimation. Chapter 5 provides the close-form ZZB for multi-source 1D DOA estimation problem with linear arrays. Chapter 6 further derives the close-form ZZB expressions for multi-source 2D DOA estimation problem and azimuth/elevation estimation under 2D DOA model. Chapters 7 summarizes the research content of this dissertation and highlight further research directions and challenging frontier issues in the ZZB for nonlinear parameter estimation problems in target localization.

1.3 Publications

During the Ph.D. program, the author has worked on ZZB derivation and analysis. All journal and conference papers completed so far are listed as follows:

1.3.1 Book Chapter

1. **Zongyu Zhang**, Zhiguo Shi, and Arye Nehorai, “Ziv-Zakai bound for multi-source DOA estimation,” (Chapter 14) in *Information-Theoretic Radar Signal Processing* (Edited by Yujie Gu and Yimin D. Zhang), *Wiley-IEEE Press*, 2024 (in press).

1.3.2 Journal Papers

1. **Zongyu Zhang**, Zhiguo Shi, Cunqi Shao, Jiming Chen, Maria Sabrina Greco, and Fulvio Gini, “Ziv-Zakai bound for 2D-DOAs estimation”, *IEEE Transactions on Signal Processing*, vol. 72, pp. 2483 - 2497, 2024.
2. **Zongyu Zhang**, Zhiguo Shi, and Yujie Gu, “Ziv-Zakai bound for DOAs estimation”, *IEEE Transactions on Signal Processing*, vol. 71, pp. 136-149, 2023. **(ESI Highly**

**Cited Paper)**

3. **Zongyu Zhang**, Zhiguo Shi, Chengwei Zhou, Chenggang Yan, and Yujie Gu, “Ziv-Zakai bound for compressive time delay estimation”, *IEEE Transactions on Signal Processing*, vol. 70, pp. 4006-4019, 2022.
4. **Zongyu Zhang**, Zhiguo Shi, Yujie Gu, Maria Sabrina Greco, and Fulvio Gini, “Ziv-Zakai bound for compressive time delay estimation from zero-mean Gaussian signal”, *IEEE Signal Processing Letters*, vol. 30, pp. 1112-1116, 2023.
5. **Zongyu Zhang**, Chengwei Zhou, Yujie Gu, Jinfang Zhou, and Zhiguo Shi, “An IDFT approach for coprime array direction-of-arrival estimation”, *Digital Signal Processing*, vol. 94, pp. 45-55, Nov. 2019.
6. Yaxing Yue, **Zongyu Zhang**, and Zhiguo Shi, “Generalized Widely Linear Robust Adaptive Beamforming: A Sparse Reconstruction Perspective”, *IEEE Transactions on Aerospace and Electronic Systems*, 2024, Early Access.
7. Ying Liu, **Zongyu Zhang**, Chengwei Zhou, Chenggang Yan, and Zhiguo Shi, “Robust variational Bayesian inference for direction-of-arrival estimation with sparse array”, *IEEE Transactions on Vehicular Technology*, vol. 71, no. 8, pp. 8591-8602, Nov. 2022.

1.3.3 Conference Papers

1. **Zongyu Zhang**, Yujie Gu, and Zhiguo Shi, “Explicit Ziv-Zakai bound for multiple sources DOA estimation”, in *Proceedings of IEEE International Conference on Acoustics, Speech, and Signal Processing (ICASSP 2023)*, Rhodes island, Greece, June 2023.
2. **Zongyu Zhang**, Chengwei Zhou, Chenggang Yan and Zhiguo Shi, “Deterministic Ziv-Zakai bound for compressive time delay estimation”, in *Proceedings of IEEE Radar Conference (RadarConf22)*, New York City, NY, USA, Mar. 2022.
3. **Zongyu Zhang**, Chengwei Zhou, Yujie Gu, and Zhiguo Shi, “Efficient DOA estimation for coprime array via inverse discrete Fourier transform”, in *Proceedings of IEEE Inter-*



- national Conference on Digital Signal Processing (IEEE DSP 2018)*, Shanghai, China, Nov. 2018.
4. **Zongyu Zhang**, Chengwei Zhou, Yujie Gu, and Zhiguo Shi, “FFT-based DOA estimation for coprime MIMO radar: a hardware-friendly approach”, in *Proceedings of IEEE International Conference on Digital Signal Processing (IEEE DSP 2018)*, Shanghai, China, Nov. 2018.
 5. Luning Lin, **Zongyu Zhang**, Hang Zheng, Chengwei Zhou, and Zhiguo Shi, “DOA Estimation for Joint Sensing and Communication with Nonorthogonal Waveform”, in *Proceedings of 2022 56th Asilomar Conference on Signals, Systems, and Computers*, Pacific Grove, CA, USA, Oct. 2022.
 6. Yaxing Yue, **Zongyu Zhang**, Chengwei Zhou, Fangyuan Xing, and Zhiguo Shi, “Closed-form two-dimensional DOA and polarization joint estimation using parallel non-collocated sparse COLD arrays”, in *Proceedings of 2022 IEEE 12th Sensor Array and Multichannel Signal Processing Workshop (SAM)*, Trondheim, Norway, June 2022.
 7. Yaxing Yue, **Zongyu Zhang**, Chengwei Zhou, Yuan Wu, Fangyuan Xing, and Zhiguo Shi, “Closed-form robust adaptive beamforming for sparse diversely polarized antenna array”, in *Proceedings of IEEE 34th Annual International Symposium on Personal, Indoor and Mobile Radio Communications (PIMRC)*, Toronto, ON, Canada, Sept. 2022.
 8. Sihan Wen, **Zongyu Zhang**, Chengwei Zhou, and Zhiguo Shi, “Ziv-Zakai bound for DOAs estimation with gain-phase error”, in *Proceedings of IEEE International Conference on Acoustics, Speech, and Signal Processing (ICASSP 2024)*, Seoul, Korea, Apr. 2024.

1.3.4 Issued Patents

1. **Zongyu Zhang**, Zhiguo Shi, Chengwei Zhou, and Jiming Chen, “A coprime MIMO radar DOA estimation approach based on different coarray of sum coarray signal fast Fourier transform”, No. ZL 2018 1 1218661.6, China, 12-Jan-2021.



2. **Zongyu Zhang**, Zhiguo Shi, Chengwei Zhou, and Jiming Chen, “A coprime MIMO radar DOA estimation approach based on discrete Fourier transform of multi-snapshot sum coarray signal”, No. ZL 2018 1 1218389.1, China, 11-Nov-2020.
3. **Zongyu Zhang**, Zhiguo Shi, Chengwei Zhou, and Jiming Chen, “A coprime array DOA estimation approach based on discrete Fourier transform of second-order equivalent virtual signal”, No. ZL 2018 1 0460228.7, China, 04-Sept-2020.
4. **Zongyu Zhang**, Zhiguo Shi, Chengwei Zhou, and Jiming Chen, “A coprime array DOA estimation approach based on fast Fourier transform of multi-snapshots coprime array received signal”, No. ZL 2018 1 0459732.5, China, 01-Sept-2020.
5. Zhiguo Shi, **Zongyu Zhang**, Chengwei Zhou, and Jiming Chen, “A coprime array DOA estimation approach based on angle-frequency domain fast Fourier transform”, No. ZL 2018 1 0464602.0, China, 5-June-2020.



Chapter 2. Preliminaries

This chapter includes the preliminaries about ZZB derivation, including basic derivation framework for both scalar and vector parameter estimation scenarios.

2.1 Basic ZZB derivation framework for scalar parameter estimation

The original ZZB derivation framework was proposed and improved in [54]–[56], which focus on a straightforward scalar parameter estimation problem. This section is to introduce this ZZB derivation framework.

Consider an observation \mathbf{y} as the non-linear function of a continuous scalar parameter θ , i.e., $\mathbf{y}(\theta)$. Here is an identity about the MSE on estimating θ [84]

$$\overline{\epsilon_\theta^2} = \mathbb{E} \{ |\epsilon_\theta|^2 \} = \frac{1}{2} \int_0^{+\infty} \Pr \left(|\epsilon_\theta| \geq \frac{\xi}{2} \right) \xi d\xi, \quad (2-1)$$

where $\epsilon_\theta = \hat{\theta} - \theta$ denotes the estimation error. Obviously, both ξ and $\Pr \left(|\epsilon_\theta| \geq \frac{\xi}{2} \right)$ are non-negative, such that the minimum of the MSE $\overline{\epsilon_\theta^2}$, i.e., the lower bound, is obtained by minimizing $\Pr \left(|\epsilon_\theta| \geq \frac{\xi}{2} \right)$. For a given ξ , the probability $\Pr \left(|\epsilon_\theta| \geq \frac{\xi}{2} \right)$ can be expressed by

$$\begin{aligned} \Pr \left(|\epsilon_\theta| \geq \frac{\xi}{2} \right) &= \Pr \left(\epsilon_\theta > \frac{\xi}{2} \right) + \Pr \left(\epsilon_\theta \leq -\frac{\xi}{2} \right) \\ &= \int_{-\infty}^{+\infty} f_\theta(\varphi) \Pr \left(\hat{\theta} > \varphi + \frac{\xi}{2} \middle| \theta = \varphi \right) d\varphi \\ &\quad + \int_{-\infty}^{+\infty} f_\theta(\varphi + \xi) \Pr \left(\hat{\theta} \leq \varphi + \frac{\xi}{2} \middle| \theta = \varphi + \xi \right) d\varphi \\ &= \int_{-\infty}^{+\infty} [f_\theta(\varphi) + f_\theta(\varphi + \xi)] P_e(\varphi, \varphi + \xi) d\varphi, \end{aligned} \quad (2-2)$$

where $f_\theta(\varphi) \triangleq f(\theta)|_{\theta=\varphi}$ is the probability density with $\theta = \varphi$. Obviously,

$$P_e(\varphi, \varphi + \xi) = \Pr(\mathcal{H}_0) \Pr \left(\hat{\theta} > \varphi + \frac{\xi}{2} \middle| \theta = \varphi \right) + \Pr(\mathcal{H}_1) \Pr \left(\hat{\theta} \leq \varphi + \frac{\xi}{2} \middle| \theta = \varphi + \xi \right) \quad (2-3)$$



is the probability of error of the binary hypothesis testing problem

$$\begin{aligned}\mathcal{H}_0 : \theta = \varphi, \quad \Pr(\mathcal{H}_0) &= \frac{f_\theta(\varphi)}{f_\theta(\varphi) + f_\theta(\varphi + \xi)}, \\ \mathcal{H}_1 : \theta = \varphi + \xi, \quad \Pr(\mathcal{H}_1) &= 1 - \Pr(\mathcal{H}_0)\end{aligned}\tag{2-4}$$

under the nearest neighborhood criterion

$$\begin{aligned}\text{Decide } \mathcal{H}_0 : \theta = \varphi & \quad \text{if } \hat{\theta} \leq \varphi + \frac{\xi}{2} \\ \text{Decide } \mathcal{H}_1 : \theta = \varphi + \xi & \quad \text{if } \hat{\theta} > \varphi + \frac{\xi}{2}.\end{aligned}\tag{2-5}$$

Among all the decision criteria, MAP criterion

$$\begin{aligned}\text{Decide } \mathcal{H}_0 & \quad \text{if } \Pr(\mathcal{H}_0)f(\mathbf{y}|\varphi) > \Pr(\mathcal{H}_1)f(\mathbf{y}|\varphi + \xi) \\ \text{Decide } \mathcal{H}_1 & \quad \text{if } \Pr(\mathcal{H}_0)f(\mathbf{y}|\varphi) \leq \Pr(\mathcal{H}_1)f(\mathbf{y}|\varphi + \xi)\end{aligned}\tag{2-6}$$

provides the minimum probability of error [1], where $f(\mathbf{y}|\varphi) \triangleq f(\mathbf{y}|\theta)|_{\theta=\varphi}$ is the probability density of \mathbf{y} with $\theta = \varphi$. Thus, the minimum probability of error becomes

$$\begin{aligned}P_{\min}(\varphi, \varphi + \xi) &= \Pr(\mathcal{H}_0)\Pr\left(\frac{f(\mathbf{y}|\varphi)}{f(\mathbf{y}|\varphi + \xi)} \leq \frac{\Pr(\mathcal{H}_1)}{\Pr(\mathcal{H}_0)} \middle| \theta = \varphi\right) \\ &\quad + \Pr(\mathcal{H}_1)\Pr\left(\frac{f(\mathbf{y}|\varphi)}{f(\mathbf{y}|\varphi + \xi)} > \frac{\Pr(\mathcal{H}_1)}{\Pr(\mathcal{H}_0)} \middle| \theta = \varphi + \xi\right) \\ &= \Pr(\mathcal{H}_0)\Pr(\mathcal{L}_\theta \leq \gamma | \theta = \varphi) + \Pr(\mathcal{H}_1)\Pr(\mathcal{L}_\theta > \gamma | \theta = \varphi + \xi) \\ &\triangleq \Pr(\mathcal{H}_0)\Pr(\mathcal{L}_\varphi \leq \gamma) + \Pr(\mathcal{H}_1)\Pr(\mathcal{L}_{\varphi+\xi} > \gamma).\end{aligned}\tag{2-7}$$

Here,

$$\mathcal{L}_\theta = \ln \frac{f(\mathbf{y}|\varphi)}{f(\mathbf{y}|\varphi + \xi)}\tag{2-8}$$

is the log-LRT, and

$$\gamma = \ln \frac{\Pr(\mathcal{H}_1)}{\Pr(\mathcal{H}_0)}\tag{2-9}$$

is a constant determined by the *a priori* probability of θ .

Because $P_e(\varphi, \varphi + \xi) \geq P_{\min}(\varphi, \varphi + \xi)$ always holds, $P_{\min}(\varphi, \varphi + \xi)$ is available to derive



the lower bound of $\Pr(|\epsilon_\theta| \geq \frac{\xi}{2})$ in (2-2), and the general expression of ZZB can be derived as

$$\overline{\epsilon_\theta^2} \geq \frac{1}{2} \int_0^{+\infty} \xi \int_{-\infty}^{+\infty} [f_\tau(\varphi) + f_\tau(\varphi + \xi)] P_{\min}(\varphi, \varphi + \xi) d\varphi d\xi. \quad (2-10)$$

Furthermore, because $\Pr(|\epsilon_\theta| \geq \frac{\xi}{2})$ is the non-increasing function of ξ , a valley filling function can be introduced to obtain a tighter ZZB expression as

$$\overline{\epsilon_\theta^2} \geq \frac{1}{2} \int_0^{+\infty} \xi \mathcal{V} \left\{ \int_{-\infty}^{+\infty} [f_\tau(\varphi) + f_\tau(\varphi + \xi)] P_{\min}(\varphi, \varphi + \xi) \right\} d\varphi d\xi. \quad (2-11)$$

It should be noted that, although the valley filling function theoretically results in tighter ZZB expression, it also leads to more challenges for closed-form ZZB derivation. Also, it has been proven that the valley filling function does not bring significant improvement on the tightness of ZZB in many specific estimation scenarios [57]. Hence, it is usually ignored in current ZZB derivation.

2.2 Basic ZZB derivation framework for scalar parameter estimation

In [57], the ZZB derivation framework for vector parameter estimation was extended, which is introduced in this section.

Consider an observation \mathbf{y} as the non-linear function of a K -dimensional vector parameter $\boldsymbol{\theta}$, i.e., $\mathbf{y}(\boldsymbol{\theta})$. Then, the error correlation matrix for estimating $\boldsymbol{\theta}$ is defined as

$$\mathbf{R}_\epsilon = \mathbb{E} \{ \boldsymbol{\epsilon} \boldsymbol{\epsilon}^T \} = \mathbb{E} \{ (\hat{\boldsymbol{\theta}} - \boldsymbol{\theta})(\hat{\boldsymbol{\theta}} - \boldsymbol{\theta})^T \}. \quad (2-12)$$

Different from scalar parameter estimation, the estimation error for K -dimensional vector parameter $\boldsymbol{\theta}$ needs to be expressed with the error correlation matrix. To give the expression of MSE, a weighted summation on the estimation error $\boldsymbol{\epsilon}$, i.e., $\mathbf{w}^T \boldsymbol{\epsilon} = \mathbf{w}^T (\hat{\boldsymbol{\theta}} - \boldsymbol{\theta})$ is considered, such that the quadratic form is obtained as

$$\mathbf{w}^T \mathbf{R}_\epsilon \mathbf{w} = \mathbb{E} \left\{ |\mathbf{w}^T \boldsymbol{\epsilon}|^2 \right\} = \frac{1}{2} \int_0^{+\infty} \Pr \left(|\mathbf{w}^T \boldsymbol{\epsilon}| \geq \frac{h}{2} \right) h dh. \quad (2-13)$$



Here, \mathbf{w} is a K -dimensional weighted vector following the unit Euclidean norm $\|\mathbf{w}\|_2 = 1$. Similar to the scalar parameter estimation scenario, the probability $\Pr(|\mathbf{w}^T \boldsymbol{\epsilon}| \geq \frac{h}{2})$ can be expressed as

$$\begin{aligned} \Pr\left(|\mathbf{w}^T \boldsymbol{\epsilon}| \geq \frac{h}{2}\right) &= \Pr\left(\mathbf{w}^T \boldsymbol{\epsilon} \leq -\frac{h}{2}\right) + \Pr\left(\mathbf{w}^T \boldsymbol{\epsilon} > \frac{h}{2}\right) \\ &= \int_{\mathbb{R}^K} f_{\boldsymbol{\theta}}(\boldsymbol{\varphi} + \boldsymbol{\delta}) \Pr\left(\mathbf{w}^T \hat{\boldsymbol{\theta}} \leq \mathbf{w}^T \boldsymbol{\varphi} + \mathbf{w}^T \boldsymbol{\delta} - \frac{h}{2} \middle| \boldsymbol{\theta} = \boldsymbol{\varphi} + \boldsymbol{\delta}\right) d\boldsymbol{\varphi} \\ &\quad + \int_{\mathbb{R}^K} f_{\boldsymbol{\theta}}(\boldsymbol{\varphi}) \Pr\left(\mathbf{w}^T \hat{\boldsymbol{\theta}} > \mathbf{w}^T \boldsymbol{\varphi} + \frac{h}{2} \middle| \boldsymbol{\theta} = \boldsymbol{\varphi}\right) d\boldsymbol{\varphi}, \end{aligned} \quad (2-14)$$

where \mathbb{R}^K denotes the K -dimensional real space. For a given h , the probability $\Pr(|\mathbf{w}^T \boldsymbol{\epsilon}| \geq \frac{h}{2})$ can be further expressed as

$$\begin{aligned} \Pr\left(|\mathbf{w}^T \boldsymbol{\epsilon}| \geq \frac{h}{2}\right) &= \int_{\mathbb{R}^K} f_{\boldsymbol{\theta}}(\boldsymbol{\varphi}) \Pr\left(\mathbf{w}^T \hat{\boldsymbol{\theta}} > \mathbf{w}^T \boldsymbol{\varphi} + \frac{h}{2} \middle| \boldsymbol{\theta} = \boldsymbol{\varphi}\right) d\boldsymbol{\varphi} \\ &\quad + \int_{\mathbb{R}^K} f_{\boldsymbol{\theta}}(\boldsymbol{\varphi} + \boldsymbol{\delta}) \Pr\left(\mathbf{w}^T \hat{\boldsymbol{\theta}} \leq \mathbf{w}^T \boldsymbol{\varphi} + \frac{h}{2} \middle| \boldsymbol{\theta} = \boldsymbol{\varphi} + \boldsymbol{\delta}\right) d\boldsymbol{\varphi} \\ &= \int_{\mathbb{R}^K} [f_{\boldsymbol{\theta}}(\boldsymbol{\varphi}) + f_{\boldsymbol{\theta}}(\boldsymbol{\varphi} + \boldsymbol{\delta})] P_e(\boldsymbol{\varphi}, \boldsymbol{\varphi} + \boldsymbol{\delta}) d\boldsymbol{\varphi} \end{aligned} \quad (2-15)$$

if

$$\mathbf{w}^T \boldsymbol{\delta} = h. \quad (2-16)$$

Here, $P_e(\boldsymbol{\varphi}, \boldsymbol{\varphi} + \boldsymbol{\delta})$ is the probability of error of the binary hypothesis testing problem

$$\begin{aligned} \mathcal{H}_0 : \boldsymbol{\theta} = \boldsymbol{\varphi}, \quad \Pr(\mathcal{H}_0) &= \frac{f_{\boldsymbol{\theta}}(\boldsymbol{\varphi})}{f_{\boldsymbol{\theta}}(\boldsymbol{\varphi}) + f_{\boldsymbol{\theta}}(\boldsymbol{\varphi} + \boldsymbol{\delta})}, \\ \mathcal{H}_1 : \boldsymbol{\theta} = \boldsymbol{\varphi} + \boldsymbol{\delta}, \quad \Pr(\mathcal{H}_1) &= 1 - \Pr(\mathcal{H}_0) \end{aligned} \quad (2-17)$$

with the nearest neighborhood criterion

$$\begin{aligned} \text{Decide } \mathcal{H}_0 : \boldsymbol{\theta} = \boldsymbol{\varphi} &\quad \text{if } \mathbf{w}^T \hat{\boldsymbol{\theta}} \leq \mathbf{w}^T \boldsymbol{\varphi} + \frac{h}{2} \\ \text{Decide } \mathcal{H}_1 : \boldsymbol{\theta} = \boldsymbol{\varphi} + \boldsymbol{\delta} &\quad \text{if } \mathbf{w}^T \hat{\boldsymbol{\theta}} > \mathbf{w}^T \boldsymbol{\varphi} + \frac{h}{2}. \end{aligned} \quad (2-18)$$

Similar to the scalar parameter estimation scenario, the minimum probability of error can



be obtained via the MAP criterion, such that the lower bound of probability of error becomes

$$\Pr\left(|\mathbf{w}^T \boldsymbol{\epsilon}| \geq \frac{h}{2}\right) \geq \int_{\mathbb{R}^K} [f_{\theta}(\boldsymbol{\varphi}) + f_{\theta}(\boldsymbol{\varphi} + \boldsymbol{\delta})] P_{\min}(\boldsymbol{\varphi}, \boldsymbol{\varphi} + \boldsymbol{\delta}) d\boldsymbol{\varphi}. \quad (2-19)$$

Accordingly, the general expression of ZZB for vector parameter estimation with the valley filling function is

$$\mathbf{w}^T \mathbf{R}_{\boldsymbol{\epsilon}} \mathbf{w} \geq \frac{1}{2} \int_0^{\infty} \mathcal{V} \left\{ \max_{\boldsymbol{\delta}: \mathbf{w}^T \boldsymbol{\delta} = h} \left[\int_{\mathbb{R}^K} (f_{\theta}(\boldsymbol{\varphi}) + f_{\theta}(\boldsymbol{\varphi} + \boldsymbol{\delta})) P_{\min}(\boldsymbol{\varphi}, \boldsymbol{\varphi} + \boldsymbol{\delta}) d\boldsymbol{\varphi} \right] \right\} h dh. \quad (2-20)$$

2.3 Summary

This chapter introduces the basic ZZB derivation framework for two types of parameter estimation scenarios, and provide preliminaries for the following chapters.



Chapter 3. ZZB for Compressive Time Delay Estimation

Compressive radar receiver can keep a good balance between sub-Nyquist sampling and high resolution. To evaluate the performance of compressive time delay estimators, CRB has been derived for lower bounding the MSE, which, unfortunately, is a local bound being tight in the asymptotic region only. In this chapter, we use the ZZB methodology to develop a Bayesian MSE bound on compressive time delay estimation by incorporating the *a priori* information of the unknown time delay. Specifically, we respectively derive deterministic ZZB and stochastic ZZB as functions of CS kernel, where there is no restriction on CS kernels and Gaussian noise colors. Simulation results demonstrate that compared with BCRB, ZZB provides a better performance prediction for MMSE estimator of compressive time delay estimation over a wide range of SNRs, where different CS kernels, CRs, *a priori* distributions and Gaussian noise colors are tested.

3.1 Introduction

Time delay estimation is a canonical nonlinear parameter estimation problem, which has been widely used for ranging, localization, synchronization, radiolocation, geolocation and others in many applications including radar, sonar, seismic, remote sensing, wireless communication, IoT (see, for example [61], [85]–[89], and the references therein). Waveform bandwidth is an essential factor in determining estimation accuracy, i.e., time delay estimation accuracy can be improved via enhanced range resolution by increasing the waveform bandwidth. Hence, in the past decades, more and more wideband signals have been adopted to improve the estimation performance and imaging quality.

However, it also brings significant challenges for high-rate A/D converters w.r.t. required sampling rate, system cost, and power consumption. To mitigate the cost and power consumption due to high-rate A/D converters and data handling hardware, CS [90] is a good solution to keep a balance between sampling rate and range resolution. Unlike the classical Nyquist sampling theory, CS theory states that signals can be acquired at sub-Nyquist sampling rates



and then reconstructed with accuracy comparable to Nyquist sampling, given signals of interest being sparse or compressible [91]. Due to the sparsity of radar signals in the time domain, radar receiver can compressively sample the target echoes at a fixed A/D conversion rate lower than the Nyquist sampling rate, which means the range resolution has been simultaneously improved because of the wideband radar waveform. Hence, CS radar has attracted great interest in the past decade [92]–[102], among which the investigation of compressive time delay estimation is helpful for understanding and demonstrating fundamental concepts [97], [101].

Similarly as in the Nyquist sampling, the classical estimators including matched filter, ML estimator, and MMSE estimator, can also be applied to estimate time delay from the compressed measurements (see, for example, [63], [101], [103]). In addition, under the framework of CS, the sparsity can be specifically exploited to formulate the time delay estimation as a sparse signal reconstruction problem [89]. Besides the well known sparse reconstruction algorithms, the more recently developed algorithms for time delay estimation include atomic norm minimization-based algorithm [103], interpolation-based recovery algorithm [104], and manifold-based optimization algorithm [105], etc.

Same as most nonlinear parameter estimation, there is no exact closed-form solution for the minimum MSE of compressive time delay estimation. To this end, researchers prefer to find the lower bound on the MSE in estimating the parameter of interest including time delay. Among numerous lower bounds, CRB [5], [106], [107] is the most commonly used one, considering that it is generally easier to evaluate than other bounds. The CRB for parameter estimation from compressed measurements is analyzed in [108]–[110], where the parameters are treated as deterministic. However, deterministic assumption may limit CRB utilizing the *a priori* information from the parameters (e.g., the range or *a priori* distribution of the parameters). The analysis and derivation of BCRB for compressive parameter estimation are provided in [63], [101], in which the parameters are regarded as random variables with certain *a priori* distribution, enabling the utilization of the *a priori* distribution of the parameter to provide a tighter bound. However, it is well known that, either CRB or BCRB behaves as a local bound and does not show a threshold effect. In other words, both CRB and BCRB are only tight in the asymptotic region (say, high SNR situation). To overcome the locality of BCRB, numer-



ous Bayesian bounds are proposed to enable better performance [3], [111], such as WWB [38], RMB [45], BAB [42], BZB [44], etc. However, all aforementioned bounds are based on covariance inequalities [39], where tighter bounds rely on higher order derivative, optimization over free variables and empirical testing point selection [3], limiting their application in specific parameter estimation.

Different from covariance inequality based bounds, ZZB relates the MSE in the estimation problem to the probability of error in a binary hypothesis testing problem, and provides a global tight bound on the MSE over a wide range of SNR [3], [112]. ZZB was originally proposed for time delay estimation [54], [56], [113], where the unknown parameter follows a uniform *a priori* distribution. After that, the framework of ZZB was extended to arbitrary *a priori* distribution parameter for general parameter estimation [57]. In the past few decades, ZZBs have been widely studied in different parameter estimation problems [58]–[60], [62], [67], [114], [115]. It is worth noting that, however, all aforementioned researches assumed the Nyquist sampling on the received signal. To the best knowledge of the authors, there is rare study of ZZB on compressive parameter estimators. Although [63] formulates the effect of CS kernel on ZZB as a constant penalty related to CR such that the compressive ZZB can be approximately expressed in a Nyquist ZZB manner, the derivation there is restricted by the random CS kernel and white Gaussian noise assumptions. Hence, it is demanding to propose a more general ZZB under the CS framework to predict the performance of compressive parameter estimators and the locations of the asymptotic region threshold.

In this chapter, we derive the explicit deterministic ZZB and stochastic ZZB for compressive time delay estimation as functions of CS kernels, which respectively corresponds to compressive measurement with deterministic amplitude and stochastic amplitude. Given the basic ZZB expression proposed in [57], the required minimum probability of error in the binary hypothesis testing problem for compressive time delay estimation can be explicitly derived as a function of CS kernel either for deterministic signal model or for stochastic signal model. Correspondingly, the ZZBs are calculated by integrals of product involving the *a priori* distribution of the unknown time delay and the corresponding minimum probability of error. Considering that there is not any restriction on CS kernels and the color of Gaussian noise, the derived ZZBs



are applicable for arbitrary CS kernels and arbitrary Gaussian noise. In addition, for better comparison with the stochastic ZZB, we also generalize the stochastic BCRB for compressive time delay estimation from [101], where the stochastic BCRB is only applicable for the zero-mean compressive measurement model. Simulation are designed to demonstrate the advantage of the derived ZZBs and BCRBs in a wide range of SNR under different scenarios, including different CS kernels, CRs, *a priori* distribution and Gaussian noise colors. Compared with BCRBs, the ZZBs derived in this chapter can provide a more accurate prediction on compressive parameter estimation performance and the location of the asymptotic region threshold under different compressive ratios.

The rest of the chapter is organized as follows. In Section 3.2, we present the CS radar receiver model and provide deterministic and stochastic BCRBs for compressive time delay estimation. In Section 3.3, we derive the deterministic ZZB and stochastic ZZB. In Section 3.4, we compare the ZZBs using random CS kernels and information-theoretic CS kernels against the MMSE estimator and the corresponding CRBs via simulations. Finally, we make conclusions in Section 3.5.

3.2 Signal Model and CRB

Considering an active radar illuminates a far-field point source target, the target echo signal at time t can be modeled as

$$r(t) = \alpha\psi(t - \tau) + n(t), \quad (3-1)$$

where α is complex-valued signal amplitude, $\psi(t - \tau)$ is the radar waveform delayed by an unknown time τ , and $n(t)$ is the complex additive Gaussian noise sampled from a stationary process. Obviously, the radar received signal is sparse in the time domain, and the sparsity depends on the number of targets in the range of interest. According to the CS theory, it is highly promising to estimate the unknown time delay τ from much less samples than that required by the Nyquist sampling theorem. In detail, by projecting the received signal $r(t)$ onto M measurement kernels $\{\phi_m(t), m = 1, 2, \dots, M\}$, where M is much less than the number of Nyquist samples, we can obtain M measurements $\{y_m, m = 1, 2, \dots, M\}$, among which the



m -th measurement y_m is the inner product of $\phi_m(t)$ and $r(t)$ during $[0, T]$, i.e.,

$$\begin{aligned}
 y_m &= \langle r(t), \phi_m(t) \rangle_{t \in [0, T]} \\
 &\triangleq \int_0^T r(t) \phi_m^*(t) dt \\
 &\approx \Delta \sum_{l=1}^L r(l) \phi_m^*(l).
 \end{aligned} \tag{3-2}$$

Here, T is the maximum duration of $r(t)$, which is divided into L small intervals of width Δ , i.e., $\Delta = T/L$. To ensure that the discrete approximation in (3-2) is accurate, Δ must be much smaller than the reciprocal of the bandwidths of $\phi_m(t)$ and $r(t)$ so that there is no significant variation in the signals within an interval Δ . Hence, L is much larger than the number of measurement M .

By stacking the measurements as $\mathbf{y} = [y_1, y_2, \dots, y_M]^T$, it can be written in matrix-vector form as

$$\mathbf{y} \approx \mathbf{\Phi} \mathbf{r} = \mathbf{\Phi} (\alpha \psi(\tau) + \mathbf{n}), \tag{3-3}$$

where the CS kernel $\mathbf{\Phi} = [\phi_1^*, \phi_2^*, \dots, \phi_M^*]^T \in \mathbb{C}^{M \times L}$ contains M measurement kernels with $\phi_m \in \mathbb{C}^L$ denoting discrete-time representation of $\phi_m(t)$, $\mathbf{r} \in \mathbb{C}^L$ and $\psi(\tau) \in \mathbb{C}^L$ are discrete-time representations of the received echo signal and the transmitted radar waveform delayed by τ , and $\mathbf{n} \in \mathbb{C}^L$ follows zero-mean complex Gaussian distribution $\mathcal{CN}(\mathbf{0}, \mathbf{R}_{nn})$ and is independent of τ . The system block diagrams of the traditional radar receiver and the CS radar receiver are compared in Fig. 3.1. Different from the traditional radar receiver that requires high-rate A/D converter, the CS radar receiver uses analog multiplication and analog integration to reduce the number of samples, which hence requires sub-Nyquist rate A/D converters only. Although extra analog components and D/A converters are required in the CS radar receiver, we do not need high-rate A/D converters to satisfy the Nyquist sampling since they may be unavailable or too expensive to commercialize [101].

There are two commonly used models of (3-3) depending on the signal amplitude α , i.e., deterministic model assuming α to be an unknown deterministic quantity and stochastic model assuming α to be a random variable. For the deterministic model, it is observed that for a given

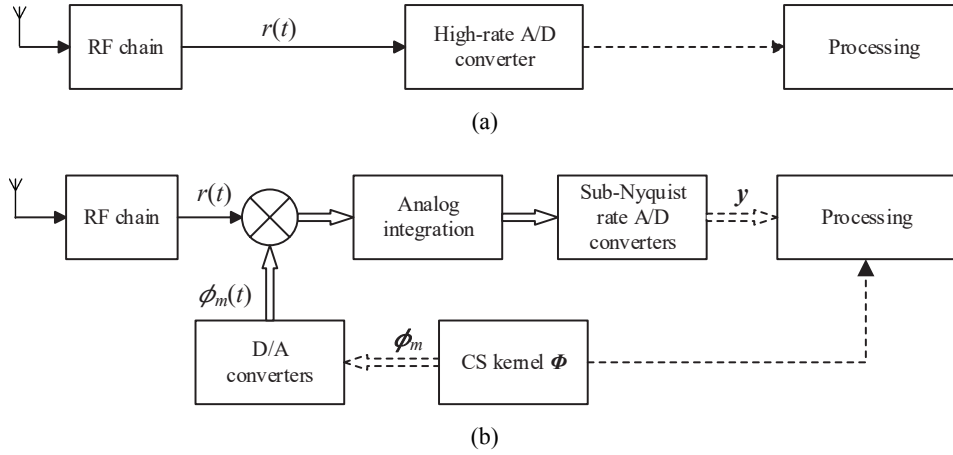


Figure 3.1 Radar receiver block diagram. (a) Traditional radar receiver; (b) CS radar receiver. The solid arrows denote the signal processed in analog domain, and the dashed arrows denote the signal processed in digital domain. The hollow arrows denote M parallel processing chains.

time delay τ , the measurement vector \mathbf{y} follows a complex Gaussian distribution $\mathcal{CN}(\bar{\mathbf{y}}_\tau, \mathbf{R}_{\mathbf{y}\mathbf{y}})$ with the mean vector $\bar{\mathbf{y}}_\tau = \alpha \Phi \psi(\tau)$ and the covariance matrix $\mathbf{R}_{\mathbf{y}\mathbf{y}} = \Phi \mathbf{R}_{nn} \Phi^H$. Correspondingly, the conditional PDF of the measurement vector \mathbf{y} given time delay τ can be expressed as

$$f(\mathbf{y}|\tau) = \frac{1}{\pi^M |\mathbf{R}_{\mathbf{y}\mathbf{y}}|} e^{-(\mathbf{y}-\bar{\mathbf{y}}_\tau)^H \mathbf{R}_{\mathbf{y}\mathbf{y}}^{-1} (\mathbf{y}-\bar{\mathbf{y}}_\tau)}. \quad (3-4)$$

For the stochastic model, here we assume that α follows a complex-valued Gaussian distribution $\mathcal{CN}(\mu_\alpha, \sigma_\alpha^2)$. It is then observed that for a given τ , \mathbf{y} follows a complex Gaussian distribution $\mathcal{CN}(\bar{\mathbf{y}}_\tau, \mathbf{R}_{\mathbf{y}\mathbf{y}|\tau})$ with $\bar{\mathbf{y}}_\tau = \mu_\alpha \Phi \psi(\tau)$ and $\mathbf{R}_{\mathbf{y}\mathbf{y}|\tau} = \Phi (\sigma_\alpha^2 \psi(\tau) \psi^H(\tau) + \mathbf{R}_{nn}) \Phi^H$. Thus, the conditional PDF of \mathbf{y} given τ becomes

$$f(\mathbf{y}|\tau) = \frac{1}{\pi^M |\mathbf{R}_{\mathbf{y}\mathbf{y}|\tau}|} e^{-(\mathbf{y}-\bar{\mathbf{y}}_\tau)^H \mathbf{R}_{\mathbf{y}\mathbf{y}|\tau}^{-1} (\mathbf{y}-\bar{\mathbf{y}}_\tau)}. \quad (3-5)$$

The CRB provides a lower bound on the variance of any unbiased estimate of a deterministic parameter, stating that the variance of any such estimator is at least as high as the inverse of the Fisher information. When the PDF of the time delay τ , i.e., $f(\tau)$, is *a priori* known, the Bayesian version of the Fisher information J_B consists of two parts [2] as

$$J_B = J_D + J_P, \quad (3-6)$$



where J_D denotes the information due to the measurement data, and

$$J_P = \mathbb{E}_\tau \left\{ -\frac{d^2 \ln f(\tau)}{d\tau^2} \right\} \quad (3-7)$$

denotes the information due to the *a priori* knowledge.

Following a similar derivation as in [101], the Fisher information J_D for the non-zero mean stochastic model is

$$J_D = \mathbb{E}_\tau \left\{ -2\sigma_\alpha^2 \Re \left[\boldsymbol{\psi}^H(\tau) \boldsymbol{\Phi}^H \frac{d\mathbf{R}_{yy}^{-1}}{d\tau} \boldsymbol{\Phi} \frac{d\boldsymbol{\psi}(\tau)}{d\tau} \right] + 2|\mu_\alpha|^2 \frac{d\boldsymbol{\psi}^H(\tau)}{d\tau} \boldsymbol{\Phi}^H \mathbf{R}_{yy}^{-1} \boldsymbol{\Phi} \frac{d\boldsymbol{\psi}(\tau)}{d\tau} \right\}. \quad (3-8)$$

It is clear that this Fisher information contains two terms. The first one (i.e., Eq. (39) in [101]) is the Fisher information reflecting the stochastic part in \mathbf{y} with $\mu_\alpha = 0$, while the second one (i.e., Eq. (28) in [101]) is the Fisher information reflecting the deterministic part in \mathbf{y} with $\sigma_\alpha^2 = 0$. Hence, the Fisher information in (3-8) is applicable for arbitrary Gaussian model including both zero-mean and zero-variance cases. Meanwhile, it is also observed that, the Fisher information J_P due to the *a priori* knowledge degrades to zero when τ follows a uniform distribution, which indicates that it makes no contribution to the BCRB.

3.3 ZZB Derivation

According to basic ZZB derivation framework introduced in Section 2.1, this section derive the ZZB with both deterministic and stochastic models.

3.3.1 Minimum Probability of Error for Deterministic Model

According to (3-4), the log-LRT is calculated as

$$\mathcal{L}_\tau = (\mathbf{y} - \bar{\mathbf{y}}_{\varphi+\xi})^H \mathbf{R}_{yy}^{-1} (\mathbf{y} - \bar{\mathbf{y}}_{\varphi+\xi}) - (\mathbf{y} - \bar{\mathbf{y}}_\varphi)^H \mathbf{R}_{yy}^{-1} (\mathbf{y} - \bar{\mathbf{y}}_\varphi), \quad (3-9)$$

where $\bar{\mathbf{y}}_\varphi \triangleq \bar{\mathbf{y}}_{\tau=\varphi} = \alpha \boldsymbol{\Phi} \boldsymbol{\psi}(\varphi)$, and thus \mathcal{L}_τ is a function of unknown time delay τ via \mathbf{y} . To calculate $\Pr(\mathcal{L}_\varphi \leq \gamma)$ and $\Pr(\mathcal{L}_{\varphi+\xi} > \gamma)$ in (2-7), it is necessary to find the distributions of \mathcal{L}_φ



and $\mathcal{L}_{\varphi+\xi}$. Given $\tau = \varphi$, we have

$$\begin{aligned}\mathcal{L}_{\varphi} &= (\mathbf{y}_{\varphi} - \bar{\mathbf{y}}_{\varphi+\xi})^{\text{H}} \mathbf{R}_{yy}^{-1} (\mathbf{y}_{\varphi} - \bar{\mathbf{y}}_{\varphi+\xi}) - (\mathbf{y}_{\varphi} - \bar{\mathbf{y}}_{\varphi})^{\text{H}} \mathbf{R}_{yy}^{-1} (\mathbf{y}_{\varphi} - \bar{\mathbf{y}}_{\varphi}) \\ &= (\bar{\mathbf{y}}_{\varphi} - \bar{\mathbf{y}}_{\varphi+\xi})^{\text{H}} \mathbf{R}_{yy}^{-1} (\bar{\mathbf{y}}_{\varphi} - \bar{\mathbf{y}}_{\varphi+\xi}) + 2\Re \left[(\bar{\mathbf{y}}_{\varphi} - \bar{\mathbf{y}}_{\varphi+\xi})^{\text{H}} \mathbf{R}_{yy}^{-1} \Phi \mathbf{n} \right],\end{aligned}\quad (3-10)$$

where $\mathbf{y}_{\varphi} \triangleq \mathbf{y}|_{\tau=\varphi} = \Phi [\alpha\psi(\varphi) + \mathbf{n}]$. Obviously, since the only random variable in \mathcal{L}_{φ} is the Gaussian noise \mathbf{n} , \mathcal{L}_{φ} follows a Gaussian distributions $\mathcal{N}(\mu_{\mathcal{L}_{\varphi}}, \sigma_{\mathcal{L}_{\varphi}}^2)$ with

$$\begin{aligned}\mu_{\mathcal{L}_{\varphi}} &= (\bar{\mathbf{y}}_{\varphi} - \bar{\mathbf{y}}_{\varphi+\xi})^{\text{H}} \mathbf{R}_{yy}^{-1} (\bar{\mathbf{y}}_{\varphi} - \bar{\mathbf{y}}_{\varphi+\xi}) \\ &= |\alpha|^2 [\psi(\varphi) - \psi(\varphi + \xi)]^{\text{H}} \Phi^{\text{H}} \mathbf{R}_{yy}^{-1} \Phi [\psi(\varphi) - \psi(\varphi + \xi)],\end{aligned}\quad (3-11)$$

and

$$\sigma_{\mathcal{L}_{\varphi}}^2 = 4\mathbb{V} \left\{ \Re \left[(\bar{\mathbf{y}}_{\varphi} - \bar{\mathbf{y}}_{\varphi+\xi})^{\text{H}} \mathbf{R}_{yy}^{-1} \Phi \mathbf{n} \right] \right\}.\quad (3-12)$$

Since $\mathbf{n} \sim \mathcal{CN}(\mathbf{0}, \mathbf{R}_{nn})$, we have

$$\mathbb{V} \left\{ \Re \left[(\bar{\mathbf{y}}_{\varphi} - \bar{\mathbf{y}}_{\varphi+\xi})^{\text{H}} \mathbf{R}_{yy}^{-1} \Phi \mathbf{n} \right] \right\} = \frac{\mu_{\mathcal{L}_{\varphi}}}{2}\quad (3-13)$$

due to

$$\mathbb{V} \left\{ (\bar{\mathbf{y}}_{\varphi} - \bar{\mathbf{y}}_{\varphi+\xi})^{\text{H}} \mathbf{R}_{yy}^{-1} \Phi \mathbf{n} \right\} = (\bar{\mathbf{y}}_{\varphi} - \bar{\mathbf{y}}_{\varphi+\xi})^{\text{H}} \mathbf{R}_{yy}^{-1} (\bar{\mathbf{y}}_{\varphi} - \bar{\mathbf{y}}_{\varphi+\xi}).\quad (3-14)$$

Thus, the distribution of \mathcal{L}_{φ} can be determined as $\mathcal{N}(\mu_{\mathcal{L}_{\varphi}}, 2\mu_{\mathcal{L}_{\varphi}})$. Similarly, given $\tau = \varphi + \xi$, then

$$\mathcal{L}_{\varphi+\xi} = -(\bar{\mathbf{y}}_{\varphi} - \bar{\mathbf{y}}_{\varphi+\xi})^{\text{H}} \mathbf{R}_{yy}^{-1} (\bar{\mathbf{y}}_{\varphi} - \bar{\mathbf{y}}_{\varphi+\xi}) + 2\Re \left[(\bar{\mathbf{y}}_{\varphi} - \bar{\mathbf{y}}_{\varphi+\xi})^{\text{H}} \mathbf{R}_{yy}^{-1} \Phi \mathbf{n} \right]\quad (3-15)$$

follows $\mathcal{N}(-\mu_{\mathcal{L}_{\varphi}}, 2\mu_{\mathcal{L}_{\varphi}})$. Hence, $\text{P}_{\min}(\varphi, \varphi + \xi)$ becomes

$$\text{P}_{\min}(\varphi, \varphi + \xi) = \Pr(\mathcal{H}_0) \mathcal{Q} \left(\frac{\mu_{\mathcal{L}_{\varphi}} - \gamma}{\sqrt{2\mu_{\mathcal{L}_{\varphi}}}} \right) + \Pr(\mathcal{H}_1) \mathcal{Q} \left(\frac{\mu_{\mathcal{L}_{\varphi}} + \gamma}{\sqrt{2\mu_{\mathcal{L}_{\varphi}}}} \right).\quad (3-16)$$



Thus, the MSE for compressive time delay estimation with deterministic signals can be correspondingly lower bounded by deterministic ZZB as

$$\bar{\epsilon}_\tau^2 \geq \frac{1}{2} \int_0^T \xi \int_0^{T-\xi} [f_\tau(\varphi) + f_\tau(\varphi + \xi)] \left[\Pr(\mathcal{H}_0) \mathcal{Q} \left(\frac{\mu_{\mathcal{L}_\varphi} - \gamma}{\sqrt{2\mu_{\mathcal{L}_\varphi}}} \right) + \Pr(\mathcal{H}_1) \mathcal{Q} \left(\frac{\mu_{\mathcal{L}_\varphi} + \gamma}{\sqrt{2\mu_{\mathcal{L}_\varphi}}} \right) \right] d\varphi d\xi \quad (3-17)$$

due to both φ and $\varphi + \xi$ located in $[0, T]$. It is observed that the derived ZZB is formulated as an explicit function of the CS kernel Φ via $\mu_{\mathcal{L}_\varphi}$. Moreover, since there is no restriction on CS kernels, the derived deterministic ZZB can be applicable for arbitrary CS kernels rather than random ones only [63]. Specifically, if τ follows a uniform distribution in $[0, T]$, i.e., $f_\tau(\varphi) = f_\tau(\varphi + \xi) = \frac{1}{T}$, (3-16) becomes

$$P_{\min}(\varphi, \varphi + \xi) = \mathcal{Q} \left(\sqrt{\frac{\mu_{\mathcal{L}_\varphi}}{2}} \right), \quad (3-18)$$

and (3-17) degrades to

$$\bar{\epsilon}_\tau^2 \geq \frac{1}{T} \int_0^T \xi \int_0^{T-\xi} \mathcal{Q} \left(\sqrt{\frac{\mu_{\mathcal{L}_\varphi}}{2}} \right) d\varphi d\xi. \quad (3-19)$$

With the assumption of white noise (say, $\mathbf{C}_{nn} = \sigma_n^2 \mathbf{I}_L$ with noise power σ_n^2) and row orthonormalization of the sensing kernel ($\Phi\Phi^H = \mathbf{I}_M$), (3-19) can be further simplified as

$$\bar{\epsilon}_\tau^2 \geq \frac{1}{T} \int_0^T \xi \int_0^{T-\xi} \mathcal{Q} \left(\sqrt{\frac{|\alpha|^2}{\sigma_n^2} \frac{1}{2} \|\Phi[\psi(\varphi) - \psi(\varphi + \xi)]\|_2^2} \right) d\varphi d\xi, \quad (3-20)$$

where $\frac{|\alpha|^2}{\sigma_n^2}$ denotes the input SNR of the target signal.

In practical applications, when the signal amplitude α is not *a priori* known, it can be assumed as a deterministic nuisance parameter that must be estimated. In such case, the log-GLRT [1]

$$\ell_\tau = \ln \frac{f(\mathbf{y}|\varphi, \hat{\alpha}_\varphi)}{f(\mathbf{y}|\varphi + \xi, \hat{\alpha}_{\varphi+\xi})} \quad (3-21)$$



is an effective approximation of the log-LRT \mathcal{L}_τ for the ZZB derivation, where

$$\hat{\alpha}_\tau = \frac{\Re[\boldsymbol{\psi}^H(\tau)\boldsymbol{\Phi}^H\mathbf{R}_{yy}^{-1}\mathbf{y}]}{\boldsymbol{\psi}^H(\tau)\boldsymbol{\Phi}^H\mathbf{R}_{yy}^{-1}\boldsymbol{\Phi}\boldsymbol{\psi}(\tau)}, \tau = \varphi, \varphi + \xi \quad (3-22)$$

is the MLE of the nuisance parameter α given $\tau = \varphi$ or $\tau = \varphi + \xi$. By performing a derivation similar to (3-9) to (3-15), we have $\ell_\varphi \sim \mathcal{N}(\mu_{\ell_\varphi}, 2\mu_{\ell_\varphi})$ and $\ell_{\varphi+\xi} \sim \mathcal{N}(-\mu_{\ell_\varphi}, 2\mu_{\ell_\varphi})$, respectively, where

$$\mu_{\ell_\varphi} = [\hat{\alpha}_\varphi\boldsymbol{\psi}(\varphi) - \hat{\alpha}_{\varphi+\xi}\boldsymbol{\psi}(\varphi + \xi)]^H \boldsymbol{\Phi}^H \mathbf{R}_{yy}^{-1} \boldsymbol{\Phi} [\hat{\alpha}_\varphi\boldsymbol{\psi}(\varphi) - \hat{\alpha}_{\varphi+\xi}\boldsymbol{\psi}(\varphi + \xi)]. \quad (3-23)$$

Thus, by replacing $\mu_{\mathcal{L}_\varphi}$ in (3-17) with μ_{ℓ_φ} , the deterministic ZZB with deterministic nuisance amplitude α is obtained.

Unlike $\mu_{\mathcal{L}_\varphi}$ in (3-11), the MLEs of α under different hypothesis (say, $\tau = \varphi$ and $\tau = \varphi + \xi$) are involved in the final expression of deterministic ZZB with μ_{ℓ_φ} in (3-23). Hence, the estimation error of α also affects the ZZB performance. Specifically, in high SNR situation the nuisance parameter α can be accurately estimated due to the asymptotic optimality of log-GLRT, such that the ZZB with nuisance parameter α is still tight in high SNR situation [62]. On the contrary, in the low SNR situation, the optimality of log-GLRT can not be guaranteed [1], such that the ZZB may suffer from the large estimation error of α and not keep tight.

3.3.2 Minimum Probability of Error for Stochastic Model

According to (3-5), the log-LRT can be calculated as

$$\mathcal{L}_\tau = c + (\mathbf{y} - \bar{\mathbf{y}}_{\varphi+\xi})^H \mathbf{R}_{yy|\varphi+\xi}^{-1} (\mathbf{y} - \bar{\mathbf{y}}_{\varphi+\xi}) - (\mathbf{y} - \bar{\mathbf{y}}_\varphi)^H \mathbf{R}_{yy|\varphi}^{-1} (\mathbf{y} - \bar{\mathbf{y}}_\varphi), \quad (3-24)$$

where $c = \ln \frac{|\mathbf{R}_{yy|\varphi+\xi}|}{|\mathbf{R}_{yy|\varphi}|}$ is a constant given φ and $\varphi + \xi$, $\bar{\mathbf{y}}_\varphi = \mu_\alpha \boldsymbol{\Phi} \boldsymbol{\psi}(\varphi)$ here due to $\alpha \sim \mathcal{CN}(\mu_\alpha, \sigma_\alpha^2)$. To obtain the distribution of \mathcal{L}_τ , we rearrange (3-24) as

$$\mathcal{L}_\tau = c + \tilde{\mathbf{y}}^H \mathbf{X} \tilde{\mathbf{y}}, \quad (3-25)$$



where

$$\tilde{\mathbf{y}} = \begin{bmatrix} \mathbf{y} - \bar{\mathbf{y}}_{\varphi+\xi} \\ \mathbf{y} - \bar{\mathbf{y}}_{\varphi} \end{bmatrix} \quad (3-26)$$

and

$$\mathbf{X} = \begin{bmatrix} \mathbf{R}_{\mathbf{y}\mathbf{y}|\varphi+\xi}^{-1} & \mathbf{0}_{M \times M} \\ \mathbf{0}_{M \times M} & -\mathbf{R}_{\mathbf{y}\mathbf{y}|\varphi}^{-1} \end{bmatrix}. \quad (3-27)$$

Obviously, $\tilde{\mathbf{y}}$ follows a complex Gaussian distribution $\mathcal{CN}(\boldsymbol{\mu}_{\tilde{\mathbf{y}}}, \mathbf{R}_{\tilde{\mathbf{y}}\tilde{\mathbf{y}}|\tau})$ with

$$\boldsymbol{\mu}_{\tilde{\mathbf{y}}} = \begin{bmatrix} \bar{\mathbf{y}}_{\tau} - \bar{\mathbf{y}}_{\varphi+\xi} \\ \bar{\mathbf{y}}_{\tau} - \bar{\mathbf{y}}_{\varphi} \end{bmatrix} \quad (3-28)$$

and

$$\mathbf{R}_{\tilde{\mathbf{y}}\tilde{\mathbf{y}}|\tau} = \begin{bmatrix} \mathbf{R}_{\mathbf{y}\mathbf{y}|\tau} & \mathbf{R}_{\mathbf{y}\mathbf{y}|\tau} \\ \mathbf{R}_{\mathbf{y}\mathbf{y}|\tau} & \mathbf{R}_{\mathbf{y}\mathbf{y}|\tau} \end{bmatrix}, \quad (3-29)$$

where $\boldsymbol{\mu}_{\tilde{\mathbf{y}}}$ is a function of τ via $\bar{\mathbf{y}}_{\tau} = \mu_{\alpha} \boldsymbol{\Phi} \boldsymbol{\psi}(\tau)$.

Since \mathcal{L}_{τ} is a quadratic form of general complex Gaussian vector, it is difficult to intuitively formulate \mathcal{L}_{τ} as a commonly used distribution. To evaluate the distribution \mathcal{L}_{τ} , we consider the MGF

$$\Theta_{\mathcal{L}_{\tau}}(s) = \mathbb{E} \{ e^{s\mathcal{L}_{\tau}} \} = \mathbb{E} \left\{ e^{s(c + \tilde{\mathbf{y}}^{\text{H}} \mathbf{X} \tilde{\mathbf{y}})} \right\}, \quad (3-30)$$

where the expectation is taken over the Gaussian random variable $\tilde{\mathbf{y}}$. Since $\mathbf{R}_{\tilde{\mathbf{y}}\tilde{\mathbf{y}}|\tau}$ is a positive semidefinite Hermitian matrix with rank M , it can be decomposed as

$$\mathbf{R}_{\tilde{\mathbf{y}}\tilde{\mathbf{y}}|\tau} = \mathbf{D}_{\tau} \mathbf{D}_{\tau}^{\text{H}}, \quad (3-31)$$

where $\mathbf{D}_{\tau} \in \mathbb{C}^{2M \times M}$. Now, we consider a linear transformation

$$\tilde{\mathbf{y}} = \boldsymbol{\mu}_{\tilde{\mathbf{y}}} + \mathbf{D}_{\tau} \mathbf{z} \quad (3-32)$$



with $z \in \mathbb{C}^M$ and $z \sim \mathcal{CN}(\mathbf{0}_M, \mathbf{I}_M)$. By substituting (3-32) into (3-30), we have

$$\begin{aligned}
 \Theta_{\mathcal{L}_\tau}(s) &= \mathbb{E} \left\{ e^{s[c+(\boldsymbol{\mu}_{\tilde{y}}+D_\tau z)^H \mathbf{X}(\boldsymbol{\mu}_{\tilde{y}}+D_\tau z)]} \right\} \\
 &= \int_{\mathbf{p}} e^{s[c+(\boldsymbol{\mu}_{\tilde{y}}+D_\tau \mathbf{p})^H \mathbf{X}(\boldsymbol{\mu}_{\tilde{y}}+D_\tau \mathbf{p})]} f_z(\mathbf{p}) d\mathbf{p} \\
 &= e^{sc+s\boldsymbol{\mu}_{\tilde{y}}^H \mathbf{X} \boldsymbol{\mu}_{\tilde{y}}} \int_{\mathbf{p}} \frac{1}{\pi^M} e^{-(\mathbf{p}^H \mathbf{K}_\tau \mathbf{p} - \mathbf{p}^H \mathbf{g}_\tau - \mathbf{g}_\tau^H \mathbf{p})} d\mathbf{p},
 \end{aligned} \tag{3-33}$$

where $\mathbf{K}_\tau = \mathbf{I}_M - sD_\tau^H \mathbf{X} D_\tau$, $\mathbf{g}_\tau = sD_\tau^H \mathbf{X} \boldsymbol{\mu}_{\tilde{y}}$, and $f_z(\mathbf{p}) \triangleq f(z)|_{z=\mathbf{p}}$ with $f(z)$ being the PDF of z

$$f(z) = \frac{1}{\pi^M} e^{-z^H z}. \tag{3-34}$$

Assuming s located in a small neighbourhood of zero, i.e., $|s| \rightarrow 0$, \mathbf{K}_τ is still a nonsingular matrix so that \mathbf{K}_τ^{-1} exists. Then, the MGF in (3-33) becomes

$$\begin{aligned}
 \Theta_{\mathcal{L}_\tau}(s) &= e^{s(c+\boldsymbol{\mu}_{\tilde{y}}^H \mathbf{X} \boldsymbol{\mu}_{\tilde{y}})+\mathbf{g}_\tau^H \mathbf{K}_\tau^{-1} \mathbf{g}_\tau} \int_{\mathbf{p}} \frac{1}{\pi^M} e^{-(\mathbf{p}-\mathbf{K}_\tau^{-1} \mathbf{g}_\tau)^H \mathbf{K}_\tau (\mathbf{p}-\mathbf{K}_\tau^{-1} \mathbf{g}_\tau)} d\mathbf{p} \\
 &= |\mathbf{K}_\tau|^{-1} e^{s(c+\boldsymbol{\mu}_{\tilde{y}}^H \mathbf{X} \boldsymbol{\mu}_{\tilde{y}})+\mathbf{g}_\tau^H \mathbf{K}_\tau^{-1} \mathbf{g}_\tau},
 \end{aligned} \tag{3-35}$$

which indicates that \mathcal{L}_τ follows a generalized chi-square distribution without a simple closed-form PDF. Hence, to make it solvable, we consider a reasonable approximation $\mathbf{K}_\tau = \mathbf{I}_M - sD_\tau^H \mathbf{X} D_\tau \approx \mathbf{I}_M$ and $|\mathbf{K}_\tau|^{-1} \approx 1$ in the case of small $|s|$. Thus, we make an approximation for (3-35) as

$$\begin{aligned}
 \Theta_{\mathcal{L}_\tau}(s) &\approx e^{s(c+\boldsymbol{\mu}_{\tilde{y}}^H \mathbf{X} \boldsymbol{\mu}_{\tilde{y}})+\mathbf{g}_\tau^H \mathbf{g}_\tau} \\
 &= e^{s(c+\boldsymbol{\mu}_{\tilde{y}}^H \mathbf{X} \boldsymbol{\mu}_{\tilde{y}})+\frac{s^2}{2}(2\boldsymbol{\mu}_{\tilde{y}}^H \mathbf{X}^H \mathbf{R}_{\tilde{y}|\tau} \mathbf{X} \boldsymbol{\mu}_{\tilde{y}})},
 \end{aligned} \tag{3-36}$$

which corresponds to a Gaussian distribution $\mathcal{L}_\tau \sim \mathcal{N}(\mu_{\mathcal{L}_\tau}, \sigma_{\mathcal{L}_\tau}^2)$ with

$$\mu_{\mathcal{L}_\tau} = c + \boldsymbol{\mu}_{\tilde{y}}^H \mathbf{X} \boldsymbol{\mu}_{\tilde{y}} \tag{3-37}$$

and

$$\sigma_{\mathcal{L}_\tau}^2 = 2\boldsymbol{\mu}_{\tilde{y}}^H \mathbf{X}^H \mathbf{R}_{\tilde{y}|\tau} \mathbf{X} \boldsymbol{\mu}_{\tilde{y}}. \tag{3-38}$$



Given $\tau = \varphi$, we have $\mathcal{L}_\varphi \sim \mathcal{N}(\mu_{\mathcal{L}_\varphi}, \sigma_{\mathcal{L}_\varphi}^2)$ with

$$\mu_{\mathcal{L}_\varphi} = c + (\bar{\mathbf{y}}_\varphi - \bar{\mathbf{y}}_{\varphi+\xi})^H \mathbf{R}_{\mathbf{y}\mathbf{y}|\varphi+\xi}^{-1} (\bar{\mathbf{y}}_\varphi - \bar{\mathbf{y}}_{\varphi+\xi}) \quad (3-39)$$

and

$$\sigma_{\mathcal{L}_\varphi}^2 = 2 (\bar{\mathbf{y}}_\varphi - \bar{\mathbf{y}}_{\varphi+\xi})^H \mathbf{R}_{\mathbf{y}\mathbf{y}|\varphi+\xi}^{-1} \mathbf{R}_{\mathbf{y}\mathbf{y}|\varphi} \mathbf{R}_{\mathbf{y}\mathbf{y}|\varphi+\xi}^{-1} (\bar{\mathbf{y}}_\varphi - \bar{\mathbf{y}}_{\varphi+\xi}). \quad (3-40)$$

Similarly, given $\tau = \varphi + \xi$, we have $\mathcal{L}_{\varphi+\xi} \sim \mathcal{N}(\mu_{\mathcal{L}_{\varphi+\xi}}, \sigma_{\mathcal{L}_{\varphi+\xi}}^2)$ with

$$\mu_{\mathcal{L}_{\varphi+\xi}} = c - (\bar{\mathbf{y}}_\varphi - \bar{\mathbf{y}}_{\varphi+\xi})^H \mathbf{R}_{\mathbf{y}\mathbf{y}|\varphi}^{-1} (\bar{\mathbf{y}}_\varphi - \bar{\mathbf{y}}_{\varphi+\xi}) \quad (3-41)$$

and

$$\sigma_{\mathcal{L}_{\varphi+\xi}}^2 = 2 (\bar{\mathbf{y}}_\varphi - \bar{\mathbf{y}}_{\varphi+\xi})^H \mathbf{R}_{\mathbf{y}\mathbf{y}|\varphi}^{-1} \mathbf{R}_{\mathbf{y}\mathbf{y}|\varphi+\xi} \mathbf{R}_{\mathbf{y}\mathbf{y}|\varphi}^{-1} (\bar{\mathbf{y}}_\varphi - \bar{\mathbf{y}}_{\varphi+\xi}). \quad (3-42)$$

Then, $P_{\min}(\varphi, \varphi + \xi)$ in (2-7) can be explicitly expressed as

$$P_{\min}(\varphi, \varphi + \xi) = \Pr(\mathcal{H}_0) \mathcal{Q} \left(\frac{\mu_{\mathcal{L}_\varphi} - \gamma}{\sigma_{\mathcal{L}_\varphi}} \right) + \Pr(\mathcal{H}_1) \mathcal{Q} \left(\frac{\gamma - \mu_{\mathcal{L}_{\varphi+\xi}}}{\sigma_{\mathcal{L}_{\varphi+\xi}}} \right). \quad (3-43)$$

Correspondingly, stochastic ZZB for compressive time delay estimation can be derived as

$$\bar{\epsilon}_\tau^2 \geq \frac{1}{2} \int_0^T \xi \int_0^{T-\xi} [f_\tau(\varphi) + f_\tau(\varphi + \xi)] \left[\Pr(\mathcal{H}_0) \mathcal{Q} \left(\frac{\mu_{\mathcal{L}_\varphi} - \gamma}{\sigma_{\mathcal{L}_\varphi}} \right) + \Pr(\mathcal{H}_1) \mathcal{Q} \left(\frac{\gamma - \mu_{\mathcal{L}_{\varphi+\xi}}}{\sigma_{\mathcal{L}_{\varphi+\xi}}} \right) \right] d\varphi d\xi, \quad (3-44)$$

in which the ZZB is a function of CS kernel Φ via $\mu_{\mathcal{L}_\varphi}$, $\mu_{\mathcal{L}_{\varphi+\xi}}$, $\sigma_{\mathcal{L}_\varphi}^2$ and $\sigma_{\mathcal{L}_{\varphi+\xi}}^2$. Specifically, when τ follows a uniform distribution in $[0, T]$, (3-43) becomes

$$P_{\min}(\varphi, \varphi + \xi) = \frac{1}{2} \left[\mathcal{Q} \left(\frac{\mu_{\mathcal{L}_\varphi}}{\sigma_{\mathcal{L}_\varphi}} \right) + \mathcal{Q} \left(\frac{-\mu_{\mathcal{L}_{\varphi+\xi}}}{\sigma_{\mathcal{L}_{\varphi+\xi}}} \right) \right], \quad (3-45)$$

and accordingly the ZZB in (3-44) is simplified as

$$\bar{\epsilon}_\tau^2 \geq \frac{1}{2T} \int_0^T \xi \int_0^{T-\xi} \left[\mathcal{Q} \left(\frac{\mu_{\mathcal{L}_\varphi}}{\sigma_{\mathcal{L}_\varphi}} \right) + \mathcal{Q} \left(\frac{-\mu_{\mathcal{L}_{\varphi+\xi}}}{\sigma_{\mathcal{L}_{\varphi+\xi}}} \right) \right] d\varphi d\xi. \quad (3-46)$$

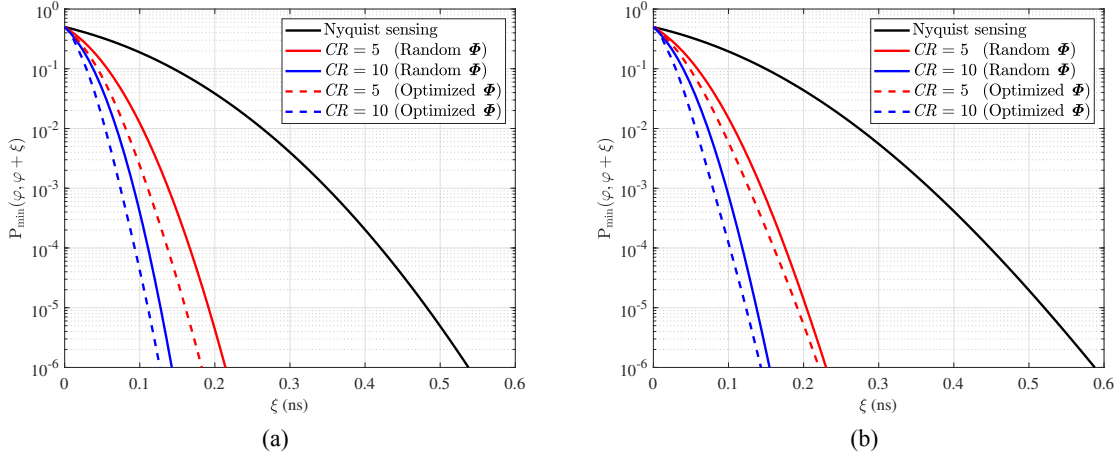


Figure 3.2 The influence of different compressive sensing kernels on the minimum probability of error. (a) Deterministic model; (b) Stochastic model.

It is worth noting that, when $\sigma_\alpha^2 = 0$, we have $\mu_{\mathcal{L}_{\varphi+\xi}} = -\mu_{\mathcal{L}_\varphi}$ and $\sigma_{\mathcal{L}_\varphi}^2 = \sigma_{\mathcal{L}_{\varphi+\xi}}^2 = 2\mu_{\mathcal{L}_\varphi}$ since $c = 0$ and $\mathbf{R}_{yy|\varphi} = \mathbf{R}_{yy|\varphi+\xi} = \mathbf{R}_{yy}$, and thus the stochastic ZZB in (3-44) degrades to the deterministic ZZB in (3-17).

In summary, the derived ZZB either for deterministic model or for stochastic model is a function of compressive sensing kernels Φ through the minimum probability of error $P_{\min}(\varphi, \varphi + \xi)$. Hence, we investigate the influence of different CRs and compression strategies on the minimum probability of error in Fig. 3.2. It is assumed that the SNR is fixed to 40 dB, and the time delay τ follows a uniform *a priori* distribution in $[0, 0.8]\mu s$. In addition, it is assumed that $\frac{\mu_\alpha}{\sigma_\alpha^2} = 20$ for the stochastic model. We fix the sampling rate of 100 MHz at the receiver, while scale up the transmitted waveform bandwidth CR times at the transmitter. It is observed that, $P_{\min}(\varphi, \varphi + \xi)$ converges to 0.5 regardless of compression or not for both deterministic and stochastic models when ξ tends to zero, indicating that the binary hypothesis testing problem (2-4) makes a decision randomly between \mathcal{H}_0 and \mathcal{H}_1 with equal probability. With ξ increasing, $P_{\min}(\varphi, \varphi + \xi)$ decreases in all scenarios, and the more compression, the lower the minimum probability of error. The root reason is that, compared with Nyquist sensing, compressive sensing enables more transmit bandwidth, such that it has better naive resolution. Consequently, it leads to the lower minimum probability of error, which will be subsequently reflected in ZZBs. Moreover, the information-theoretic CS kernel [101] makes the minimum probability of error



decrease sharper than the random Gaussian kernel, indicating that the optimized CS kernel enables a lower minimum probability of error for the ZZBs. It is also observed that deterministic $P_{\min}(\varphi, \varphi + \xi)$ decreases sharper than the stochastic $P_{\min}(\varphi, \varphi + \xi)$ regardless of compression or not, which indicates that the less the stochastic, the lower the minimum probability of error. Furthermore, compared with random compressive sensing, information-theoretic compressive sensing can decrease the minimum probability of error more in the deterministic scenario than in the stochastic scenario. It is worth noting that, the derived minimum probability of error and the corresponding ZZBs are for the first time appropriate for optimized CS kernels, which generalizes the ZZB derivation from random compressive sensing only (see, [63]) to both random and optimized compressive sensing.

3.4 Simulation

In this section, we evaluate the derived ZZBs for the compressive time delay estimation. We also study the effect of CRs, the *a priori* distributions, and the Gaussian noise colors on the ZZBs especially on the asymptotic region threshold. In our simulations, we keep the A/D converter operating at a fixed sampling rate of $B = 100$ MHz, while scale up the radar waveform bandwidth to $\text{CR} \times B$ at the radar transmitter. As such, we can achieve CR times compression at the radar receiver. For example, when the CRs are five and ten, the transmitted waveform bandwidth are respectively $5 \times 100 \text{ MHz} = 500 \text{ MHz}$ and $10 \times 100 \text{ MHz} = 1 \text{ GHz}$. Without loss of generality, we adopt the widely used LFM signal as the radar waveform. It is noted that other radar waveforms are also applicable since the derived ZZBs do not require the *a priori* knowledge of the radar waveform. According to the signal model, the input SNR in the simulations is defined as $\text{SNR} = \frac{|\alpha|^2}{\sigma_n^2}$ for deterministic signals and $\text{SNR} = \frac{\sigma_\alpha^2 + |\mu_\alpha|^2}{\sigma_n^2}$ for stochastic signals. The time delay is assumed between $0 \mu\text{s}$ and $0.8 \mu\text{s}$, which corresponds to the range of a target from the radar being between 0 meters and 120 meters.

We choose the RMSE of the time delay estimation as the performance metric for the derived ZZBs. Meanwhile, both BCRBs and MMSE estimator are also presented for a comparison. For

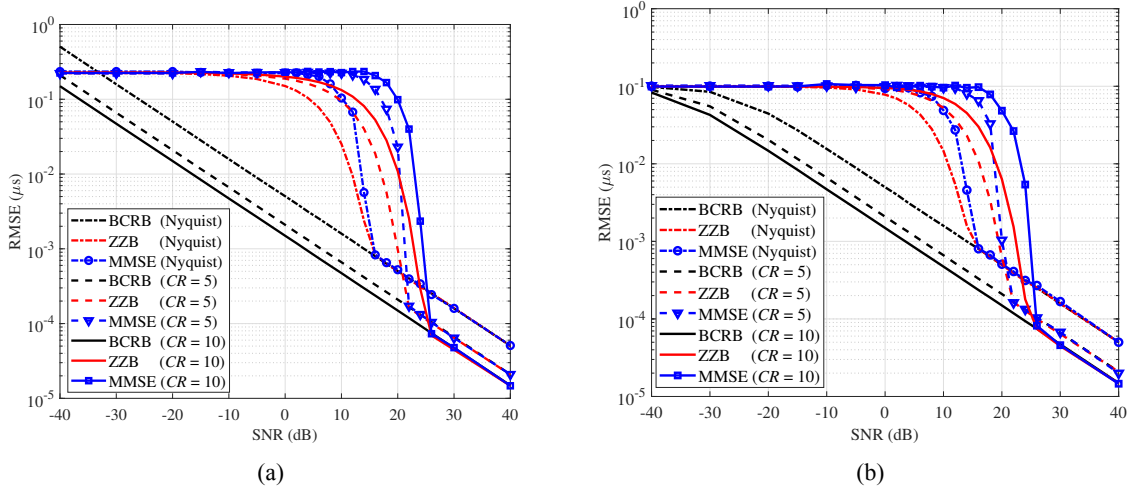


Figure 3.3 RMSE comparison of deterministic ZZB, BCRB, and MMSE estimator with random Gaussian CS kernel. (a) $\tau \sim \mathcal{U}[0, \frac{80}{B}]$; (b) $\tau \sim \mathcal{N}(\frac{40}{B}, (\frac{10}{B})^2)$.

the MMSE estimate of the time delay

$$\hat{\tau} = \mathbb{E}_{\tau|\mathbf{y}}\{\tau\} = \int \tau f(\tau|\mathbf{y})d\tau = \int \frac{\tau f(\mathbf{y}|\tau)f(\tau)}{f(\mathbf{y})}d\tau \quad (3-47)$$

with $f(\mathbf{y}) = \int f(\mathbf{y}|\tau)f(\tau)d\tau$, we run $K = 1,000$ Monte-Carlo trials for each SNR to obtain the RMSE. Here, the RMSE is defined as

$$\text{RMSE} = \sqrt{\frac{1}{K} \sum_{k=1}^K (\hat{\tau}_k - \tau_k)^2}, \quad (3-48)$$

where $\hat{\tau}_k$ is the MMSE estimate of the true time delay τ_k in the k -th Monte-Carlo trial.

3.4.1 Deterministic Model

For deterministic signals, we consider two typical distributions of time delay, i.e., a uniform distribution $\tau \sim \mathcal{U}[0, \frac{80}{B}]$ and a normal distribution $\tau \sim \mathcal{N}(\frac{40}{B}, (\frac{10}{B})^2)$. In Fig. 3.3, we compare the deterministic ZZB with the deterministic BCRB and the MMSE estimator, where the random Gaussian CS kernels are applied. It is observed that the ZZB effectively lower bounds the MSE in all regions regardless of compression or not, namely, the ZZB converges to the BCRB in the asymptotic region and converges to the *a priori* variance of τ in the low SNR situation.



Table 3.1 Threshold points of ZZBs with different CRs.

CR	2	3	4	5	6	7	8	9	10
Threshold (dB)	17.5	19	20.5	22	22.5	23	24	25	26

On the contrary, the BCRB cannot provide a tight bound outside the asymptotic region. The reason is that, different from utilizing limited Fisher information in the low SNR situation, the ZZB lower bounds the MSE by minimizing the probability of error via MAP detector, which makes a decision between \mathcal{H}_0 and \mathcal{H}_1 by the *a priori* distribution $f(\tau)$. Moreover, the ZZB with $\tau \sim \mathcal{N}\left(\frac{40}{B}, \left(\frac{10}{B}\right)^2\right)$ is lower than that with $\tau \sim \mathcal{U}[0, \frac{80}{B}]$ in the low SNR situation, which is because the normal distribution provides more *a priori* information than the uniform distribution and has a lower *a priori* variance.

From Fig. 3.3 it is also observed that, there is an intersection point between ZZBs with different CRs, which is located between the two threshold points. On the one hand, the ZZB converges to the *a priori* variance of τ in the low SNR situation regardless of the CRs, but with SNR increasing, higher CR makes the ZZB achieve the asymptotic region at a higher SNR to make up the SNR loss during the compression. For example, in Fig. 3.3a the asymptotic regions of the ZZBs with Nyquist sampling (i.e., CR = 1), compressive sampling with CR = 5 and CR = 10 start from around 14 dB, 22 dB, and 26 dB, respectively. On the other hand, higher CR enables lower ZZB in the asymptotic region. Thus, there must be an intersection point between two ZZBs with different CRs, which motivates us to prefer higher CR for SNR above the intersection point to obtain a lower ZZB. On the contrast, we have to choose lower CR to have lower ZZB when the SNR is below the intersection point.

To find the relationship between the intersection point and the corresponding thresholds, we plot all the intersection points among ZZBs from CR = 2 to CR = 10 in Fig. 3.4. Meanwhile, according to the thresholds under different CRs listed in Table 3.1, we also plot all linear interpolation points between different pair of thresholds in Fig. 3.4. For example, the linear interpolation of thresholds between ZZBs with CR = 4 and CR = 7 is $20.5 \times \frac{4}{4+7} + 23 \times \frac{7}{4+7} \approx 22.1$ dB. It is observed that, the linear interpolation can be used to approximately predict the intersection point of the ZZBs with different CRs. Thus, once we obtain two threshold points of

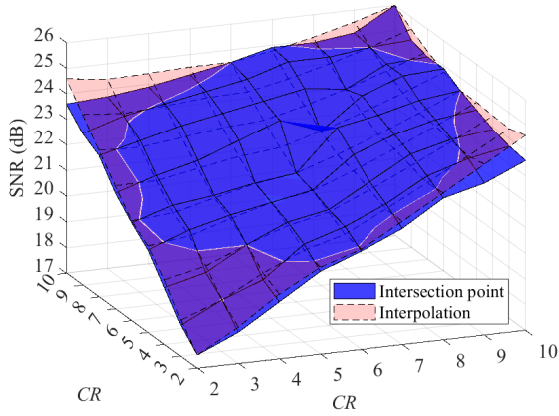


Figure 3.4 Intersection points of ZZBs with different CRs.

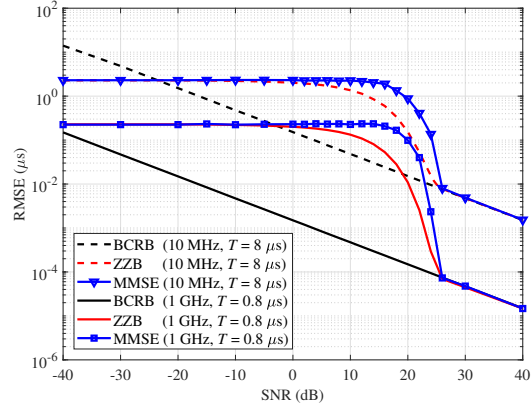


Figure 3.5 Influence of time-bandwidth product on the derived ZZB.

the ZZBs under different CRs, we can approximately predict the intersection point of these two ZZBs according to such linear interpolation, which may help us to choose proper CRs in different SNRs.

Then, we investigate the influence of time-bandwidth product on the derived ZZB. We compare the 1 GHz bandwidth waveform as in Fig. 3.3 with a 10 MHz bandwidth waveform whose time delay follows a uniform distribution in $[0, 8]\mu\text{s}$. Thus, the time-bandwidth product of 1 GHz bandwidth waveform is 10 times greater than that of 10 MHz bandwidth waveform, where both CRs are fixed to $\text{CR} = 10$. The comparison of ZZB, BCRB and MMSE estimator under different time-bandwidth products are plotted in Fig. 3.5. Obviously, in the low SNR situation, the derived ZZB effectively lower bounds the MSE of the MMSE estimator to the *a priori* variance of τ , which does not depend on the actual bandwidth (say, 10 MHz or 1 GHz). On the other hand, in the asymptotic region, the ZZB converges to the BCRB in each scenario. More specifically, the ZZB for 10 MHz waveform bandwidth is 100 times greater than that for 1 GHz waveform bandwidth, indicating that the ZZB in the asymptotic region is inversely proportional to the bandwidth. Moreover, it is worth noting that, the threshold points of two scenarios occur at the same SNR (say, 26 dB), which means that changing time-bandwidth product will not change the threshold point of the derived ZZB for a given CR. Hence, the derived ZZB for different time-bandwidth products can be predicted according to the *a priori* variance of τ in the low SNR situation and the waveform bandwidth in the asymptotic region.

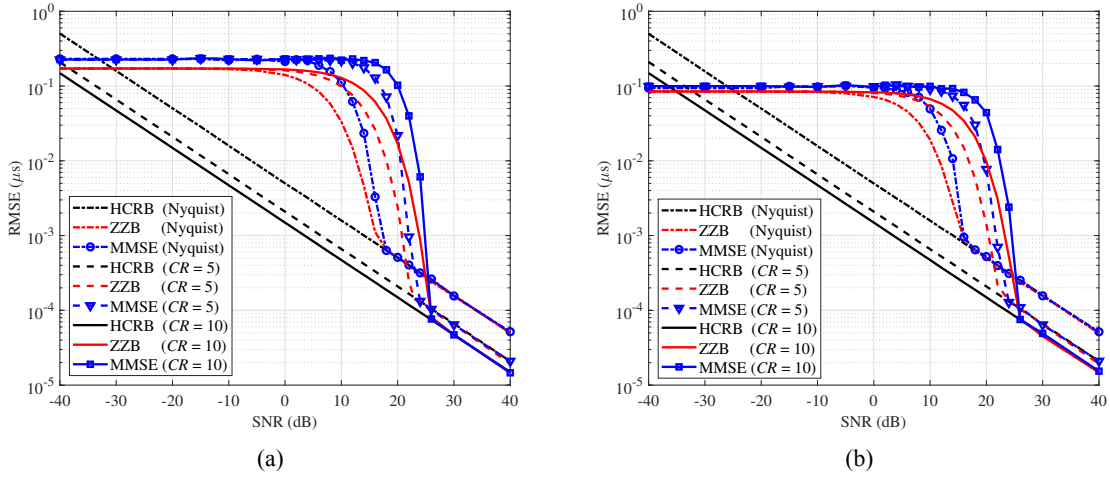


Figure 3.6 RMSE comparison of deterministic ZZB, HCRB, and MMSE estimator considering nuisance unknown α with random Gaussian CS kernel. (a) $\tau \sim \mathcal{U}[0, \frac{80}{B}]$; (b) $\tau \sim \mathcal{N}(\frac{40}{B}, (\frac{10}{B})^2)$.

In Fig. 3.6, we investigate the effect of nuisance parameter α on the derived ZZB. For comparison, both the MMSE estimator incorporating the MLE of α in (3-22) and the HCRB [107] are also plotted. Other simulation parameters are same as those in Fig. 3.3. It is observed that, the derived ZZBs in Fig. 3.6 are same as those in Fig. 3.3 in the asymptotic region, indicating the asymptotic optimality of the log-GLRT [1]. In the high SNR situation, the nuisance parameter α can be accurately estimated such that the ZZB converges to the HCRB and is tight for lower bounding the MSE of the MMSE estimator. In the low SNR situation, affected by the MLE in (3-22), the deterministic ZZB does not converge to the *a priori* variance of τ , making the ZZB not tight as that in Fig. 3.3. However, compared with the HCRB, the ZZB still provides a tighter bound in the low SNR situation. Moreover, it is worth noting that, compared with Fig. 3.3, the existence of nuisance parameter α does not obviously affect the threshold point location of the derived ZZB.

Since the ZZB is a function of the CS kernel, it is reasonable to optimize the CS kernel to lower the ZZB. In Fig. 3.7, we compare the ZZB with the information-theoretic CS kernel [97],

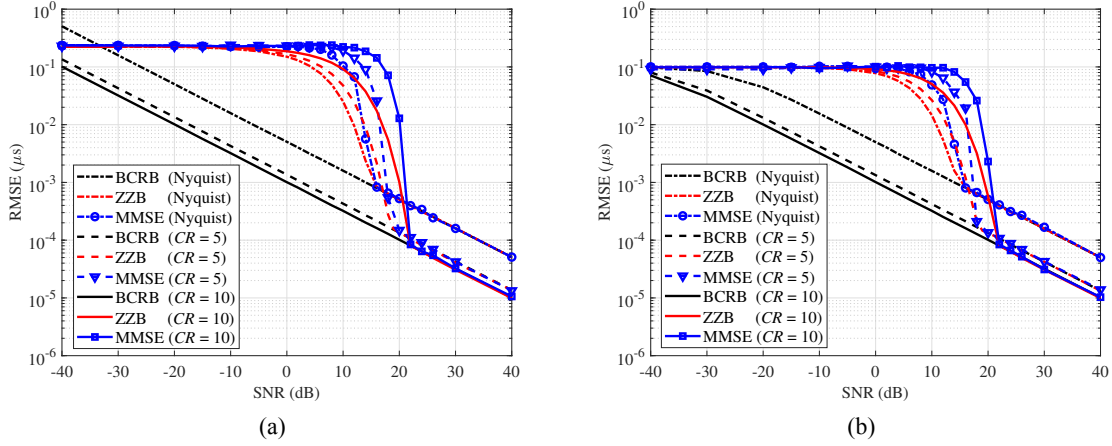


Figure 3.7 RMSE comparison of deterministic ZZB, BCRB, and MMSE estimator with information-theoretic CS kernel proposed in [101]. (a) $\tau \sim \mathcal{U}[0, \frac{80}{B}]$; (b) $\tau \sim \mathcal{N}(\frac{40}{B}, (\frac{10}{B})^2)$.

[101], which is obtained by solving the mutual information maximization problem

$$\begin{aligned} & \max_{\Phi} I(\mathbf{y}; \tau) \\ & \text{s.t. } \Phi\Phi^H = \mathbf{I}, \end{aligned} \quad (3-49)$$

where the objective function $I(\mathbf{y}; \tau)$ denotes the Shannon mutual information between the compressive measurement \mathbf{y} and the time delay τ , and the row orthogonal constraint is used to avoid increasing the mutual information by simply scaling up the CS kernel. By comparing Fig. 3.7 to Fig. 3.3, we can see that the BCRB has a constant decrease in all regions, but the ZZB only decreases in the transition region and the asymptotic region. Obviously, the ZZB still can predict the estimation performance correctly in all regions, which means in the low SNR situation, the ZZB is more tighter than the BCRB for the information-theoretic CS kernel than the random CS kernel. In addition, we also can see that for a fixed CR (e.g., CR = 5), the ZZB using information-theoretic CS kernels starts the asymptotic region at lower SNR (18 dB) than that using random CS kernels (22 dB). Correspondingly, the intersection point between two ZZBs with different CRs also occurs at lower SNR, e.g., about 21.2 dB for ZZBs with CR = 5 and CR = 10 in Fig. 3.7a versus 24.2 dB in Fig. 3.3a. Another significant observation is that in the transition region, the ZZB using information-theoretic CS kernel is much closer to the ZZB

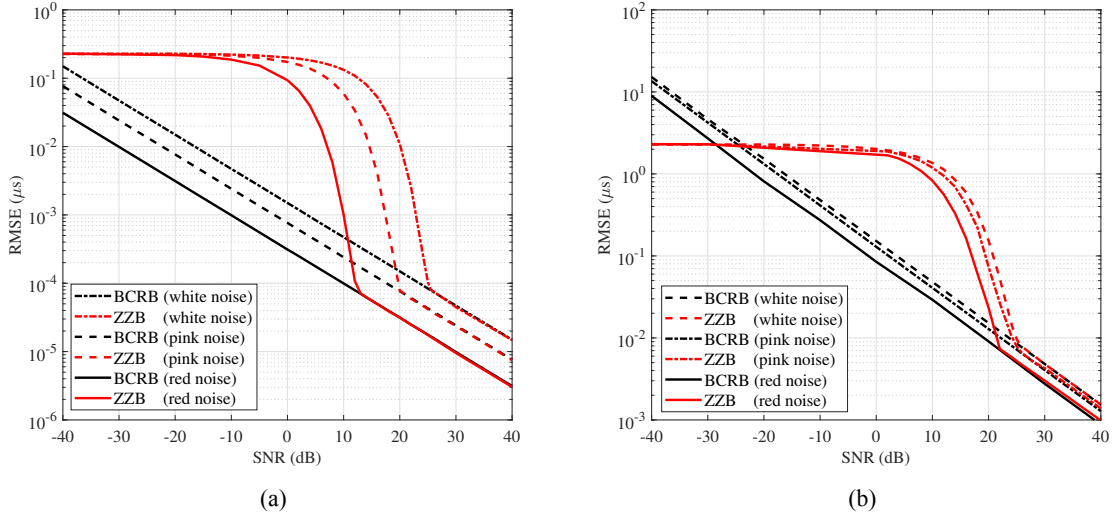


Figure 3.8 Performance comparison of deterministic ZZB and BCRB under different colored Gaussian noises with $CR = 10$. (a) 1 GHz waveform bandwidth; (b) 10 MHz waveform bandwidth.

of Nyquist sampling (i.e., without compression) than the ZZB using random CS kernel. This advantage is also verified by the MMSE performance comparison.

Since there is no restriction on the color of the Gaussian noise, we investigate the performance of the deterministic ZZB under colored Gaussian noises in Fig. 3.8, where pink noise (whose power spectral density is inversely proportional to the frequency) and red noise (whose power spectral density is inversely proportional to the square of frequency) are considered¹. As a comparison, both ZZB and BCRB with under Gaussian noise are also plotted. Other simulation parameters are same as those in Fig. 3.5. It is observed that, in the low SNR situation, all ZZBs converge to the *a priori* variance of the time delay τ , regardless of the colors of the Gaussian noises. On the contrary, in the asymptotic region, the ZZBs under different colored noises respectively converge to the corresponding BCRBs. Hence, the derived ZZB always outperforms the corresponding BCRB regardless of the Gaussian noise colored or not. It is also observed that compared with white noise, both red noise and pink noise can bring the lower bounds (ZZB and BCRB) from the transition region to the asymptotic region. Correspondingly, red noise and pink noise make their individual ZZBs achieve the asymptotic region at lower input SNR than white noise. The reason is that, the power spectral densities of red/pink noises attenuate with

¹Both the pink noise and red noise are generated by MATLAB[®] with in-built function `dsp.ColoredNoise(·)`.

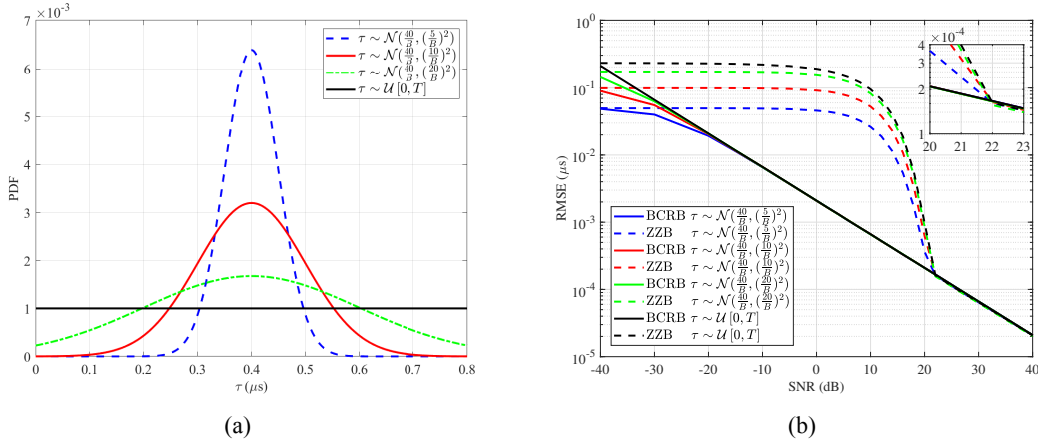


Figure 3.9 Sensitivity analysis of the deterministic ZZB. (a) PDFs of time delay τ ; (b) The corresponding ZZBs and BCRBs.

the frequency increasing, indicating that for the same SNR, the high-frequency components of the red and pink noises are much smaller than those of white noise. As such, the received signals contaminated by red or pink noise have larger equivalent SNR than the received signals contaminated by white noise, which enables a lower ZZB accordingly. Correspondingly, by comparing Fig. 3.8a and Fig. 3.8b, we can see that the larger the waveform bandwidth, the larger difference of ZZBs between colored Gaussian noises and white Gaussian noise.

Similarly as the BCRB, the ZZB depends on the *a priori* distribution of the unknown time delay. Hence, in Fig. 3.9, we study the sensitivity of ZZB w.r.t. the *a priori* distribution, where the BCRB is also plotted for the reference. Without loss of generality, a random Gaussian CS kernel with $\text{CR} = 5$ is applied here. Obviously, the ZZB is sensitive to the *a priori* distribution of the unknown parameter in the low SNR situation and in the transition region. By comparing Fig. 3.9a and Fig. 3.9b, we can see that the lower variance of τ brings the lower ZZB in the low SNR situation and transition region, where the *a priori* distribution $f(\tau)$ provides more information than the observation in lower bounding the MSE. However, the effect of the *a priori* distribution on the ZZB will vanish as long as the SNR increases to the asymptotic region threshold, in which region the ZZB is limited by the radar waveform bandwidth via the CR. By contrast, all BCRBs with different *a priori* distributions $f(\tau)$ almost coincide, indicating that the *a priori* distribution $f(\tau)$ performs little effect on the BCRB, which explains the reason why the ZZB is more tighter in the transition region.

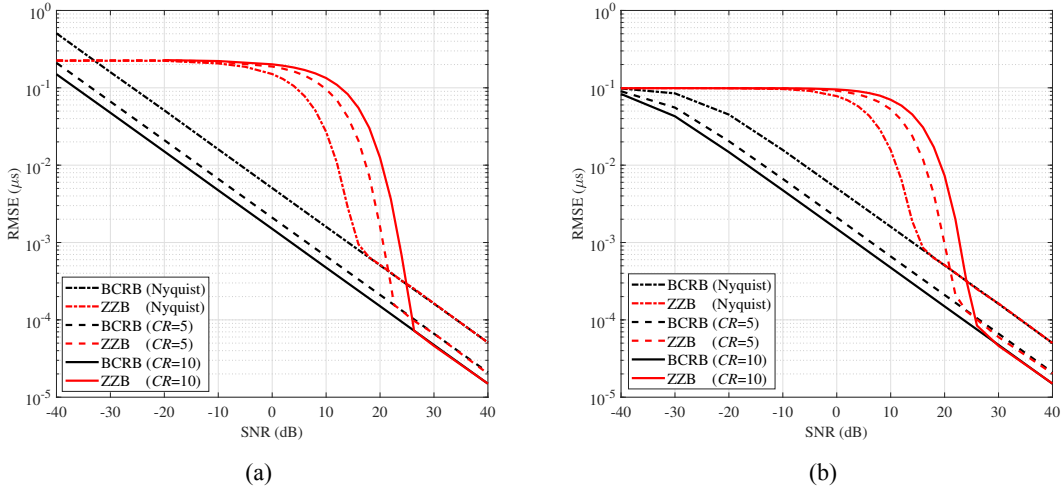


Figure 3.10 RMSE comparison of stochastic ZZB and stochastic BCRB with random Gaussian CS kernel. (a) $\tau \sim \mathcal{U}[0, \frac{80}{B}]$; (b) $\tau \sim \mathcal{N}(\frac{40}{B}, (\frac{10}{B})^2)$.

3.4.2 Stochastic Model

Now let's take a look at the stochastic ZZB with general Gaussian signal amplitude α , which variance σ_α^2 is assumed to be fixed to 1 in our simulations. In Fig. 3.10, we compare the stochastic ZZB and the stochastic BCRB, where random Gaussian CS kernels are applied and the signal amplitude α follows a Gaussian distribution $\mathcal{CN}(\mu_\alpha, \sigma_\alpha^2)$ with $\frac{|\mu_\alpha|}{\sigma_\alpha} = 10$. Similar as the deterministic case, the stochastic ZZB is also tighter than the stochastic BCRB in the low SNR situation and in the transition region regardless that the *a priori* distribution of τ is uniform or normal. In the asymptotic region, the stochastic ZZB converges to the stochastic BCRB as expected. That is to say, although we introduced the approximation of the quadratic form of complex Gaussian vector during the derivation of the stochastic ZZB, it can still effectively lower bound the MSE over a wide range of SNR.

Finally, we investigate the influence of the stochasticity of the signals on the stochastic ZZB by selecting $\frac{|\mu_\alpha|}{\sigma_\alpha}$ as the metric of the stochasticity of the signals. The stochastic ZZBs with different $\frac{|\mu_\alpha|}{\sigma_\alpha}$ are compared in Fig. 3.11, where the stochastic BCRB² is also plotted for the reference. It is observed that the stochastic ZZB converges to the deterministic ZZB with $\frac{|\mu_\alpha|}{\sigma_\alpha}$

²We note that, unlike the stochastic ZZB, the stochastic BCRB is not sensitive to $\frac{|\mu_\alpha|}{\sigma_\alpha}$. Hence, we only plot one stochastic BCRB in Fig. 3.11 for the comparison rather than plotting all stochastic BCRBs of all tested $\frac{|\mu_\alpha|}{\sigma_\alpha}$ cases.

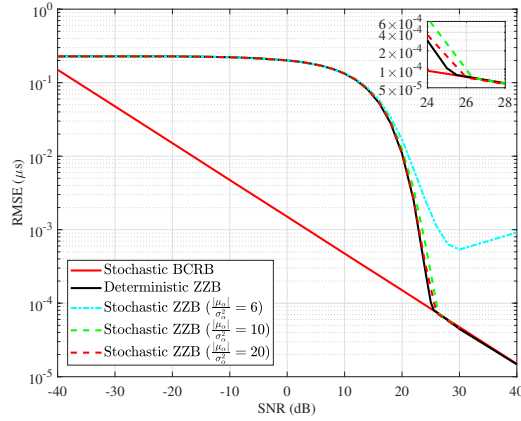


Figure 3.11 Asymptotic region threshold comparison of stochastic ZZB.

increasing and, correspondingly, has the lower asymptotic region threshold. For example, the thresholds of ZZBs for $\frac{|\mu_\alpha|}{\sigma_\alpha^2} = 10$ and 20 are respectively SNR = 26.2 dB and 26 dB. However, it is worth mentioning that, when $\frac{|\mu_\alpha|}{\sigma_\alpha^2} = 6$, the derived stochastic ZZB cannot effectively lower bound the MSE in the asymptotic region, since it may suffer from the approximation in (3-36). Nevertheless, the stochastic ZZB still works reliable in the low SNR situation and is tighter than the BCRB. More accurate stochastic ZZB for small $\frac{|\mu_\alpha|}{\sigma_\alpha^2}$ remains further study.

3.5 Summary

In this chapter, we derived the deterministic ZZB and the stochastic ZZB for compressive time delay estimation as functions of CS kernels. Because there is no restriction on the CS kernel, the derived ZZBs are for the first time applicable for arbitrary CS kernels either random one (e.g., Gaussian CS kernels) or optimized one (e.g., information-theoretic CS kernels [101]). Besides white Gaussian noise, the derived ZZBs are also effective for other colored Gaussian noises. Simulation results demonstrate that, besides consistent with the BCRB in the asymptotic region, the derived ZZB regardless of the deterministic one or the stochastic one is tighter than the BCRB in the low SNR situation and the transition region. Hence, it is effective to lower bound the MSE over a wide range of SNR. Also, the relationship between the time-bandwidth product and the derived ZZB is investigated. In the derived stochastic BCRB, an approximation of quadratic form of complex Gaussian vector is adopted, which makes the stochastic ZZB



inaccurate in the asymptotic region with small $\frac{|\mu_\alpha|}{\sigma_\alpha^2}$. Hence, we will consider to derive a more accurate expression for the stochastic ZZB. In the future work, we will also consider some more specific scenarios, such as multipath model, frequency selective channel, extended targets, etc. Finally, although the ZZBs of this chapter are derived for compressive time delay estimation, we believe that the basic conclusions are valid for compressive estimation of other nonlinear parameters [116]–[119].



Chapter 4. ZZB for Compressive Time Delay Estimation with Zero-Mean Gaussian Signals

Existing stochastic ZZB for compressive time delay estimation from compressed measurement relies on a Gaussian approximation, which makes it inaccurate in the asymptotic region when the stochastic component dominates the received signals. In this chapter, we apply different random projections on zero-mean Gaussian received signal to obtain multiple compressed measurements, based on which the log-LRT is exactly formulated as the difference of two generalized integer Gamma variables. Accordingly, we further derive the exact expression of the stochastic ZZB for compressive time delay estimation from zero-mean Gaussian signal. Simulation results show that the derived ZZB is globally tight to accurately predict the estimation performance regardless of the number of compressed measurements, and it can also accurately predict the threshold SNR for the estimator when the number of compressed measurements is large.

4.1 Introduction

Time delay estimation is a fundamental nonlinear parameter estimation problem with numerous applications in radar, sonar, seismic, remote sensing, wireless communication, industrial IoT, etc [61], [85]–[88], [120]. Due to the high range resolution, wideband signals have been widely adopted as the radar transmit waveforms in the recent years to improve the estimation accuracy. Nevertheless, it also becomes challenging for radar receivers w.r.t. high-rate A/D converters, system cost and power consumption. CS [90], [91] provides a promising solution to use sub-Nyquist A/D converters to sample wideband signal while keeping its high resolution. Hence, CS radar has received a lot of interest in the past decade [92], [95], [97], [98], [101], [121], among which compressive time delay estimation is one typical application.

As a typical nonlinear parameter estimation problem, there is also no exact closed-form expression, under the CS framework, for minimum MSE on time delay estimation. To this end,



it has aroused interest in the derivation of tight lower bounds for the MSE of compressive time delay estimation. Among them, CRB [5], [12]–[14], [122]–[124] is the most frequently used one due to its easy evaluation with the closed-form expression and asymptotic tightness at high SNR. However, the classic CRB depends on the actual value of the parameter only, and fails to use the *a priori* statistical information on the parameter to obtain a tight bound in the non-asymptotic region. Although BCRB utilizes the *a priori* probability density of the parameter, it does not provide a global tight bound for compressive time delay estimation [101].

Different from CRB and BCRB, the ZZB is a global bound on the MSE tight over a wide range of SNR [3]. It was originally proposed for time delay estimation under the assumption of uniform *a priori* distribution of the time delay [54] and then was extended for arbitrary *a priori* distributions [57]. Since then, the ZZB has been applied for evaluating various parameter estimation problems, see for instance [58], [60], [62], [64], [65], [72], [115]. In particular, we derived both deterministic ZZB and stochastic ZZB for compressive time delay estimation, which are suitable for arbitrary CS kernels and Gaussian noise regardless of white or not [64]. However, it was observed that the Gaussian approximation during the derivation of stochastic ZZB makes it inaccurate in the asymptotic region when the stochastic component dominates received signals, even makes it completely invalid when the received signals are zero-mean Gaussian.

In this chapter, we derive an explicit expression of the stochastic ZZB for compressive time delay estimation from zero-mean Gaussian signal, without introducing any approximation. We apply different random CS kernels on the zero-mean Gaussian received signal to obtain multiple compressed measurements. Based on these compressed measurements, the log-LRT can be exactly formulated as the difference of two generalized integer Gamma random variables. Consequently, we derive the minimum probability of error of the required binary hypothesis testing problem and the exact expression of the stochastic ZZB. Simulation results demonstrate that the derived ZZB can accurately predict the threshold SNR of the MMSE estimator when the number of measurements is large.



4.2 Signal Model

For an active radar, the received signal reflected from a far-field point target at time t can be modeled as

$$r(t) = \alpha\psi(t - \tau) + n(t), \quad (4-1)$$

where $\alpha \in \mathbb{C}$ is the signal amplitude following a zero-mean circular complex Gaussian distribution $\mathcal{CN}(0, \sigma_\alpha^2)$, $\psi(t - \tau)$ is the radar waveform delayed by an unknown time τ , and $n(t)$ is the complex-valued additive Gaussian noise. Due to the sparsity of radar signal in the time domain, the unknown time delay τ can be estimated from compressed measurements according to the CS theory. By projecting the received signal $r(t)$ onto K different random CS kernels $\{\Phi_1, \Phi_2, \dots, \Phi_K\}$, we obtain the compressed measurement matrix $\mathbf{Y} = [\mathbf{y}_1, \mathbf{y}_2, \dots, \mathbf{y}_K] \in \mathbb{C}^{M \times K}$, where

$$\mathbf{y}_k = \Phi_k \mathbf{r} = \Phi_k (\alpha\psi(\tau) + \mathbf{n}), k = 1, 2, \dots, K. \quad (4-2)$$

Here, $\Phi_k \in \mathbb{C}^{M \times L}$ is the k -th CS kernel ($M \ll L$) satisfying $\Phi_k \Phi_k^H = \mathbf{I}$ and $\Phi_k \Phi_m^H = \mathbf{0}, \forall k \neq m$, $\psi(\tau) \in \mathbb{C}^L$ is the discrete-time representation of the delayed radar waveform $\psi(t - \tau)$, and $\mathbf{n} \in \mathbb{C}^L$ is the zero-mean circular complex Gaussian noise following $\mathcal{CN}(\mathbf{0}, \mathbf{C}_{nn})$.

For a given time delay τ , each compressed measurement \mathbf{y}_k follows a zero-mean complex Gaussian distribution $\mathcal{CN}(\mathbf{0}, \mathbf{C}_{\mathbf{y}\mathbf{y}|\tau}^{(k)})$ with covariance matrix

$$\mathbf{C}_{\mathbf{y}\mathbf{y}|\tau}^{(k)} = \Phi_k (\sigma_\alpha^2 \psi(\tau) \psi^H(\tau) + \mathbf{C}_{nn}) \Phi_k^H. \quad (4-3)$$

Accordingly, the conditional PDF of the compressed measurement matrix \mathbf{Y} given time delay τ , is expressed as

$$f(\mathbf{Y}|\tau) = \frac{1}{\pi^{KM} \prod_{k=1}^K |\mathbf{C}_{\mathbf{y}\mathbf{y}|\tau}^{(k)}|} e^{-\sum_{k=1}^K \mathbf{y}_k^H [\mathbf{C}_{\mathbf{y}\mathbf{y}|\tau}^{(k)}]^{-1} \mathbf{y}_k}. \quad (4-4)$$

The classical CRB is a lower bound on the variance for any unbiased estimator [2]. Different from the classic CRB, BCRB utilizes the *a priori* information of the time delay, and is



given in (3-6), where

$$J_D = -2\sigma_\alpha^2 \sum_{k=1}^K \mathbb{E}_\tau \left\{ \Re \left[\boldsymbol{\psi}^H(\tau) \boldsymbol{\Phi}_k^H \frac{d \left[\mathbf{C}_{\mathbf{y}\mathbf{y}|\tau}^{(k)} \right]^{-1}}{d\tau} \boldsymbol{\Phi}_k \frac{d\boldsymbol{\psi}(\tau)}{d\tau} \right] \right\} \quad (4-5)$$

represents the Fisher information of the measurement data derived by following the framework given in [101], and J_P is the same as (3-7).

4.3 ZZB Derivation

According to (4-4), the log-LRT becomes

$$\mathcal{L}_\tau = c + \sum_{k=1}^K \mathbf{y}_k^H \left(\left[\mathbf{C}_{\mathbf{y}\mathbf{y}|\varphi+\xi}^{(k)} \right]^{-1} - \left[\mathbf{C}_{\mathbf{y}\mathbf{y}|\varphi}^{(k)} \right]^{-1} \right) \mathbf{y}_k, \quad (4-6)$$

where

$$c = \sum_{k=1}^K \ln \frac{\left| \mathbf{C}_{\mathbf{y}\mathbf{y}|\varphi+\xi}^{(k)} \right|}{\left| \mathbf{C}_{\mathbf{y}\mathbf{y}|\varphi}^{(k)} \right|} \quad (4-7)$$

is a constant given φ and ξ .

Due to $\mathbf{y}_k \sim \mathcal{CN}(\mathbf{0}, \mathbf{C}_{\mathbf{y}\mathbf{y}|\tau}^{(k)})$, we have $\mathbf{z}_k = \left[\mathbf{C}_{\mathbf{y}\mathbf{y}|\tau}^{(k)} \right]^{-\frac{1}{2}} \mathbf{y}_k \sim \mathcal{CN}(\mathbf{0}, \mathbf{I})$. Thus, \mathcal{L}_τ can be formulated as a quadratic form of the complex Gaussian vector $\tilde{\mathbf{z}} = [\mathbf{z}_1^T, \mathbf{z}_2^T, \dots, \mathbf{z}_K^T]^T \in \mathbb{C}^{MK}$ as

$$\mathcal{L}_\tau = c + \tilde{\mathbf{z}}^H \boldsymbol{\Gamma}_\tau \tilde{\mathbf{z}}, \quad (4-8)$$

where

$$\boldsymbol{\Gamma}_\tau = \text{block diag} [\boldsymbol{\Omega}_1, \boldsymbol{\Omega}_2, \dots, \boldsymbol{\Omega}_K] \quad (4-9)$$

is a Hermitian block diagonal matrix with

$$\boldsymbol{\Omega}_k = \left[\mathbf{C}_{\mathbf{y}\mathbf{y}|\tau}^{(k)} \right]^{\frac{1}{2}} \left(\left[\mathbf{C}_{\mathbf{y}\mathbf{y}|\varphi+\xi}^{(k)} \right]^{-1} - \left[\mathbf{C}_{\mathbf{y}\mathbf{y}|\varphi}^{(k)} \right]^{-1} \right) \left[\mathbf{C}_{\mathbf{y}\mathbf{y}|\tau}^{(k)} \right]^{\frac{1}{2}}. \quad (4-10)$$



Then, the matrix $\mathbf{\Gamma}_\tau$ can be eigen-decomposed as

$$\mathbf{\Gamma}_\tau = \mathbf{U}_\tau \mathbf{\Lambda}_\tau \mathbf{U}_\tau^H, \quad (4-11)$$

where \mathbf{U}_τ is a unitary matrix and $\mathbf{\Lambda}_\tau$ is a diagonal matrix containing eigenvalues of $\mathbf{\Gamma}_\tau$. Now, by substituting (4-11) into (4-8), we have

$$\mathcal{L}_\tau = c + \tilde{\mathbf{z}}^H \mathbf{U}_\tau \mathbf{\Lambda}_\tau \mathbf{U}_\tau^H \tilde{\mathbf{z}} = c + \mathbf{w}^H \mathbf{\Lambda}_\tau \mathbf{w}, \quad (4-12)$$

where $\mathbf{w} = \mathbf{U}_\tau^H \tilde{\mathbf{z}} \sim \mathcal{CN}(\mathbf{0}, \mathbf{I})$. Hence, the log-LRT is expressed via a linear combination of chi-square random variables as

$$\mathcal{L}_\tau = c + \sum_{i=1}^{\text{rank}(\mathbf{\Gamma}_\tau)} \frac{\lambda_{\tau,i}}{2} \chi_2^2 \triangleq c + X_\tau, \quad (4-13)$$

where $\text{rank}(\mathbf{\Gamma}_\tau) = 2K$ is the rank of $\mathbf{\Gamma}_\tau$ ¹, $\lambda_{\tau,i}$ denotes the i -th non-zero eigenvalue in $\mathbf{\Lambda}_\tau$, and χ_2^2 denotes the chi-square distributed random variable with 2 degrees of freedom.

Obviously, there are both positive and negative eigenvalues contained in $\mathbf{\Lambda}_\tau$ since $\mathbf{\Gamma}_\tau$ is an indefinite matrix. Then, X_τ results in a difference of two generalized integer Gamma distribution with the exact CDF [125]

$$F_{X_\tau}(x) = \begin{cases} 1 - G^+ G^- \sum_{j=1}^{p^+} P_j^+ e^{-\kappa_j^+ x}, & x \geq 0, \\ G^+ G^- \sum_{\ell=1}^{p^-} P_\ell^- e^{\kappa_\ell^- x}, & x < 0, \end{cases} \quad (4-14)$$

where $\kappa_j^+ = \frac{1}{\lambda_j^+}$ and $\kappa_\ell^- = \frac{1}{\lambda_\ell^-}$ with λ_j^+ and λ_ℓ^- respectively representing modulus of the j -th positive eigenvalue and the ℓ -th negative eigenvalue in $\mathbf{\Lambda}_\tau$, p^+ and p^- respectively denote the

¹It is easy to prove by applying the Sherman-Morrison formula on (4-10).



number of positive and negative eigenvalues. Here,

$$G^+ = \prod_{j=1}^{p^+} \kappa_j^+, \quad (4-15)$$

$$G^- = \prod_{\ell=1}^{p^-} \kappa_\ell^-, \quad (4-16)$$

$$P_j^+ = \sum_{\ell=1}^{p^-} \prod_{\substack{v=1 \\ v \neq \ell}}^{p^-} \frac{1}{(\kappa_v^- - \kappa_\ell^-) (\kappa_j^+ + \kappa_\ell^-) \kappa_j^+} \prod_{\substack{u=1 \\ u \neq j}}^{p^+} \frac{1}{\kappa_u^+ - \kappa_j^+}, \quad (4-17)$$

and

$$P_\ell^- = \sum_{j=1}^{p^+} \prod_{\substack{u=1 \\ u \neq j}}^{p^+} \frac{1}{(\kappa_u^+ - \kappa_j^+) (\kappa_j^+ + \kappa_\ell^-) \kappa_\ell^-} \prod_{\substack{v=1 \\ v \neq \ell}}^{p^-} \frac{1}{\kappa_v^- - \kappa_\ell^-}. \quad (4-18)$$

Then, by respectively substituting $\tau = \varphi$ and $\tau = \varphi + \xi$ into (4-9) and calculating (4-11) to (4-18), we have

$$\Pr(\mathcal{L}_\varphi < \gamma) = F_{X_\varphi}(\gamma - c), \quad (4-19)$$

and

$$\Pr(\mathcal{L}_{\varphi+\xi} \geq \gamma) = 1 - F_{X_{\varphi+\xi}}(\gamma - c). \quad (4-20)$$

Thus, the minimum probability of error $P_{\min}(\varphi, \varphi + \xi)$ is explicitly expressed as

$$P_{\min}(\varphi, \varphi + \xi) = \Pr(\mathcal{H}_0) F_{X_\varphi}(\gamma - c) + \Pr(\mathcal{H}_1) (1 - F_{X_{\varphi+\xi}}(\gamma - c)). \quad (4-21)$$

and the stochastic ZZB becomes

$$\begin{aligned} \text{MSE} \geq & \frac{1}{2} \int_0^{+\infty} \xi \int_{-\infty}^{+\infty} [f_\tau(\varphi) + f_\tau(\varphi + \xi)] \times \\ & [\Pr(\mathcal{H}_0) F_{X_\varphi}(\gamma - c) + \Pr(\mathcal{H}_1) (1 - F_{X_{\varphi+\xi}}(\gamma - c))] d\varphi d\xi. \end{aligned} \quad (4-22)$$



4.4 Simulation

In this section, we compare the effect of the number of CS kernels on the exact stochastic ZZB for compressive time delay estimation, where the Gaussian random CS kernel is adopted. Without loss of generality, in our simulations, we use a 1-MHz-bandwidth A/D converter to sample 10-MHz-bandwidth radar received signal², i.e., the compressive sampling ratio equals to 0.1, where the radar waveform is a typical LFM signal. The dimension of the obtained compressed measurement \mathbf{y}_k is $M = 16$. Due to the zero-mean assumption, the SNR at the receiver is defined as $\text{SNR} = \frac{\sigma_a^2}{\sigma_n^2}$. Here, we assume the time delay τ follows a normal distribution as $\tau \sim \mathcal{N}(4\mu\text{s}, (1\mu\text{s})^2)$ in $[0, 8]\mu\text{s}^3$, which means that a target locates from 0 meters to 1,200 meters away from the radar receiver. In all simulations, we perform numerical integration to evaluate the ZZBs according to the trapezoidal rule, and run $Q = 1,000$ Monte-Carlo trials to obtain the BCRB (i.e., J_B^{-1}) and the RMSE

$$\text{RMSE} = \sqrt{\frac{1}{Q} \sum_{q=1}^Q (\hat{\tau}_q - \tau_q)^2} \quad (4-23)$$

of the MMSE estimator [101]

$$\hat{\tau} = \int \frac{\tau f(\mathbf{Y}|\tau)f(\tau)}{f(\mathbf{Y})} d\tau \quad (4-24)$$

for each SNR point, where $\hat{\tau}_q$ is the MMSE estimate of the true time delay τ_q in the q -th Monte-Carlo trial, and $f(\mathbf{Y}) = \int f(\mathbf{Y}|\tau)f(\tau)d\tau$.

Due to the applicability limitation of the Gaussian-approximated stochastic ZZB [64], in the first example, we compare it with the exact stochastic ZZB (4-22) under the single compressed measurement. It is observed from Fig. 4.1 that, the Gaussian-approximated ZZB is completely invalid for evaluating the MMSE estimator outside the *a priori* performance region, because for zero-mean Gaussian received signal, $P_{\min}(\varphi, \varphi + \xi)$ in Eq. (50) of [64] degrades

²The effect of waveform bandwidth on ZZB was investigated in our pervious work [64]. Hence, the simulation in this chapter can be used to effectively predict the cases with larger waveform bandwidth.

³The derived ZZB is appropriate for arbitrary *a priori* distribution of τ .

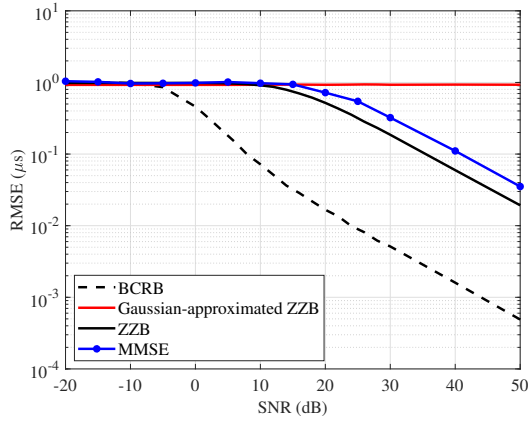


Figure 4.1 RMSE comparison of BCRB, Gaussian-approximated ZZB, ZZB, and the MMSE estimator with single CS kernel ($K = 1$).

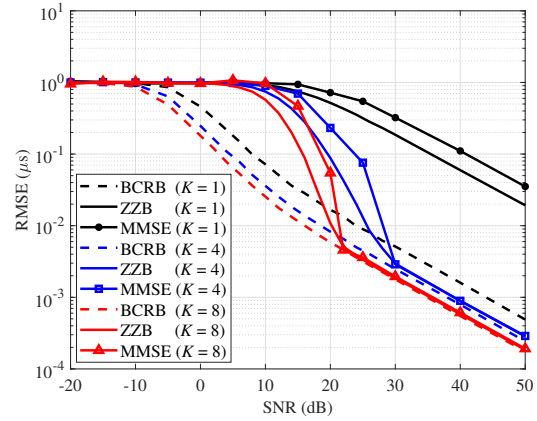


Figure 4.2 RMSE comparison of BCRB, ZZB, and the MMSE estimator with different number of CS kernels.

to either $\Pr(\mathcal{H}_0)$ if $c > \gamma$ or $\Pr(\mathcal{H}_1)$ if $c \leq \gamma$. It implies that the Gaussian-approximated ZZB is dominated by the *a priori* distribution of τ only, such that it fails to lower bound the MSE anymore. Compared with the Gaussian-approximated ZZB, the BCRB provides a loose bound in the transition region although it does converge to the *a priori* variance of the time delay τ in the *a priori* performance region. On the contrast, the ZZB derived in this chapter can predict the estimation performance of the MMSE estimator from the *a priori* performance region to the asymptotic region. Meanwhile, it is also observed that the ZZB does not tend to coincide with the BCRB in the asymptotic region. The reason is that, as a local bound, the BCRB only captures the local small errors, and becomes loose in the presence of catastrophic errors even in high SNR situation. By contrast, the ZZB captures both small and catastrophic errors to provide a global tight bound.

In the second example, we compare the ZZB with the BCRB and the RMSE of the MMSE estimator under different number of CS kernels. It is observed from Fig. 4.2 that, all the ZZBs converge to the *a priori* variance of the time delay τ regardless of the number of CS kernels, and provide global tight bound to predict the RMSE of the MMSE estimator. Compared with the single compressed measurement ($K = 1$), the ZZB tends to the corresponding BCRB with the SNR increasing for multiple compressed measurements (e.g., $K = 4$), which implies that the catastrophic errors on the RMSE in the asymptotic region can be mitigated or even eliminated by increasing the number of CS kernels. Furthermore, the gap between the ZZB and the BCRB in



the asymptotic region becomes smaller as the number of compressed measurements increases. The reason is that, more random CS kernels increase the rank of Γ_τ in (4-9) and bring more non-zero eigenvalues accordingly, leading to a negligible $P_{\min}(\varphi, \varphi + \xi)$ in (2-7) for large ξ . Correspondingly, the effect of catastrophic errors on the RMSE is mitigated in the asymptotic region, and finally the ZZB coincides with the BCRB (see $K = 8$). Moreover, unlike the BCRB without threshold effect, the ZZBs for $K = 4$ and $K = 8$ accurately predict the threshold SNRs for the MMSE estimator. Obviously, the threshold SNR predicted by the ZZB becomes lower with more compressed measurements (30 dB for $K = 4$ versus 22 dB for $K = 8$), indicating that the ZZB enters the asymptotic region earlier.

4.5 Summary

In this chapter, we derived the stochastic ZZB for compressive time delay estimation from multiple random compressed measurements on zero-mean Gaussian received signal. From the multiple compressed measurements, we derived the exact expression of the log-LRT as the difference of two generalized integer Gamma distributed variables, based on which we further derived the minimum probability of error of the binary hypothesis problem and the corresponding stochastic ZZB without any approximation. Simulation results demonstrate that the stochastic ZZB derived in this chapter consistently provides a global tight bound, from the *a priori* performance region to the asymptotic region, on evaluating the MMSE estimator for zero-mean Gaussian signal, regardless of the number of compressed measurements. In addition, the derived stochastic ZZB can also accurately predict the threshold SNR for the MMSE estimator, provided the number of measurements is large. It is noting that, besides the ZZB, the family of WWB also provide tight bounds for parameter estimation (see, [126] and the references therein), which motivates us to further evaluate the WWB for compressive time delay estimation and provides more insight for the comparison between ZZB and WWB in our future work.



Chapter 5. ZZB for 1D DOAs Estimation

Lower bounds on MSE play an important role in evaluating the DOA estimation performance. Among numerous bounds for DOA estimation, the local CRB is only tight asymptotically. By contrast, the existing global tight ZZB is appropriate for evaluating the single source estimation only. In this chapter, we derive an explicit ZZB applicable for evaluating hybrid coherent/incoherent multiple sources DOA estimation. It is first shown that, a straightforward generalization of ZZB from single source estimation to multiple sources estimation cannot keep the bound valid in the *a priori* performance region. To derive a global tight ZZB, we then introduce order statistics to describe the change of the *a priori* distribution of DOAs caused by ordering process during the MSE calculation. The derived ZZB is for the first time formulated as a function of coherent coefficients between coherent sources, and reveals the relationship between the MSE convergency in the *a priori* performance region and the number of sources. Moreover, the derived ZZB also provides a unified tight bound for both overdetermined and underdetermined DOA estimation. Simulation results demonstrate the obvious advantages of the derived ZZB over the CRB on evaluating and predicting the estimation performance for multiple sources DOA.

5.1 Introduction

DOA estimation is a fundamental problem in many array processing applications including radar, sonar, navigation, and wireless communications [2]. In the past decades, multiple sources DOA estimation has attracted great research interest, the majority of which concentrated on the algorithm design. Among them, the typical ones include MUSIC [127]–[129], ESPRIT [130]–[132], sparse reconstruction-based algorithms [133]–[135], and machine learning-based algorithms [136]–[138].

MSE is commonly used to evaluate the performance of estimators. However, as a typical nonlinear parameter estimation problem, there is no exact closed-form minimum MSE for DOAs estimation, which motivates to find MSE lower bounds (see, [3] and the references



therein). Among them, CRB [5] is the most widely used one, since it is easily derived from the inverse of the FIM. Therein, the closed-form CRB for DOAs estimation is given in [6], [7]. To overcome the singularity of FIM in the underdetermined estimation, nonsingular FIM is derived in [8], [9], where the corresponding coarray CRB for underdetermined DOA estimation is also provided. As a local non-Bayesian bound, it is well known that these CRBs are only asymptotically tight in small error estimation scenario (e.g., high SNR), and cannot offer a valid bound in evaluating estimation performance under low SNR situation. In order to overcome the locality of these CRBs, numerous Bayesian bounds utilizing the *a priori* distribution of parameters had been proposed in past few decades [3], among which one typical class is covariance inequality-based bounds [39] including BCRB [2], WWB [38], RMB [45], BAB [42], and BZB [44]. However, these bounds rely on higher order derivative, optimization over free variables and empirical testing point selection to provide a global tighter solution [3].

As another typical Bayesian bound, ZZB enables to provide a global tight bound on the MSE over a wide range of SNR. ZZB was originally proposed in [54] (with improvement in [55], [56]) by considering a scalar estimation problem, where the time delay is assumed to follow a uniform *a priori* distribution. Since then, the ZZBs for specific scalar parameter estimation problems have been widely studied [61], [62], [64], [67]–[69], [115], [139], e.g., single source DOA estimation exploiting linear array [68], [69]. On the other hand, a unified expression of ZZB for vector parameter estimation with arbitrary *a priori* distribution was first derived in [57], which provides a promising framework for the derivation of ZZB on multiple sources DOA estimation. However, it remains challenges in deriving an explicit ZZB due to the involved high dimensional integration and constrained optimization. Although an explicit ZZB for two-dimensional DOA estimation was derived in [58], the involved Sherman-Morrison formula and matrix determinant lemma make it appropriate for single source estimation only. Furthermore, its uniform distribution assumption on $\sin \theta$ rather than on the DOA θ itself, is impractical for DOA estimation, because it implies that, the source signal impinges on the array from the boresight with the highest probability, and the probability gradually decreases with the DOA deviating from the boresight. Hence, the existing ZZBs for single source DOA estimation are difficult to be straightforwardly extended to multiple sources scenario, where the main



challenges are:

- With the number of sources increasing, the numerical solution suffers from heavier computational burden, such that an explicit ZZB is required.
- For multiple sources DOA estimation, there naturally exists permutation ambiguity during MSE calculation. However, the ordering process for the elimination of permutation ambiguity implicitly changes the *a priori* distribution of DOAs, which makes the ZZB derived from the existing framework invalid in the *a priori* performance region.
- For multiple sources DOA estimation, the mutual coherence among coherent sources is generally unavoidable due to multipath propagation (see, [140]–[142] and the references therein), the effect of which on the ZZB is still unclear.

Due to these difficulties, some researchers had to adopt the ZZB for single source DOA estimation [58] to evaluate their multiple sources DOA estimation [71]. In this chapter, we derive an explicit ZZB for hybrid coherent/incoherent multiple sources DOA estimation. By utilizing Woodbury matrix identity and Sylvester’s determinant theorem, we first follow the derivation in [58] to generalize the ZZB for single source DOA estimation to multiple sources DOA estimation. However, such straightforward generalization does not consider the permutation ambiguity arising in MSE calculation for multiple sources DOA estimation, which makes the generalized ZZB invalid in the *a priori* performance region. To this end, we for the first time introduce the order statistics to describe the effect of the elimination of permutation ambiguity on the ZZB, such that the ZZB keeps tight for the evaluation of DOA estimators outside the asymptotic region. The ZZB for DOAs estimation is an explicit function of the number of sources, the number of array sensors, the number of snapshots, the *a priori* distribution and SNRs of sources, array observation data, and the coherent coefficient. Furthermore, the derived ZZB provides a unified expression for both overdetermined DOA estimation and underdetermined DOA estimation, and also explicitly reveals the MSE convergency in the *a priori* performance region w.r.t. the number of sources and their *a priori* distributions. Simulations demonstrate the validity of the ZZB to predict multiple sources DOA estimation performance, benefited from



its obvious threshold effect. Compared with the widely used CRB, the derived ZZB provides a tight bound over a wider range of SNR, and clearly reveals the MSE convergency in the *a priori* performance region and the effect of the coherent coefficient in the transition region.

The rest of this chapter is organized as follows. We introduce a hybrid coherent/incoherent multiple sources model, MSE and CRB in Section 5.2. Then, in Section 5.3, we derive a ZZB as an explicit function of multiple sources, where the permutation ambiguity in DOAs estimation is also considered. We perform simulations in Section 5.4 to demonstrate the advantages of the ZZB. Finally, we make our conclusions in Section 5.5.

5.2 Signal Model, MSE and CRB

Assuming K far-field narrowband signals impinging on a linear array consisting of M sensors located at $\{d_1, d_2, \dots, d_M\}$ from directions $\boldsymbol{\theta} = [\theta_1, \theta_2, \dots, \theta_K]^T$, where, without loss of generality, the first L ($1 \leq L \leq K$) sources are assumed to be mutually coherent, while the left $K - L$ sources are incoherent with each other and independent of the first L sources. The array observation data are modeled as

$$\begin{aligned} \mathbf{x}(t) &= \sum_{k=1}^L \mathbf{a}(\theta_k) \beta_k s_1(t) + \sum_{k=L+1}^K \mathbf{a}(\theta_k) s_k(t) + \mathbf{n}(t) \\ &= \mathbf{A}(\boldsymbol{\theta}) \mathbf{s}(t) + \mathbf{n}(t), \forall t = 1, 2, \dots, T, \end{aligned} \quad (5-1)$$

where $\mathbf{A}(\boldsymbol{\theta}) = [\mathbf{a}(\theta_1), \mathbf{a}(\theta_2), \dots, \mathbf{a}(\theta_K)] \in \mathbb{C}^{M \times K}$ is the steering matrix with the k -th column

$$\mathbf{a}(\theta_k) = \left[e^{-j \frac{2\pi}{\lambda} d_1 \sin \theta_k}, \dots, e^{-j \frac{2\pi}{\lambda} d_M \sin \theta_k} \right]^T \quad (5-2)$$

denoting the steering vector of the k -th source with λ representing the wavelength, $\mathbf{s}(t) = [\beta^T s_1(t), s_{L+1}(t), \dots, s_K(t)]^T \in \mathbb{C}^K$ denotes the K signals with $\boldsymbol{\beta} = [\beta_1, \dots, \beta_L]^T \in \mathbb{C}^L$ containing the coherent coefficient β_l between the l -th ($1 \leq l \leq L$) coherent signal $\beta_l s_1(t)$ and the reference signal $s_1(t)$ (i.e., $\beta_1 = 1$), and $\mathbf{n}(t) \sim \mathcal{CN}(\mathbf{0}_M, \sigma_n^2 \mathbf{I}_M)$ is the complex zero-mean additive white Gaussian noise independent of the signals with σ_n^2 denoting the noise power. Here, T denotes the number of snapshots.



Without loss of generality, we make the following assumptions:

Assumption 5.2.1. *All the incoherent signals $s_k(t), k = 1, L + 1, \dots, K$ are sampled from zero-mean, stationary complex Gaussian stochastic processes.*

Assumption 5.2.2. *The DOAs of the signals are distinct (say, $\theta_i \neq \theta_j \forall i \neq j$).*

Assumption 5.2.3. *Each DOA follows a uniform distribution $\theta_k \sim \mathcal{U}[\vartheta_{\min}, \vartheta_{\max}]$.*

Thus, the theoretical covariance matrix of $\mathbf{x}(t)$ given $\boldsymbol{\theta}$ is

$$\mathbf{R}_{\mathbf{x}|\boldsymbol{\theta}} = \mathbb{E} \{ \mathbf{x}(t) \mathbf{x}^H(t) \} = \mathbf{A}(\boldsymbol{\theta}) \boldsymbol{\Sigma} \mathbf{A}^H(\boldsymbol{\theta}) + \sigma_n^2 \mathbf{I}_M, \quad (5-3)$$

where

$$\boldsymbol{\Sigma} = \mathbb{E} \{ \mathbf{s}(t) \mathbf{s}^H(t) \} = \text{block diag} [\boldsymbol{\Sigma}_{co}, \boldsymbol{\Sigma}_{in}] \quad (5-4)$$

with

$$\boldsymbol{\Sigma}_{co} = \boldsymbol{\beta} \boldsymbol{\beta}^H \sigma_1^2 \quad (5-5)$$

denoting the covariance matrix corresponding to the first L coherent sources, and

$$\boldsymbol{\Sigma}_{in} = \text{diag} [\sigma_{L+1}^2, \dots, \sigma_K^2] \quad (5-6)$$

denoting the power of the left $K - L$ incoherent sources. The diagonal entries of matrix $\boldsymbol{\Sigma}$ denote the power of K sources, where $|\beta_k|^2 \sigma_1^2$ ($k = 1, \dots, L$) denotes the power of the k -th coherent source, σ_k^2 , while σ_k^2 ($k = L + 1, \dots, K$) denotes the power of the k -th incoherent source.

Similar to other parameter estimation problems, the MSE defined as

$$\text{MSE} = \frac{1}{K} \sum_{k=1}^K \mathbb{E} \left\{ \left(\hat{\theta}_k - \theta_k \right)^2 \right\} = \frac{1}{K} \text{Tr} \{ \mathbf{R}_\epsilon \} \quad (5-7)$$

is a well accepted metric to evaluate the estimation accuracy of DOA estimators, where $\hat{\theta}_k$ is the estimate of θ_k . It is worth noting that, the definition of MSE for DOA estimation implies the following assumption:



Assumption 5.2.4. *All DOAs make the same contribution to MSE calculation, namely, they have an equal weight.*

As a widely used lower bound in evaluating the variance of DOA estimators, CRB is the inverse of the Fisher information, where the ι_j -th entry of the FIM \mathbf{J} w.r.t. $\boldsymbol{\theta}$ is given by [2]

$$\mathbf{J}_{\iota_j} = T \text{Tr} \left\{ \frac{\partial \mathbf{R}_{x|\boldsymbol{\theta}}}{\partial \theta_{\iota_j}} \mathbf{R}_{x|\boldsymbol{\theta}}^{-1} \frac{\partial \mathbf{R}_{x|\boldsymbol{\theta}}}{\partial \theta_{\iota_j}} \mathbf{R}_{x|\boldsymbol{\theta}}^{-1} \right\}. \quad (5-8)$$

It is observed that, due to the uniform distribution, there is no *a priori* information of $\boldsymbol{\theta}$ contributing to the Fisher information even if in BCRB [2], which makes CRB only tight in the asymptotic region.

5.3 Derivation of ZZB for DOAs Estimation

In this section, we derive a ZZB for DOAs estimation in an explicit way, where the number of sources, the number of array sensors, the number of snapshots, the *a priori* distribution and SNRs of sources, array observation data, and the coherent coefficient are served as explicit factors. In subsection 5.3.1, we first follow the derivation framework in [58] to generalize the ZZB for single source DOA estimation to multiple sources DOA estimation, which, unfortunately, is invalid for lower bounding the MSE outside the asymptotic region. Considering the permutation ambiguity arising in MSE calculation for multiple sources DOA estimation, in subsection 5.3.2, we then introduce order statistics to make the ZZB global tight in evaluating the MSE for multiple sources DOA estimation.

By ignoring the valley filling function in Eq. (2-20), the general ZZB expression here becomes

$$\mathbf{w}^T \mathbf{R}_\epsilon \mathbf{w} \geq \frac{1}{2} \int_0^\infty \max_{\boldsymbol{\delta}: \mathbf{w}^T \boldsymbol{\delta} = h} \left[\int_{\mathbb{R}^K} (f_\theta(\boldsymbol{\varphi}) + f_\theta(\boldsymbol{\varphi} + \boldsymbol{\delta})) P_{\min}(\boldsymbol{\varphi}, \boldsymbol{\varphi} + \boldsymbol{\delta}) d\boldsymbol{\varphi} \right] h dh, \quad (5-9)$$

With Assumption 5.2.4, the weight vector \mathbf{w} in DOAs estimation becomes

$$\mathbf{w} = \frac{1}{\sqrt{K}} \mathbf{1}_K. \quad (5-10)$$



Thus, (5-9) can be written as

$$\frac{1}{K} \mathbf{1}_K^T \mathbf{R}_\epsilon \mathbf{1}_K \geq \frac{1}{2} \int_0^\infty \max_{\delta: \mathbf{1}_K^T \delta = \sqrt{K}h} \left[\int_{\mathbb{R}^K} (f_\theta(\boldsymbol{\varphi}) + f_\theta(\boldsymbol{\varphi} + \boldsymbol{\delta})) P_{\min}(\boldsymbol{\varphi}, \boldsymbol{\varphi} + \boldsymbol{\delta}) d\boldsymbol{\varphi} \right] h d h. \quad (5-11)$$

For single source case (i.e., $K = 1$), the vector $\boldsymbol{\theta}$ degrades to a scalar θ , $\delta = h$, and (5-11) becomes

$$\mathbb{E} \left\{ \left(\hat{\theta} - \theta \right)^2 \right\} \geq \frac{1}{2} \int_0^\infty \int_{-\infty}^{+\infty} (f_\theta(\varphi) + f_\theta(\varphi + h)) P_{\min}(\varphi, \varphi + h) d\varphi h d h, \quad (5-12)$$

which also has been investigated in [58]. On the contrary, for multiple sources case (i.e., $K \geq 2$), it's still challenging for ZZB to evaluate the performance of DOA estimators straightforwardly due to K -dimensional integration and optimization in (5-11).

5.3.1 Generalized ZZB for Multiple Sources DOA Estimation

It is worth noting that, the utilization of Sherman-Morrison formula and matrix determinant lemma in [58] makes it appropriate for single source case only, which, accordingly, hinders the ZZB derivation in multiple sources scenario. Instead, for the hybrid coherent/incoherent multiple sources considered in this chapter, we introduce Woodbury matrix identity and Sylvester's determinant theorem to generalize the ZZB as an explicit function of multiple sources.

For the array observation data matrix $\mathbf{X} = [\mathbf{x}(1), \dots, \mathbf{x}(T)] \in \mathbb{C}^{M \times T}$, $P_{\min}(\boldsymbol{\varphi}, \boldsymbol{\varphi} + \boldsymbol{\delta})$ is lower bounded as [143]

$$P_{\min}(\boldsymbol{\varphi}, \boldsymbol{\varphi} + \boldsymbol{\delta}) \geq e^{\left[\mu(p; \boldsymbol{\delta}) + \frac{1}{8} \frac{\partial^2 \mu(p; \boldsymbol{\delta})}{\partial p^2} \right]} \mathcal{Q} \left(\frac{1}{2} \sqrt{\frac{\partial^2 \mu(p; \boldsymbol{\delta})}{\partial p^2}} \right) \Bigg|_{p=\frac{1}{2}} \triangleq P(\boldsymbol{\delta}), \quad (5-13)$$

where

$$\mu(p; \boldsymbol{\delta}) = \ln \int f(\mathbf{X} | \boldsymbol{\varphi} + \boldsymbol{\delta})^p f(\mathbf{X} | \boldsymbol{\varphi})^{1-p} d\mathbf{X} \quad (5-14)$$

is the semi-invariant moment generating function.



For the observation data matrix \mathbf{X} with T snapshots, $\mu(p; \boldsymbol{\delta})$ is given in [143]

$$\mu(p; \boldsymbol{\delta}) = T \left[p \ln |\mathbf{R}_{x|\varphi}| + (1-p) \ln |\mathbf{R}_{x|\varphi+\delta}| - \ln |p\mathbf{R}_{x|\varphi} + (1-p)\mathbf{R}_{x|\varphi+\delta}| \right], \quad (5-15)$$

where $\mathbf{R}_{x|\varphi} \triangleq \mathbf{R}_{x|\theta=\varphi}$ and $\mathbf{R}_{x|\varphi+\delta} \triangleq \mathbf{R}_{x|\theta=\varphi+\delta}$.

The first derivative of $\mu(p; \boldsymbol{\delta})$ w.r.t. p is

$$\frac{\partial \mu(p; \boldsymbol{\delta})}{\partial p} = T \left[\ln |\mathbf{R}_{x|\varphi}| - \ln |\mathbf{R}_{x|\varphi+\delta}| - \text{Tr} \left\{ [p\mathbf{R}_{x|\varphi} + (1-p)\mathbf{R}_{x|\varphi+\delta}]^{-1} \mathbf{R}_- \right\} \right] \quad (5-16)$$

by denoting $\mathbf{R}_- = \mathbf{R}_{x|\varphi} - \mathbf{R}_{x|\varphi+\delta}$, and then the second derivative of $\mu(p; \boldsymbol{\delta})$ w.r.t. p is

$$\frac{\partial^2 \mu(p; \boldsymbol{\delta})}{\partial p^2} = T \text{Tr} \left\{ \left[[p\mathbf{R}_{x|\varphi} + (1-p)\mathbf{R}_{x|\varphi+\delta}]^{-1} \mathbf{R}_- \right]^2 \right\}. \quad (5-17)$$

Hence, by denoting $\mathbf{R}_+ = \mathbf{R}_{x|\varphi} + \mathbf{R}_{x|\varphi+\delta}$, $\mu(p; \boldsymbol{\delta})|_{p=\frac{1}{2}}$ and $\frac{\partial^2 \mu(p; \boldsymbol{\delta})}{\partial p^2}|_{p=\frac{1}{2}}$ respectively become

$$\mu(p; \boldsymbol{\delta})|_{p=\frac{1}{2}} = T \left[\frac{\ln (|\mathbf{R}_{x|\varphi}| |\mathbf{R}_{x|\varphi+\delta}|)}{2} - \ln \left| \frac{\mathbf{R}_+}{2} \right| \right], \quad (5-18)$$

and

$$\frac{\partial^2 \mu(p; \boldsymbol{\delta})}{\partial p^2} \Big|_{p=\frac{1}{2}} = 4T \text{Tr} \left\{ (\mathbf{R}_+^{-1} \mathbf{R}_-)^2 \right\}. \quad (5-19)$$

By performing the second-order Taylor series expansion of $\mu(p; \boldsymbol{\delta})|_{p=\frac{1}{2}}$ and $\frac{\partial^2 \mu(p; \boldsymbol{\delta})}{\partial p^2} \Big|_{p=\frac{1}{2}}$ around the point $\boldsymbol{\delta} = \mathbf{0}_K$, we have

$$\mu(p; \boldsymbol{\delta})|_{p=\frac{1}{2}} \approx -\frac{1}{8} \boldsymbol{\delta}^T \mathbf{J} \boldsymbol{\delta}, \quad (5-20)$$

and

$$\frac{\partial^2 \mu(p; \boldsymbol{\delta})}{\partial p^2} \Big|_{p=\frac{1}{2}} \approx \boldsymbol{\delta}^T \mathbf{J} \boldsymbol{\delta}. \quad (5-21)$$

Thus, by substituting (5-20) and (5-21) into (5-13), $P(\boldsymbol{\delta})$ is approximated as

$$P_S(\boldsymbol{\delta}) = \mathcal{Q} \left(\frac{1}{2} \sqrt{\boldsymbol{\delta}^T \mathbf{J} \boldsymbol{\delta}} \right), \quad (5-22)$$



Although the result is consistent with Eq. (D. 12) in [58], the derivation here is generalized to multiple sources DOA estimation.

Since the approximation $P(\boldsymbol{\delta}) \approx P_S(\boldsymbol{\delta})$ is only appropriate for $\boldsymbol{\delta}$ located in a small region Δ around $\mathbf{0}_K$, we further investigate (5-13) for $\boldsymbol{\delta}$ outside the region Δ . According to Sylvester's determinant theorem

$$|\mathbf{I}_M + \mathbf{UV}| = |\mathbf{I}_K + \mathbf{VU}| \quad (5-23)$$

for $\mathbf{U} \in \mathbb{C}^{M \times K}$ and $\mathbf{V} \in \mathbb{C}^{K \times M}$, the determinants in (5-18) can be respectively written as

$$|\mathbf{R}_{x|\varphi}| = \sigma_n^{2M} \left| \mathbf{I}_K + \frac{1}{\sigma_n^2} \mathbf{A}^H(\varphi) \mathbf{A}(\varphi) \boldsymbol{\Sigma} \right|, \quad (5-24)$$

$$|\mathbf{R}_{x|\varphi+\boldsymbol{\delta}}| = \sigma_n^{2M} \left| \mathbf{I}_K + \frac{1}{\sigma_n^2} \mathbf{A}^H(\varphi + \boldsymbol{\delta}) \mathbf{A}(\varphi + \boldsymbol{\delta}) \boldsymbol{\Sigma} \right|, \quad (5-25)$$

and

$$\left| \frac{1}{2} \mathbf{R}_+ \right| = \sigma_n^{2M} \left| \mathbf{I}_{2K} + \frac{1}{2\sigma_n^2} \mathbf{B}^H \mathbf{B} \mathbf{D} \right|, \quad (5-26)$$

where

$$\mathbf{B} = [\mathbf{A}(\varphi), \mathbf{A}(\varphi + \boldsymbol{\delta})], \quad (5-27)$$

and

$$\mathbf{D} = \text{block diag}[\boldsymbol{\Sigma}_{co}, \boldsymbol{\Sigma}_{in}, \boldsymbol{\Sigma}_{co}, \boldsymbol{\Sigma}_{in}]. \quad (5-28)$$

Obviously, $\mathbf{A}^H(\varphi) \mathbf{A}(\varphi)$, $\mathbf{A}^H(\varphi + \boldsymbol{\delta}) \mathbf{A}(\varphi + \boldsymbol{\delta})$, and $\mathbf{B}^H \mathbf{B}$ are related to the array beampattern, whose null points coincide with the minima of $P(\boldsymbol{\delta})$. The null points of the array beampattern occur at

$$|\mathbf{a}^H(\theta) \mathbf{a}(\theta + \boldsymbol{\delta})| = 0 \quad (5-29)$$

for single source case [58], which implies the steering vector $\mathbf{a}(\theta + \boldsymbol{\delta})$ is orthogonal to $\mathbf{a}(\theta)$. By generalizing (5-29) for multiple sources case, we propose the following approximation

$$\mathbf{A}^H(\boldsymbol{\theta}) \mathbf{A}(\boldsymbol{\theta}) \approx M \mathbf{I}_K \quad (5-30)$$



by considering that multiple steering vectors are approximately orthogonal to each other, from which we have¹

$$\mathbf{B}^H \mathbf{B} \approx M \mathbf{I}_{2K}. \quad (5-31)$$

As such, (5-18) can be approximated as

$$\begin{aligned} \mu(p; \boldsymbol{\delta})|_{p=\frac{1}{2}} &\approx T \ln \frac{\left| \mathbf{I}_K + \frac{M}{\sigma_n^2} \boldsymbol{\Sigma} \right|}{\left| \mathbf{I}_{2K} + \frac{M}{2\sigma_n^2} \mathbf{D} \right|} \\ &= T \ln \frac{4(1 + M \|\boldsymbol{\beta}\|_2^2 \eta_1)}{(2 + M \|\boldsymbol{\beta}\|_2^2 \eta_1)^2} + T \sum_{k=L+1}^K \ln \frac{4(1 + M \eta_k)}{(2 + M \eta_k)^2}, \end{aligned} \quad (5-32)$$

where $\eta_k = \frac{\sigma_k^2}{\sigma_n^2}$ is the SNR of the k -th source. Then, \mathbf{R}_+ and \mathbf{R}_- in (5-19) can be further written as

$$\mathbf{R}_+ = 2\sigma_n^2 \mathbf{I}_M + \mathbf{B} \mathbf{D} \mathbf{B}^H, \quad (5-33)$$

and

$$\mathbf{R}_- = \mathbf{B} \tilde{\mathbf{D}} \mathbf{B}^H, \quad (5-34)$$

respectively, where

$$\tilde{\mathbf{D}} = \text{block diag}[\boldsymbol{\Sigma}_{co}, \boldsymbol{\Sigma}_{in}, -\boldsymbol{\Sigma}_{co}, -\boldsymbol{\Sigma}_{in}]. \quad (5-35)$$

According to Woodbury matrix identity, the inverse of \mathbf{R}_+ can be approximated as

$$\mathbf{R}_+^{-1} \approx \frac{1}{2\sigma_n^2} \mathbf{I}_M - \frac{1}{4\sigma_n^4} \mathbf{B} \mathbf{D} \mathbf{Y} \mathbf{B}^H \quad (5-36)$$

with the approximation condition (5-31), where

$$\mathbf{Y} = \left(\mathbf{I}_{2K} + \frac{M}{2\sigma_n^2} \mathbf{D} \right)^{-1} = \text{block diag}[\mathbf{Y}_{co}, \mathbf{Y}_{in}, \mathbf{Y}_{co}, \mathbf{Y}_{in}] \quad (5-37)$$

¹To obtain the minimum value of $P(\boldsymbol{\delta})$, we only consider the case there is no same value in $\boldsymbol{\varphi}$ and $\boldsymbol{\varphi} + \boldsymbol{\delta}$, such that the steering vectors in $\mathbf{A}(\boldsymbol{\varphi})$ are also orthogonal to those $\mathbf{A}(\boldsymbol{\varphi} + \boldsymbol{\delta})$.



with

$$\begin{aligned} \mathbf{Y}_{co} &= \left(\mathbf{I}_L + \frac{M}{2\sigma_n^2} \boldsymbol{\Sigma}_{co} \right)^{-1} \\ &= \mathbf{I}_L - \frac{M\eta_1}{2 + M\|\boldsymbol{\beta}\|_2^2\eta_1} \boldsymbol{\beta}\boldsymbol{\beta}^H \end{aligned} \quad (5-38)$$

according to Sherman-Morrison formula, and

$$\begin{aligned} \mathbf{Y}_{in} &= \left(\mathbf{I}_{K-L} + \frac{M}{2\sigma_n^2} \boldsymbol{\Sigma}_{in} \right)^{-1} \\ &= \text{diag} \left[\left(1 + \frac{M\eta_{L+1}}{2} \right)^{-1}, \dots, \left(1 + \frac{M\eta_K}{2} \right)^{-1} \right]. \end{aligned} \quad (5-39)$$

Accordingly, we have

$$(\mathbf{R}_+^{-1} \mathbf{R}_-)^2 \approx \frac{M}{4\sigma_n^4} \left(\mathbf{B}\mathbf{D}^2\mathbf{B}^H - \frac{M}{\sigma_n^2} \mathbf{B}\mathbf{D}^3\mathbf{Y}\mathbf{B}^H + \frac{M^2}{4\sigma_n^4} \mathbf{B}\mathbf{D}^4\mathbf{Y}^2\mathbf{B}^H \right) \quad (5-40)$$

since

$$\mathbf{D}^2 = \tilde{\mathbf{D}}^2. \quad (5-41)$$

Then, (5-19) is approximated as

$$\left. \frac{\partial^2 \mu(p; \boldsymbol{\delta})}{\partial p^2} \right|_{p=\frac{1}{2}} \approx \frac{TM^2}{\sigma_n^4} \text{Tr} \left\{ \left(\mathbf{D}^2 - \frac{M}{\sigma_n^2} \mathbf{D}^3\mathbf{Y} + \frac{M^2}{4\sigma_n^4} \mathbf{D}^4\mathbf{Y}^2 \right) \right\}, \quad (5-42)$$

where the trace of \mathbf{D}^2 , $\mathbf{D}^3\mathbf{Y}$, and $\mathbf{D}^4\mathbf{Y}^2$ are respectively expressed as

$$\text{Tr}\{\mathbf{D}^2\} = 2\|\boldsymbol{\beta}\|_2^4\sigma_1^4 + \sum_{k=L+1}^K 2\sigma_k^4, \quad (5-43)$$

$$\text{Tr}\{\mathbf{D}^3\mathbf{Y}\} = \frac{4\|\boldsymbol{\beta}\|_2^6\sigma_1^6}{2 + M\|\boldsymbol{\beta}\|_2^2\eta_1} + \sum_{k=L+1}^K \frac{4\sigma_k^6}{2 + M\eta_k}. \quad (5-44)$$

and

$$\text{Tr}\{\mathbf{D}^4\mathbf{Y}^2\} = \frac{8\|\boldsymbol{\beta}\|_2^8\sigma_1^8}{(2 + M\|\boldsymbol{\beta}\|_2^2\eta_1)^2} + \sum_{k=L+1}^K \frac{8\sigma_k^8}{(2 + M\eta_k)^2}. \quad (5-45)$$



Finally, (5-42) becomes

$$\left. \frac{\partial^2 \mu(p; \boldsymbol{\delta})}{\partial p^2} \right|_{p=\frac{1}{2}} \approx 8T \left[\left(\frac{M \|\boldsymbol{\beta}\|_2^2 \eta_1}{2 + M \|\boldsymbol{\beta}\|_2^2 \eta_1} \right)^2 + \sum_{k=L+1}^K \left(\frac{M \eta_k}{2 + M \eta_k} \right)^2 \right], \quad (5-46)$$

which is a function of SNR η_k , the number of array sensors M , the number of sources K and the coherent coefficient $\boldsymbol{\beta}$. By substituting (5-32) and (5-46) into (5-13), $P(\boldsymbol{\delta})$ for $\boldsymbol{\delta}$ outside the region Δ is approximated as

$$\begin{aligned} P_L = e &^T \left[\ln \frac{4(1+M\|\boldsymbol{\beta}\|_2^2\eta_1)}{(2+M\|\boldsymbol{\beta}\|_2^2\eta_1)^2} + \left(\frac{M\|\boldsymbol{\beta}\|_2^2\eta_1}{2+M\|\boldsymbol{\beta}\|_2^2\eta_1} \right)^2 + \sum_{k=L+1}^K \left[\ln \frac{4(1+M\eta_k)}{(2+M\eta_k)^2} + \left(\frac{M\eta_k}{2+M\eta_k} \right)^2 \right] \right] \\ &\times \mathcal{Q} \left(\sqrt{2T \left[\left(\frac{M\|\boldsymbol{\beta}\|_2^2\eta_1}{2 + M\|\boldsymbol{\beta}\|_2^2\eta_1} \right)^2 + \sum_{k=L+1}^K \left(\frac{M\eta_k}{2 + M\eta_k} \right)^2 \right]} \right). \end{aligned} \quad (5-47)$$

The boundary of the region Δ occurs at $P_S(\boldsymbol{\delta}) = P_L$. However, the explicit boundary is difficult to calculate. Similar to [58], considering that $\mathcal{Q}(z)$ is a decreasing function w.r.t. z , the region Δ can be approximately given by

$$\frac{\sqrt{\boldsymbol{\delta}^T \mathbf{J} \boldsymbol{\delta}}}{2} \leq \sqrt{2T \left[\left(\frac{M\|\boldsymbol{\beta}\|_2^2\eta_1}{2 + M\|\boldsymbol{\beta}\|_2^2\eta_1} \right)^2 + \sum_{k=L+1}^K \left(\frac{M\eta_k}{2 + M\eta_k} \right)^2 \right]}, \quad (5-48)$$

which is the interior of an ellipse given in

$$\Delta = \left\{ \boldsymbol{\delta} : \boldsymbol{\delta}^T \mathbf{J} \boldsymbol{\delta} \leq 8T \left[\left(\frac{M\|\boldsymbol{\beta}\|_2^2\eta_1}{2 + M\|\boldsymbol{\beta}\|_2^2\eta_1} \right)^2 + \sum_{k=L+1}^K \left(\frac{M\eta_k}{2 + M\eta_k} \right)^2 \right] \right\}. \quad (5-49)$$

Accordingly, $P(\boldsymbol{\delta})$ is expressed as

$$P(\boldsymbol{\delta}) \approx \begin{cases} P_S(\boldsymbol{\delta}), & \boldsymbol{\delta} \in \Delta \\ P_L, & \boldsymbol{\delta} \notin \Delta \end{cases}. \quad (5-50)$$

It should be pointed out that, the $P_S(\boldsymbol{\delta})$ derived here is appropriate for multiple sources case although it has the same expression as Eq. (D. 13) in [58]. To be more specific, the determinants of $\mu(p; \boldsymbol{\delta})|_{p=\frac{1}{2}}$ in [58] are calculated using matrix determinant lemma in the Eq.



(B. 16) in [58] and the Eq. (B. 17) in [58], from which the $P_S(\boldsymbol{\delta})$ is finally derived. Considering the fact that the use of matrix determinant lemma in [58] implies the single source assumption, the $P_S(\boldsymbol{\delta})$ derived there is naturally appropriate for single source only. On the contrary, we perform the Taylor expansion directly on $\mu(p; \boldsymbol{\delta})|_{p=\frac{1}{2}}$ and $\frac{\partial^2 \mu(p; \boldsymbol{\delta})}{\partial p^2}|_{p=\frac{1}{2}}$ that preserves the matrix determinants to derive the $P_S(\boldsymbol{\delta})$, during which the assumption about number of sources has not been involved. Therefore, the $P_S(\boldsymbol{\delta})$ derived here is appropriate for both single source and multiple sources simultaneously. Besides, we adopt Woodbury matrix identity and Sylvester's determinant theorem rather than Sherman-Morrison formula and matrix determinant lemma in [58] to derive the P_L , which, not only makes it work for multiple sources, but also enables us for the first time to formulate it as an explicit function of coherent coefficients $\boldsymbol{\beta}$. Moreover, the derived P_L is also a function of the number of sources, which is approximately² same as that in [58] when $K = 1$.

Since K DOAs are independent, the K -dimensional integration in (5-11) becomes

$$\begin{aligned} \frac{1}{2} \int_{\mathbb{R}^K} (f_{\theta}(\boldsymbol{\varphi}) + f_{\theta}(\boldsymbol{\varphi} + \boldsymbol{\delta})) P_{\min}(\boldsymbol{\varphi}, \boldsymbol{\varphi} + \boldsymbol{\delta}) d\boldsymbol{\varphi} &\geq \frac{P(\boldsymbol{\delta})}{\zeta^K} \int_{\Phi} d\boldsymbol{\varphi} \\ &= \frac{P(\boldsymbol{\delta})}{\zeta^K} \prod_{k=1}^K (\zeta - |\delta_k|), \end{aligned} \quad (5-51)$$

where

$$\Phi = \{\boldsymbol{\varphi} | \varphi_k \in [\vartheta_{\min}, \vartheta_{\max} - |\delta_k|], k = 1, 2, \dots, K\} \quad (5-52)$$

is the K -dimensional integration region, $\zeta = \vartheta_{\max} - \vartheta_{\min}$ denotes the range of DOAs, and $|\delta_k|$ is the absolute value of the k -th element in $\boldsymbol{\delta}$.

By substituting (5-50) into (5-51), we have

$$\frac{P(\boldsymbol{\delta})}{\zeta^K} \prod_{k=1}^K (\zeta - |\delta_k|) \approx \frac{P_L}{\zeta^K} \prod_{k=1}^K (\zeta - |\delta_k|) + \begin{cases} P_S(\boldsymbol{\delta}) - P_L & \boldsymbol{\delta} \in \Delta \\ 0 & \boldsymbol{\delta} \notin \Delta \end{cases}, \quad (5-53)$$

based on which the corresponding optimization problem in (5-11) can be divided into three

²Our derivation of P_L is consistent with the Eq. (C. 13) in [58]. However, an extra approximation was made in Eq. (C. 13) in [58]. Hence, we mention "approximately" here.



separated terms as

$$\max_{\delta: \mathbf{1}_K^T \delta = \sqrt{K}h} \frac{P(\boldsymbol{\delta})}{\zeta^K} \prod_{k=1}^K (\zeta - |\delta_k|) \approx \max_{\delta: \mathbf{1}_K^T \delta = \sqrt{K}h} \frac{P_L}{\zeta^K} \prod_{k=1}^K (\zeta - |\delta_k|) + \max_{\delta \in \Delta: \mathbf{1}_K^T \delta = \sqrt{K}h} P_S(\boldsymbol{\delta}) - P_L. \quad (5-54)$$

Then, we have the following property about the maximum of $\frac{1}{\zeta^K} \prod_{k=1}^K (\zeta - |\delta_k|)$.

Property 1.

$$\max_{\delta: \mathbf{1}_K^T \delta = \sqrt{K}h} \frac{1}{\zeta^K} \prod_{k=1}^K (\zeta - |\delta_k|) = \left(1 - \frac{h}{\zeta \sqrt{K}}\right)^K. \quad (5-55)$$

Proof. Obviously, the integration region Φ in (5-52) brings the constraint

$$|\delta_k| \leq \zeta, \forall k = 1, 2, \dots, K, \quad (5-56)$$

such that all the $\zeta - |\delta_k|$ must be positive. With the constraint

$$\mathbf{1}_K^T \boldsymbol{\delta} = \sqrt{K}h, \quad (5-57)$$

the maximum of $\prod_{k=1}^K (\zeta - |\delta_k|)$ must occur in the region $\Omega = \{\delta_k > 0, \forall k = 1, 2, \dots, K\}$, because given any $\boldsymbol{\delta}$ containing negative elements, there always exists a certain $\boldsymbol{\delta}$ in the region δ^+ leading to a larger $\prod_{k=1}^K (\zeta - |\delta_k|)$. Thus, we have

$$\sum_{k=1}^K \zeta - |\delta_k| = \sum_{k=1}^K \zeta - \delta_k = K\zeta - \sqrt{K}h, \quad (5-58)$$

which is a positive constant. Based on the arithmetic-geometric mean inequality, the maximum of $\prod_{k=1}^K (\zeta - |\delta_k|)$ occurs if and only if $\delta_k = \frac{h}{\sqrt{K}}, \forall k = 1, 2, \dots, K$, and thus Property 1 is proved. \square

Accordingly, the first term in (5-54) becomes

$$\max_{\delta: \mathbf{1}_K^T \delta = \sqrt{K}h} \frac{P_L}{\zeta^K} \prod_{k=1}^K (\zeta - |\delta_k|) = P_L \left(1 - \frac{h}{\sqrt{K}\zeta}\right)^K. \quad (5-59)$$



The maximum of the second term in (5-54) occurs at [58]³

$$\boldsymbol{\delta} = \sqrt{K}h \frac{\mathbf{J}^{-1}\mathbf{1}_K}{\mathbf{1}_K^T \mathbf{J}^{-1} \mathbf{1}_K}, \quad (5-60)$$

such that it becomes

$$\max_{\boldsymbol{\delta} \in \Delta: \mathbf{1}_K^T \boldsymbol{\delta} = \sqrt{K}h} P_S(\boldsymbol{\delta}) = \mathcal{Q} \left(\frac{\sqrt{K}h}{2\sqrt{\mathbf{1}_K^T \mathbf{J}^{-1} \mathbf{1}_K}} \right). \quad (5-61)$$

Correspondingly, (5-54) is further written as

$$\begin{aligned} & \max_{\boldsymbol{\delta}: \mathbf{1}_K^T \boldsymbol{\delta} = \sqrt{K}h} \frac{P(\boldsymbol{\delta})}{\zeta^K} \prod_{k=1}^K (\zeta - |\delta_k|) \\ & \approx P_L \left(1 - \frac{h}{\sqrt{K}\zeta} \right)^K + \begin{cases} \mathcal{Q} \left(\frac{\sqrt{K}h}{2\sqrt{\mathbf{1}_K^T \mathbf{J}^{-1} \mathbf{1}_K}} \right) - P_L & 0 \leq h \leq \tilde{h}, \\ 0 & h > \tilde{h}, \end{cases} \end{aligned} \quad (5-62)$$

where

$$\tilde{h} \approx \min \left[\sqrt{\frac{8T\mathbf{1}_K^T \mathbf{J}^{-1} \mathbf{1}_K}{K} \left[\left(\frac{M\|\boldsymbol{\beta}\|_2^2 \eta_1}{2 + M\|\boldsymbol{\beta}\|_2^2 \eta_1} \right)^2 + \sum_{k=L+1}^K \left(\frac{M\eta_k}{2 + M\eta_k} \right)^2 \right]}, \sqrt{K}\zeta \right] \quad (5-63)$$

is the threshold derived by

$$\frac{\sqrt{K}\tilde{h}}{2\sqrt{\mathbf{1}_K^T \mathbf{J}^{-1} \mathbf{1}_K}} \approx \sqrt{2T \left[\left(\frac{M\|\boldsymbol{\beta}\|_2^2 \eta_1}{2 + M\|\boldsymbol{\beta}\|_2^2 \eta_1} \right)^2 + \sum_{k=L+1}^K \left(\frac{M\eta_k}{2 + M\eta_k} \right)^2 \right]} \quad (5-64)$$

with the constraint $0 \leq \tilde{h} \leq \sqrt{K}\zeta$.

³Since the array observation data are related to the wanted random parameters (i.e., DOAs) and other unwanted random parameters (e.g., sources and noise power), we cannot simply calculate \mathbf{J}^{-1} only considering the Fisher information w.r.t. $\boldsymbol{\theta}$ [2]. In this case, the parameter vector containing all random parameters is $\boldsymbol{\alpha} = [\boldsymbol{\theta}^T, \boldsymbol{\sigma}^T]^T$ with $\boldsymbol{\sigma} = [\sigma_1^2, \sigma_2^2, \dots, \sigma_K^2, \sigma_n^2]^T$ denoting the unwanted parameter vector, and the complete FIM \mathbf{J}_α can be calculated according to (5-8) or (5-94) by replacing $\boldsymbol{\theta}$ into $\boldsymbol{\alpha}$. Then, \mathbf{J}^{-1} should be calculated as the first block with $K \times K$ elements in \mathbf{J}_α^{-1} , whose explicit solution is given in the Eq. (3.1) in [7] for overdetermined DOA estimation and the Eq. (43) in [9] for underdetermined DOA estimation, respectively.



Then, (5-11) can be further written as

$$\frac{1}{K} \mathbf{1}_K^T \mathbf{R}_\epsilon \mathbf{1}_K \geq P_L \int_0^{\sqrt{K}\zeta} \left(1 - \frac{h}{\sqrt{K}\zeta}\right)^K h dh + \int_0^{\tilde{h}} \left[\mathcal{Q} \left(\frac{\sqrt{K}h}{2\sqrt{\mathbf{1}_K^T \mathbf{J}^{-1} \mathbf{1}_K}} \right) - P_L \right] h dh, \quad (5-65)$$

where the first integration

$$\int_0^{\sqrt{K}\zeta} \left(1 - \frac{h}{\sqrt{K}\zeta}\right)^K h dh = \frac{12 \mathbf{1}_K^T \mathbf{R}_\theta \mathbf{1}_K}{(K+1)(K+2)}, \quad (5-66)$$

and the second integration

$$\begin{aligned} \int_0^{\tilde{h}} \left[\mathcal{Q} \left(\frac{\sqrt{K}h}{2\sqrt{\mathbf{1}_K^T \mathbf{J}^{-1} \mathbf{1}_K}} \right) - P_L \right] h dh &= \int_0^{\tilde{h}} \frac{1}{\sqrt{2\pi}} e^{-\frac{Kh^2}{8 \mathbf{1}_K^T \mathbf{J}^{-1} \mathbf{1}_K}} \frac{\sqrt{K}h^2}{4\sqrt{\mathbf{1}_K^T \mathbf{J}^{-1} \mathbf{1}_K}} dh \\ &= \Gamma_{\frac{3}{2}}(\tilde{u}) \frac{\mathbf{1}_K^T \mathbf{J}^{-1} \mathbf{1}_K}{K}. \end{aligned} \quad (5-67)$$

Here,

$$\Gamma_{\frac{3}{2}}(\tilde{u}) = \frac{1}{\Gamma(\frac{3}{2})} \int_0^{\tilde{u}} e^{-\xi} \xi^{\frac{1}{2}} d\xi \quad (5-68)$$

is the normalized incomplete Gamma function with $\Gamma(\frac{3}{2}) = \frac{\sqrt{\pi}}{2}$ and

$$\tilde{u} = \frac{K\tilde{h}^2}{8 \mathbf{1}_K^T \mathbf{J}^{-1} \mathbf{1}_K}. \quad (5-69)$$

Thus, the generalized ZZB for multiple sources DOA estimation is derived as

$$\frac{1}{K} \mathbf{1}_K^T \mathbf{R}_\epsilon \mathbf{1}_K \geq \frac{12 P_L \mathbf{1}_K^T \mathbf{R}_\theta \mathbf{1}_K}{(K+1)(K+2)} + \Gamma_{\frac{3}{2}}(\tilde{u}) \frac{\mathbf{1}_K^T \mathbf{J}^{-1} \mathbf{1}_K}{K}, \quad (5-70)$$

where

$$\mathbf{R}_\theta = \frac{\zeta^2}{12} \mathbf{I}_K \quad (5-71)$$

is the *a priori* covariance matrix of θ ,

Obviously, the generalized ZZB in (5-70) lower bounds the error correlation matrix, one special case of which is the MSE we sought. Specifically, considering that the MSE defined in (5-7) is only related to the diagonal elements of the error correlation matrix \mathbf{R}_ϵ (also, the



diagonal elements in \mathbf{J}^{-1} [144]), the MSE of DOAs estimation can be lower bounded by the generalized ZZB as

$$\text{MSE} \geq \frac{12P_L \text{Tr}\{\mathbf{R}_\theta\}}{(K+1)(K+2)} + \Gamma_{\frac{3}{2}}(\tilde{u}) \frac{\text{Tr}\{\mathbf{J}^{-1}\}}{K}. \quad (5-72)$$

Obviously, only the first term of the generalized ZZB is a function of the *a priori* distribution of θ via \mathbf{R}_θ , while the second term is a function of the FIM \mathbf{J} .

5.3.2 ZZB for Estimation with Permutation Ambiguity

In subsection 5.3.1, we generalized the ZZB of single source DOA estimation to multiple sources DOA estimation, which, however, is invalid in the *a priori* performance region. The reason is that, the ordering process is required by multiple sources DOA estimators for the elimination of permutation ambiguity, which implicitly changes the *a priori* distribution of DOAs. To better illustrate the effect of the permutation ambiguity on MSE calculation, we consider the following example.

Example 1: Assuming there are two signals impinging on the array from 30° and 45° , while their estimates are respectively 29° and 44° . Accordingly, the RMSE is calculated as $\sqrt{\frac{(30^\circ-29^\circ)^2+(45^\circ-44^\circ)^2}{2}} = 1.00^\circ$. However, when permutation ambiguity occurs, the outputs of DOAs estimator become 44° and 29° , leading to a wrong RMSE of $\sqrt{\frac{(30^\circ-44^\circ)^2+(45^\circ-29^\circ)^2}{2}} \approx 15.03^\circ$.

Although permutation ambiguity is ubiquitous for DOAs estimator, its impact on the MSE calculation is more prominent in the asymptotic region. Generally speaking, in the asymptotic region, the estimates of DOAs are around the true values, which leads to a small estimation error. On the contrary, the farther away from the asymptotic region, the larger the estimation error is. Obviously, to obtain the correct MSE, the outputs of DOAs estimators $\hat{\theta}$ should not be directly matched to the true DOAs θ during MSE calculation. To eliminate the permutation ambiguity, both the estimated DOAs and the true DOAs are respectively sorted in ascending



order before calculating the MSE. As such, the MSE should be calculated as

$$\text{MSE} = \frac{1}{K} \sum_{k=1}^K \mathbb{E} \left\{ \left(\hat{\theta}_{(k)} - \theta_{(k)} \right)^2 \right\}, \quad (5-73)$$

where $\hat{\theta}_{(k)}$ and $\theta_{(k)}$ are the k -th smallest order statistic in $\hat{\boldsymbol{\theta}}$ and $\boldsymbol{\theta}$, respectively. Here, the subscript (k) enclosed in parentheses indicates the k -th order statistic of the sample.

Although the ordering process enables an accurate MSE calculation in the asymptotic region, it simultaneously has an effect on the MSE outside the asymptotic region because it implicitly changes the *a priori* distribution of DOAs $\boldsymbol{\theta}$. Actually, different DOAs are naturally assumed to be independent with each other, while such an ordering process introduces an extra dependence among the DOAs. For example, in the *a priori* performance region, each θ_k tends to be randomly estimated according to its *a priori* distribution $\theta_k \sim \mathcal{U}[\vartheta_{\min}, \vartheta_{\max}]$, and the MSE of θ_k converges to its *a priori* variance $\sigma_{\theta_k}^2$. After the ordering process, $\theta_{(k)}$ tends to be randomly estimated in the interval $[\theta_{(k-1)}, \theta_{(k+1)}]$ ⁴ rather than original $[\vartheta_{\min}, \vartheta_{\max}]$, and the MSE of $\theta_{(k)}$ converges to its *a priori* variance $\sigma_{\theta_{(k)}}^2$. Obviously, with the number of sources K increasing, the average range of $\theta_{(k)}$ becomes narrower compared with that of the original θ_k , making the MSE scale down in the *a priori* performance region due to the ordering process.

According to aforementioned discussion, the effect of ordering process on the MSE calculation is formulated as the ratio

$$\kappa = \frac{\text{Tr}\{\mathbf{R}_{(\theta)}\}}{\text{Tr}\{\mathbf{R}_{\theta}\}} \quad (5-74)$$

between the trace of the *a priori* covariance matrix of the order statistics $\{\theta_{(1)}, \dots, \theta_{(K)}\}$, i.e.,

$$\text{Tr}\{\mathbf{R}_{(\theta)}\} = \sum_{k=1}^K \sigma_{\theta_{(k)}}^2, \quad (5-75)$$

and that of the *a priori* covariance matrix of the original $\boldsymbol{\theta}$ before the ordering process, say, $\text{Tr}\{\mathbf{R}_{\theta}\}$.

⁴The interval becomes $[\vartheta_{\min}, \theta_{(2)}]$ and $[\theta_{(K-1)}, \vartheta_{\max}]$ for $\theta_{(1)}$ and $\theta_{(K)}$, respectively.



According to the *a priori* PDF of $\theta_{(k)}$ [145, p.229]

$$f(\theta_{(k)}) = \frac{K! \left(\frac{\theta_{(k)}}{\zeta}\right)^{k-1} \left(1 - \frac{\theta_{(k)}}{\zeta}\right)^{K-k}}{\zeta(k-1)!(K-k)!}, \quad (5-76)$$

the *a priori* variance of $\theta_{(k)}$ is

$$\begin{aligned} \sigma_{\theta_{(k)}}^2 &= \int_0^\zeta (\theta_{(k)} - \mathbb{E}\{\theta_{(k)}\})^2 f(\theta_{(k)}) d\theta_{(k)} \\ &= \frac{\zeta^2(K+1-k)k}{(K+1)^2(K+2)}, \end{aligned} \quad (5-77)$$

where

$$\mathbb{E}\{\theta_{(k)}\} = \int_0^\zeta \theta_{(k)} f(\theta_{(k)}) d\theta_{(k)} = \frac{k\zeta}{K+1}. \quad (5-78)$$

Thus, (5-75) becomes

$$\text{Tr}\{\mathbf{R}(\theta)\} = \frac{K\zeta^2}{6(K+1)}, \quad (5-79)$$

and correspondingly, the ratio κ in (5-74) becomes

$$\kappa = \frac{2}{K+1}, \quad (5-80)$$

which is a function of the number of sources K . For single source case (i.e., $K = 1$), we have $\kappa = 1$, namely, there is no permutation ambiguity. Furthermore, the ratio κ gets smaller with the number of sources increasing, indicating that the MSE scales down more in the *a priori* performance region after the ordering process. The reason is that, the average interval $[\theta_{(k-1)}, \theta_{(k+1)}]$ gets narrower with the number of sources increasing.

In order to make the ZZB valid in the *a priori* performance region for evaluating multiple sources DOA estimation, we incorporate the ratio κ (5-80) into the first term of (5-72) to obtain the ZZB expression as

$$\text{MSE} \geq 2P_L \frac{K\zeta^2}{(K+1)^2(K+2)} + \Gamma_{\frac{3}{2}}(\tilde{u}) \frac{\text{Tr}\{\mathbf{J}^{-1}\}}{K}. \quad (5-81)$$



Obviously, same as the generalized ZZB (5-72), the derived ZZB is also an explicit function of the number of sources, and depends on the number of snapshots, the number of array sensors, the *a priori* distribution and SNRs of sources, array observation data via the FIM, and the coherent coefficient β .

In the *a priori* performance region, the ZZB converges to the APB as

$$\lim_{\forall \eta_k \rightarrow 0} \text{MSE} \geq \frac{K\zeta^2}{(K+1)^2(K+2)}, \quad (5-82)$$

since

$$\lim_{\forall \eta_k \rightarrow 0} 2P_L = 1, \quad (5-83)$$

and

$$\lim_{\forall \eta_k \rightarrow 0} \Gamma_{\frac{3}{2}}(\tilde{u}) = 0. \quad (5-84)$$

Obviously, the estimation accuracy of DOA estimator cannot be further improved by simply increasing the number of array sensors and/or the number of snapshots when the SNR tends to zero.

In the asymptotic region, the ZZB converges to the CRB as

$$\lim_{\forall \eta_k \rightarrow +\infty} \text{MSE} \geq \frac{\text{Tr}\{\mathbf{J}^{-1}\}}{K}, \quad (5-85)$$

since

$$\lim_{\forall \eta_k \rightarrow +\infty} 2P_L = 0 \quad (5-86)$$

and

$$\lim_{\forall \eta_k \rightarrow +\infty} \Gamma_{\frac{3}{2}}(\tilde{u}) = 1. \quad (5-87)$$

Now it is clear that, the ZZB in (5-81) is a linear combination between the APB and the CRB, whose coefficients are $2P_L$ and $\Gamma_{\frac{3}{2}}(\tilde{u})$, respectively.



For fully incoherent sources (say, $L = 1$), P_L (5-47) and \tilde{u} (5-69) respectively degrade to

$$P_L = e^{T \sum_{k=1}^K \left[\ln \frac{4(1+M\eta_k)}{(2+M\eta_k)^2} + \left(\frac{M\eta_k}{2+M\eta_k} \right)^2 \right]} \mathcal{Q} \left(\sqrt{2T \sum_{k=1}^K \left(\frac{M\eta_k}{2+M\eta_k} \right)^2} \right), \quad (5-88)$$

and

$$\tilde{u} \approx \min \left[T \sum_{k=1}^K \left(\frac{M\eta_k}{2+M\eta_k} \right)^2, \frac{K^2 \zeta^2}{8 \mathbf{1}_K^T \mathbf{J}^{-1} \mathbf{1}_K} \right]. \quad (5-89)$$

When K sources have the same SNR η , P_L and \tilde{u} further become

$$P_L = e^{KT \left[\ln \frac{4(1+M\eta)}{(2+M\eta)^2} + \left(\frac{M\eta}{2+M\eta} \right)^2 \right]} \mathcal{Q} \left(\sqrt{2KT} \frac{M\eta}{2+M\eta} \right), \quad (5-90)$$

and

$$\tilde{u} \approx \min \left[KT \left(\frac{M\eta}{2+M\eta} \right)^2, \frac{K^2 \zeta^2}{8 \mathbf{1}_K^T \mathbf{J}^{-1} \mathbf{1}_K} \right]. \quad (5-91)$$

Furthermore, when $K = 1$, the ZZB is simplified to

$$\mathbb{E} \left\{ \left(\hat{\theta} - \theta \right)^2 \right\} \geq 2e^{T \left[\ln \frac{4(1+M\eta)}{(2+M\eta)^2} + \left(\frac{M\eta}{2+M\eta} \right)^2 \right]} \mathcal{Q} \left(\sqrt{2T} \frac{M\eta}{2+M\eta} \right) \sigma_\theta^2 + \Gamma_{\frac{3}{2}}(\tilde{u}) J^{-1}, \quad (5-92)$$

where $\sigma_\theta^2 = \frac{\zeta^2}{12}$ denotes the *a priori* variance of θ , and J is the scalar Fisher information. It is worth pointing out that, the ZZB (5-92) is consistent with the Eq. (C.30) in [58], if we ignore the implicit condition $\tilde{h} < \sqrt{K}\zeta$ such that

$$\tilde{u} \approx T \left(\frac{M\eta}{2+M\eta} \right)^2, \quad (5-93)$$

and introduce the approximation in the Eq. (C.14) in [58].

In Fig. 5.1, we compare combination coefficients of the ZZB versus the SNR, where a single source is assumed to follow *a priori* distribution $\mathcal{U}[-90^\circ, 90^\circ]$ w.r.t. a ULA consisting of $M = 20$ sensors. The number of snapshots is fixed to $T = 40$, and 10,000 Monte-Carlo trials are performed for each SNR point. It is observed that the coefficient $2P_L$ decreases from 1 in the *a priori* performance region to 0 in the asymptotic region as analyzed, while the co-

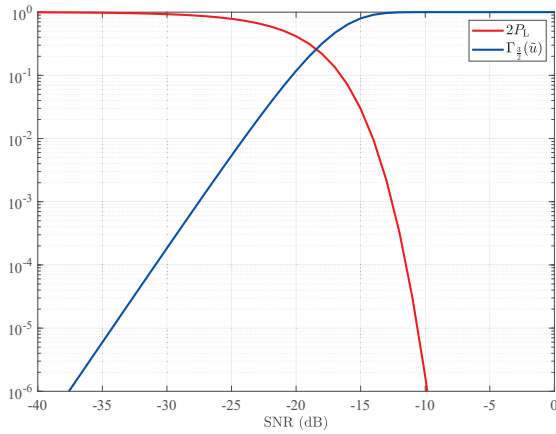


Figure 5.1 Combination coefficients versus the SNR for single source.

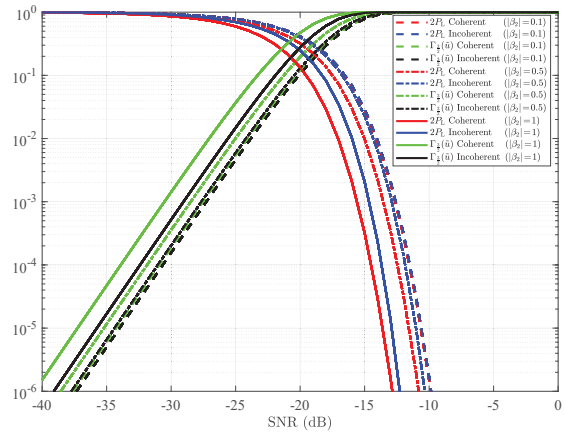


Figure 5.2 Combination coefficients versus the SNR for two sources with different coherent coefficients.

efficient $\Gamma_{\frac{3}{2}}(\tilde{u})$ has an opposite trend. That is to say, the APB dominates the ZZB in the *a priori* performance region, but sharply vanishes in the asymptotic region. On the contrary, the CRB is ignorable in the *a priori* performance region, but gradually dominates the ZZB from the transition region to the asymptotic region.

Unlike in the single source case, both combination coefficients $2P_L$ and $\Gamma_{\frac{3}{2}}(\tilde{u})$ also depend on the coherent coefficient β under coherent multiple sources case. Hence, in Fig. 5.2, we compare both combination coefficients versus the SNR for two coherent sources, where different magnitudes of the coherent coefficient β_2 are considered. Meanwhile, the corresponding combination coefficients for incoherent sources are also plotted as a reference, where the second source with power $\sigma_2^2 = |\beta_2|^2 \sigma_1^2$ is independent of the first one. It is observed that, the difference between coherent and incoherent combination coefficients becomes larger with $|\beta_2|$ increasing. The reason is that, larger $|\beta_2|$ leads to larger norm $\|\beta\|_2$ in (5-47) and (5-63), which makes the combination coefficients $2P_L$ and $\Gamma_{\frac{3}{2}}(\tilde{u})$ in coherent case more distinguishable from those in incoherent case. On the other hand, with $|\beta_2|$ increasing, $2P_L$ and $\Gamma_{\frac{3}{2}}(\tilde{u})$ respectively decreases from 1 and reaches to 1 at lower SNR, indicating that the ZZB will leave the *a priori* performance region to enter the asymptotic region at lower SNR. Furthermore, for the same $|\beta_2|$, $2P_L$ and $\Gamma_{\frac{3}{2}}(\tilde{u})$ in coherent case respectively decreases from 1 and reaches to 1 earlier than those in incoherent case, indicating that the coherent ZZB will leave from the APB to touch the CRB earlier than in incoherent case.



Remark: For underdetermined DOA estimation (say, $K > M$) using virtual coarray, the ν_j -th entry of the coarray FIM w.r.t. θ is given by [9],

$$\tilde{\mathbf{J}}_{\nu_j} = T \left[\text{vec} \left(\frac{\partial \mathbf{R}_{x|\theta}}{\partial \theta_i} \right) \right]^H (\mathbf{R}_{x|\theta}^T \otimes \mathbf{R}_{x|\theta})^{-1} \text{vec} \left(\frac{\partial \mathbf{R}_{x|\theta}}{\partial \theta_j} \right). \quad (5-94)$$

to avoid the rank defect problem. By substituting the coarray FIM into (5-81), the corresponding coarray ZZB can be used to evaluate underdetermined DOA estimation in a wide range of SNR from the *a priori* performance region to the asymptotic region.

5.4 Simulations

In this section, we evaluate the ZZB for multiple sources DOA estimation, where both the CRB and the APB are also plotted for reference. Since ZZB requires the *a priori* distribution, we assume each DOA to follow a uniform distribution $\mathcal{U}[-60^\circ, 60^\circ]$ in our simulations. We run $\mathcal{L} = 10,000$ Monte-Carlo trials for each SNR point to obtain the involved bounds and the RMSE

$$\text{RMSE} = \sqrt{\frac{1}{\mathcal{L}K} \sum_{\ell=1}^{\mathcal{L}} \sum_{k=1}^K (\hat{\theta}_{\ell,(k)} - \theta_{\ell,(k)})^2} \quad (5-95)$$

of DOAs estimation. Here, $\hat{\theta}_{\ell,(k)}$ is the estimate of $\theta_{\ell,(k)}$, the k -th DOA after ordering process in the ℓ -th Monte-Carlo trial. To keep sources resolvable, we assume a minimum interval of 10° in each θ in multiple sources case, i.e., K DOAs in each trial are sampled with at least 10° separation. Unless otherwise specified, the number of snapshots is fixed to $T = 40$, and a ULA with $M = 20$ half-wavelength inter-element spacing sensors is adopted in our simulations, although any linear array configuration is applicable.

Considering that the ZZB in [58] is only appropriate for the single source case, we first compare the derived ZZB (5-92) with the ZZB in [58] under the single source assumption. Meanwhile, the MUSIC algorithm is also plotted for a reference. It is observed from Fig. 5.3 that, due to the extra approximation in [58], the explicit ZZB in [58] enters the asymptotic region at a slightly lower input SNR than the derived ZZB, which is consistent with the numerical integration in the Fig. 4 of [58]. Besides, both the derived ZZB and the ZZB in [58] converge to

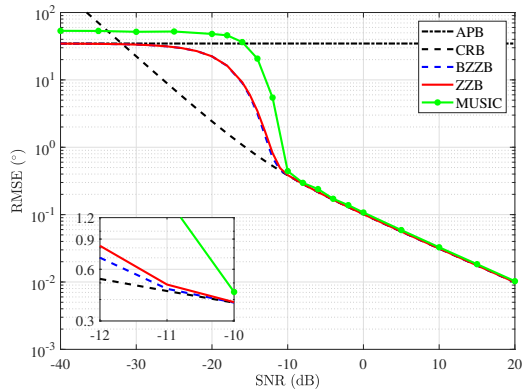


Figure 5.3 Comparison of bounds for single source case ($K = 1$).

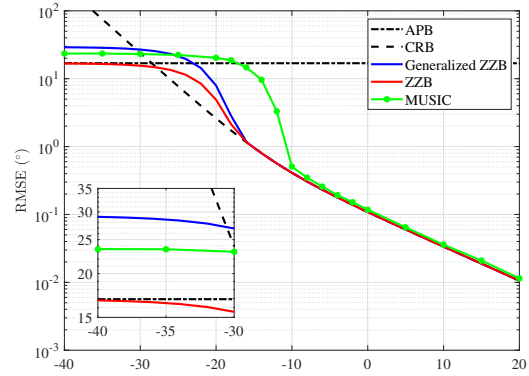


Figure 5.4 Comparison of bounds for multiple sources case ($K = 5$).

the APB in the *a priori* performance region and the CRB in the asymptotic region, respectively. Furthermore, the ZZB provides a tighter bound than the CRB outside the asymptotic region, and also predicts the threshold entering the asymptotic region for DOA estimation algorithms (e.g., MUSIC). On the contrary, since no *a priori* information is used, the CRB provides a loose bound outside the asymptotic region, and finally divergence exceeds the MSE of the MUSIC algorithm in the *a priori* performance region.

Then, we evaluate the derived ZZB under fully incoherent multiple sources assumption, where all K sources are assumed to have the same SNRs. It is observed from Fig. 5.4 that, both the generalized ZZB and the ZZB enter the asymptotic region at the same SNR, then keep consistent with the CRB in the asymptotic region. However, below the asymptotic region threshold, the generalized ZZB increases faster than the ZZB before entering the *a priori* performance region, and finally convergence exceeds the MSE of the MUSIC algorithm. The CRB still provides a loose bound in the transition region, and finally divergence exceeds the MSE of the MUSIC algorithm. On the contrary, benefited from the ratio κ (5-80) considering the ordering process required in multiple sources DOA estimation, the ZZB is consistently lower than the generalized ZZB outside the asymptotic region, and keeps valid to lower bound the MSE of the MUSIC algorithm in the *a priori* performance region. As analyzed, the ZZB converges to the APB in the *a priori* performance region. Hence, the ZZB provides a global lower bound tighter than the CRB for multiple sources DOA estimation. Furthermore, the asymptotic region threshold predicted by Fig. 5.4 appears at a lower SNR than that in Fig. 5.3, which is because

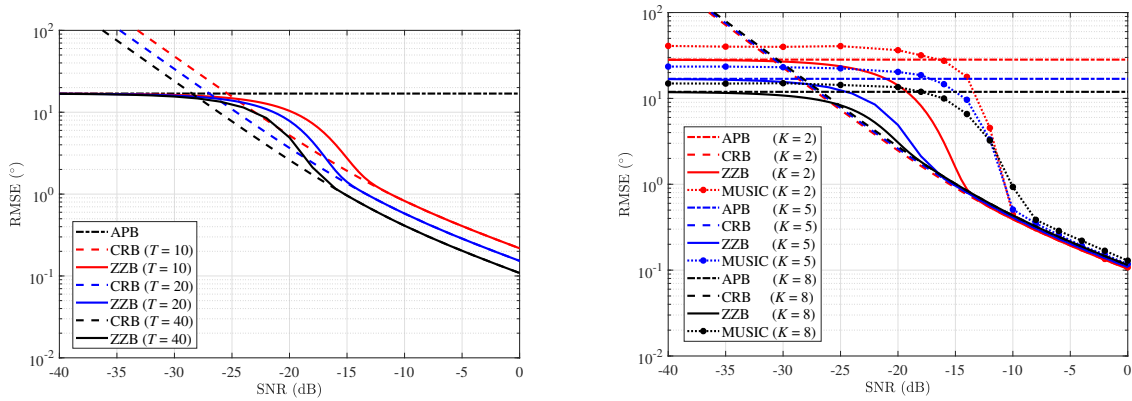


Figure 5.5 Effect of the number of snapshots on **Figure 5.6** Effect of the number of sources on ZZB. **ZZB.**

the coefficients $2P_L$ and $\Gamma_{\frac{3}{2}}(\tilde{u})$ respectively reach 0 and 1 more rapidly with K increasing.

In Fig. 5.5, we investigate the effect of the number of snapshots T on the ZZB, where the number of sources is fixed to $K = 5$. It is observed that, the ZZB converges to the APB in the *a priori* performance region regardless of the number of snapshots. This is because the MSE convergency in the *a priori* performance region only depends on the *a priori* distribution of DOAs and the number of sources. Nevertheless, we prefer more snapshots to bring the lower bound outside the *a priori* performance region, which implies the better estimation performance. Specifically, with the increase of T , the ZZB touches the CRB at a lower SNR, leading to a narrower transition region. Each double snapshots brings a fixed decrease of the threshold point, which helps to predict the asymptotic region threshold of the ZZB under different numbers of snapshots.

We then evaluate the effect of the number of sources K on the ZZB in Fig. 5.6. It is observed that, for different numbers of sources K , the ZZB always effectively lower bounds the corresponding MSE of the MUSIC algorithm, and respectively converges to the corresponding APB (5-82) in the *a priori* performance region and the CRB (5-85) in the asymptotic region. With the number of sources K increasing, the ZZB touches the corresponding CRB at a lower SNR, since the function $\Gamma_{\frac{3}{2}}(\tilde{u})$ w.r.t. K increases to 1 (i.e., ZZB converges to CRB) more rapidly. Meanwhile, the ZZB converges to a lower APB in the *a priori* performance region and a higher CRB in the asymptotic region, such that the difference between the ZZB and the cor-



responding CRB in the transition region becomes smaller. Even so, the ZZB always converges to the APB with SNR decreasing, while the CRB becomes invalid to evaluate the estimation performance of DOA estimator (e.g., MUSIC) in low SNR situation.

Now, we evaluate the ZZB for the hybrid coherent/incoherent multiple sources DOA estimation. We assume there are $K = 5$ sources, where the first $L = 3$ sources are mutually coherent with the coefficient $\beta = [1, 0.9e^{j\phi_1}, 0.8e^{j\phi_2}]$, whereas the last $K - L = 2$ sources are incoherent. Here, both ϕ_1 and ϕ_2 are random phases following a uniform distribution $\mathcal{U}[-\pi, \pi]$. In addition, we also plot the fully incoherent ZZB as a reference. For fair comparison, the SNRs of 5 sources in the fully incoherent case are $\eta_2 = |\beta_2|^2\eta_1$, $\eta_3 = |\beta_3|^2\eta_1$, $\eta_4 = \eta_5 = \eta_1$, respectively. It is observed from Fig. 5.7 that, both coherent ZZB and incoherent ZZB converge to the APB in the *a priori* performance region, which indicates that, whether coherent or not does not affect the ZZB there. On the other hand, coherent ZZB and incoherent ZZB converge to their corresponding CRBs in the asymptotic region. However, the coherent ZZB is lower than the incoherent ZZB in the transition region. The reason is that, the ZZB is a linear combination between the APB and the CRB, where the coefficient $2P_L$ in the coherent ZZB decreases from 1 more rapidly than that in the incoherent ZZB (as shown in Fig. 5.2), making the coherent ZZB decreases from the APB faster. Thus, the coherent ZZB is lower than the incoherent ZZB.

Then, we investigate the effect of the *a priori* distribution of DOAs on the ZZB for different numbers of sources. Considering that linear array does not perform well for DOAs estimation at directions close to the array endfires, actual array processing systems usually select a narrow field of view. It can be explained from the perspective of performance analysis that, the FIM \mathbf{J} at endfire DOAs close to $\pm 90^\circ$ becomes ill-conditioned, which makes the CRB invalid even in high SNR scenario. It is observed from Fig. 5.8 that, for the same number of sources K , the wider *a priori* distribution of DOAs $\mathcal{U}[-85^\circ, 85^\circ]$ leads to the larger ZZB due to the larger CRB and APB. On the other hand, with the number of sources increasing, the gap of ZZBs between the narrow *a priori* distribution of DOAs $\mathcal{U}[-60^\circ, 60^\circ]$ and the wide *a priori* distribution of DOAs $\mathcal{U}[-85^\circ, 85^\circ]$ becomes larger in the asymptotic region. The reason is that, it is of higher probability that more signals impinge from outside of $[-60^\circ, 60^\circ]$ simultaneously, which makes the estimation accuracy even worse due to the smaller effective array aperture.

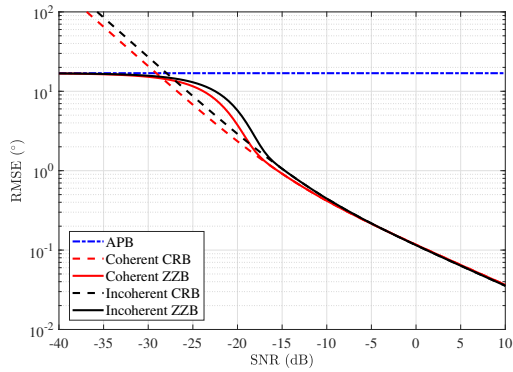


Figure 5.7 Effect of the mutual coherence on ZZB.

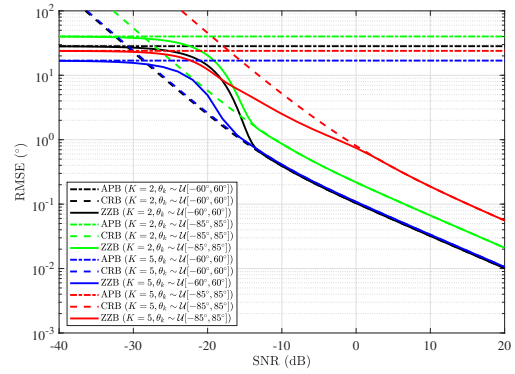


Figure 5.8 Effect of the *a priori* distribution of DOAs on ZZB.

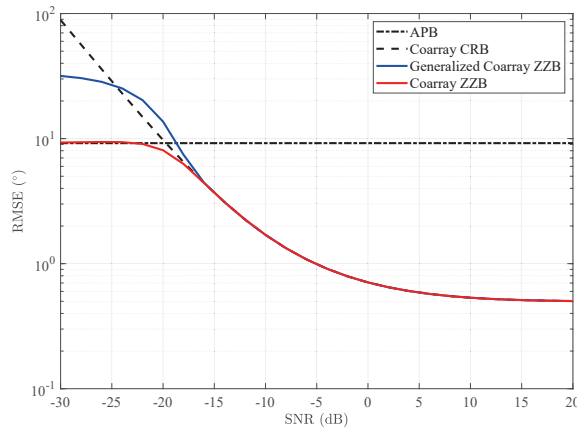


Figure 5.9 ZZB for underdetermined DOA estimation.

In addition to the overdetermined DOA estimation, the ZZB is also appropriate for the underdetermined DOA estimation by incorporating the coarray Fisher information (5-94). Here, we adopt a (3, 5) pair coprime linear array (the number of array sensors $M = 2 \times 3 + 5 - 1 = 10$) [146], [147] to estimate $K = 11$ sources following the same *a priori* distribution $\mathcal{U}[-60^\circ, 60^\circ]$ with the minimum interval of 5° . Both the coarray CRB [9] and the generalized coarray ZZB are plotted for a comparison. All the sources are assumed to be fully incoherent with the same SNR. It is observed from Fig. 5.9 that, the coarray ZZB converges to the coarray CRB in the asymptotic region, and also flattens out as analyzed when the SNR gets higher. On the other hand, the coarray ZZB converges to the APB as predicted in the *a priori* performance region. Hence, the ZZB also provides a unified bound for underdetermined DOA estimation from the *a priori* performance region to the asymptotic region.



5.5 Summary

In this chapter, we derived an explicit ZZB for hybrid coherent/incoherent multiple sources DOA estimation. Different from the single source DOA estimation, the ordering process for eliminating permutation ambiguity during MSE calculation of multiple sources DOA estimation makes the generalized ZZB invalid outside the asymptotic region. Hence, we for the first time introduced the order statistics to describe the effect of the ordering process on the ZZB, which kept it global tight for evaluating multiple sources DOA estimation. The derived ZZB for the first time revealed the relationship between the MSE convergency and the number of sources, regardless of the number of snapshots and array configuration. Simulation results demonstrate the advantages of the ZZB over the CRB in a wide range of SNR for multiple sources DOA estimation. It is also noted that, in the transition region, the ZZB may be affected by Fisher information when two sources are closely located, which will be further studied in our future work. Finally, we believe the basic conclusions observed in this chapter are valid for other multiple sources parameter estimation problems with permutation ambiguity including range, velocity, and so on.



Chapter 6. ZZB for 2D DOAs Estimation

In multi-source 2D DOA estimation, the essential matching process between the estimated and the true DOAs in the MSE calculation is often based on minimum Euclidean distance criterion, which is substantially different from 1D DOA estimation that is based on simple ordering process. Hence, the ZZB for multi-source 2D DOA estimation is not the extension of that for 1D DOA estimation provided in existing work. Facing this problem, we analyze the effect of the minimum Euclidean distance criterion on the ZZB via the stochastic Euclidean bipartite matching problem, from which we derive a globally valid ZZB with closed-form solution for multi-source 2D DOA estimation. The derived ZZB outperforms the most commonly used CRB. In addition to the hybrid coherent/uncorrelated multi-source model, we consider the partially correlated multi-source model into the ZZB derivation and formulate the ZZB as an explicit function of the correlation coefficient matrix for the first time. Moreover, according to the matching process based on minimum Euclidean distance criterion, separately estimating azimuth/elevation from 2D DOA model is a new scenario that is different from 1D DOA estimation, such that we first derive the ZZB for azimuth/elevation estimation from 2D DOA model by adopting different weight vectors. Simulation results demonstrate the advantages of the derived ZZB over the widely-accepted CRB.

6.1 Introduction

2D DOA estimation is a typical problem in radar, sonar, navigation, and wireless communications [2], [148]. Many estimation algorithms have been generalized from 1D to 2D DOA estimation in the past few decades. To name a few, subspace-based algorithms like MUSIC [127]–[129], [149], [150] and ESPRIT [130]–[132], sparse reconstruction-based algorithms [133]–[135], [147], [151]–[153], and machine learning-based algorithms [136]–[138].

MSE is commonly used to evaluate the estimation accuracy, which, however, does not have an exact closed-form minimum solution. Hence, lower bound on MSE [3] is a powerful tool that has received extensive attention over the past half-century. The CRB [5] is the most well-



accepted one benefiting from the easy derivation and asymptotic tightness. Specifically, [6], [7] provide the explicit CRB for both conditional and unconditional DOA estimation. However, it is well known that, the CRB is derived from the inverse of the Fisher information that only captures the small estimation error. Then, the conventional CRB is a local bound and does not provide effective estimation performance evaluation in the non-asymptotic region. Considering that the MSE convergence is related to the *a priori* distribution of the parameters in extremely low SNR situation (also called *a priori* performance region), Bayesian bounds have been proposed in the past few decades (see, [3] and the references therein), which successfully utilize the *a priori* distribution of parameters to provide global bounds. As one typical class of Bayesian bounds, covariance inequality-based Bayesian bounds [2], [38], [39], [42], [44], [45] incorporate the *a priori* information of the estimated parameter into non-Bayesian bounds to pursue global tightness, which, however, rely on the tradeoff between computational burden and the tightness in the non-asymptotic region [3], i.e., tighter expressions depend on higher order derivative, empirical test point selection in higher dimension, and the optimization over higher-dimensional free variables.

Different from covariance inequality-based Bayesian bounds, ZZB provides a global bound by exploiting the relationship between the lower bound on MSE and the minimum probability of error of a binary hypothesis testing problem. A scalar ZZB for time delay estimation with uniform *a priori* distribution is derived in [54]–[56]. Then, [57] extends the scalar ZZB to the vector ZZB and proposes a general ZZB expression for vector parameter estimation problem. According to these general derivation frameworks, ZZB have been considered in numerous specific parameter estimation problems [58], [61], [62], [64], [66]–[69], [72], [81]–[83], [115], [139]. Specifically, [68], [69] provide the ZZB for single source 1D DOA estimation with linear array. [58] incorporates the vector ZZB into the 2D DOA estimation and provides an explicit ZZB for single source 2D DOA estimation. In [72], the ZZB is extended from single source 1D DOA estimation to multi-source estimation. To analyze how the commonly used ordering process applicable to both estimated and true DOAs in the MSE calculation affects the ZZB, the authors first incorporated the order statistics into the ZZB derivation and provided a global tight ZZB for 1D DOA estimation, for both overdetermined estimation and underdetermined



estimation. Although the ordering process in 1D DOA estimation successfully eliminates the permutation ambiguity arising in the output of the estimated DOAs, realizes the matching between the estimated and the true DOAs, and guarantees the correct MSE result in the asymptotic region, it is inappropriate for 2D DOA estimation problem. The reason is that, in 2D DOA estimation, the matching process arises on 2D azimuth-elevation plane, such that the matching process have to be performed according to the minimum Euclidean distance criterion rather than an ordering process along the azimuth or the elevation axis. Hence, the order statistics for analyzing the effect of the matching process on the ZZB is invalid in 2D DOA estimation problem, indicating that the ZZB for 2D DOA estimation is not the extension of 1D DOA estimation scenario. The main challenge is that how the matching process based on the minimum Euclidean distance criterion affects the ZZB is still unclear. Moreover, in 2D DOA estimation problem, it is a common case of evaluating the performance of azimuth/elevation estimation separately. Even if it is a 1D DOA estimation under 2D DOA model, it is still inappropriate to use the ZZB in [72] because we have to perform the matching process based on minimum Euclidean distance criterion before calculating the MSE of azimuth/elevation estimation. Obviously, under 2D DOA estimation, there is no valid ZZB for azimuth/elevation estimation yet. Besides, [72] only considers a hybrid coherent/uncorrelated multi-source model, and does not consider the existence of partially correlated sources.

In this chapter, we derive an explicit ZZB for multi-source 2D DOA estimation, where the partially correlated sources are first considered in the signal model in addition to the hybrid coherent/uncorrelated multiple sources. The ZZB is explicitly generalized from single source to multi-source 2D DOA estimation, and then we analyze how the matching process between the estimated and the true DOAs according to the minimum Euclidean distance criterion affects the ZZB. We analyze this effect by resorting to a stochastic EBMP. By incorporating the minimum of the cost function of stochastic EBMP into the ZZB methodology, we provide a global valid ZZB for multi-source 2D DOA estimation from the non-asymptotic region to the asymptotic region. To the best of our knowledge, the derived ZZB is formulated as an explicit function of the correlation coefficient matrix for the first time. Moreover, the derived ZZB is a general expression that does not depend on the specific 2D array manifold. Considering that evaluat-



ing the performance of azimuth/elevation estimation separately from 2D DOA model is also a common scenario, we also provide two approaches to derive the ZZB on the azimuth/elevation estimation by adopting different weight vectors. Simulations demonstrate that the derived ZZB provides a global bound and outperforms the CRB. Moreover, the simulation result shows that, adopting the weight vector aiming at the azimuth/elevation estimation produces a tighter ZZB than partitioning the ZZB for joint 2D DOAs estimation. The main contributions of this chapter are:

- By analyzing the effect of the minimum Euclidean criterion on the ZZB with the formulated stochastic EBMP, we provide the explicit ZZB solution for multi-source 2D DOA estimation, which is a global valid bound in both the non-asymptotic region and the asymptotic region.
- We also derive the ZZB with closed-form solution for azimuth/elevation separate estimation from 2D DOA model by adopting different weight vectors, demonstrating the effect of the weight vector selection on the resulting ZZB in azimuth/elevation estimation for the first time.
- We incorporate the correlation coefficient matrix into the ZZB derivation framework and formulate the ZZB as the function of the correlation coefficient matrix, revealing the relationship between the correlation and the ZZB for the first time.

The rest of this chapter is organized as follows. We introduce a general multi-source model with coherent, partially correlated and uncorrelated sources in Sect. 6.2, where the fundamental of MSE and CRB are also briefly introduced. In Sect. 6.3, we derive the explicit ZZB for multi-source 2D DOA estimation. In Sect. 6.4, simulations demonstrate the advantages of the ZZB over the CRB. Finally, we draw our conclusions in Sect. 6.5.

6.2 Signal Model, MSE and CRB

We consider a general 2D array \mathbb{S} with M sensors located at $\mathbb{S} = \{(x_1, y_1), \dots, (x_M, y_M)\}$. Assume that there are K far-field narrowband signals impinging on the array \mathbb{S} from DOAs



$\{(\phi_k, \theta_k) | k = 1, 2, \dots, K\}$. Without loss of generality, the first K_{coh} sources are mutually coherent, the next K_{cor} sources are partially correlated, and the last K_{un} sources are uncorrelated with each other. Hence, we have $K = K_{\text{coh}} + K_{\text{cor}} + K_{\text{un}}$ and assume that three sets of sources are mutually independent of each other. Then, we make some assumptions on the DOAs as follows.

Assumption 6.2.1. *All the signals impinge on the array from different directions (say, $\nexists i \neq j$, $\phi_i = \phi_j$ and $\theta_i = \theta_j$).*

Assumption 6.2.2. *Each azimuth/elevation follows a uniform distribution $\phi_k \sim \mathcal{U}[\varphi_{\min}, \varphi_{\max}]$ and $\theta_k \sim \mathcal{U}[\vartheta_{\min}, \vartheta_{\max}]$, $\forall k = 1, 2, \dots, K$.*

We can obtain the T -snapshots array observation data matrix $\mathbf{Z} = [\mathbf{z}(1), \dots, \mathbf{z}(T)] \in \mathbb{C}^{M \times T}$, where

$$\begin{aligned} \mathbf{z}(t) &= \sum_{k=1}^{K_{\text{coh}}} \mathbf{a}(\phi_k, \theta_k) \beta_k s_1(t) + \sum_{k=K_{\text{coh}}+1}^K \mathbf{a}(\phi_k, \theta_k) s_k(t) + \mathbf{n}(t) \\ &= \mathbf{A}(\boldsymbol{\phi}, \boldsymbol{\theta}) \mathbf{s}(t) + \mathbf{n}(t), t = 1, 2, \dots, T \end{aligned} \quad (6-1)$$

is the array received signal observed from the t -th snapshot. Here, $\mathbf{A}(\boldsymbol{\phi}, \boldsymbol{\theta}) = [\mathbf{a}(\phi_1, \theta_1), \dots, \mathbf{a}(\phi_K, \theta_K)] \in \mathbb{C}^{M \times K}$ is the steering matrix with $\boldsymbol{\phi} = [\phi_1, \phi_2, \dots, \phi_K]^T \in \mathbb{R}^K$ and $\boldsymbol{\theta} = [\theta_1, \theta_2, \dots, \theta_K]^T \in \mathbb{R}^K$ respectively denoting the azimuth and elevation of the K sources. $\mathbf{a}(\phi_k, \theta_k)$ represents the steering vector of the k -th source whose specific expression depends on the array manifold. $\mathbf{s}(t) = [\boldsymbol{\beta}^T s_1(t), s_{K_{\text{coh}}+1}(t), \dots, s_K(t)]^T \in \mathbb{C}^K$ contains K signal waveforms, where $\boldsymbol{\beta} = [\beta_1, \dots, \beta_{K_{\text{coh}}}]^T \in \mathbb{C}^{K_{\text{coh}}}$ denotes the K_{coh} coherent coefficients w.r.t. the reference signal $s_1(t)$. $\mathbf{n}(t)$ is the complex-valued zero-mean white Gaussian noise following $\mathbf{n}(t) \sim \mathcal{CN}(\mathbf{0}_M, \sigma_n^2 \mathbf{I}_M)$ with σ_n^2 denoting the noise power. According to the widely used unconditional model [7], we assume:

Assumption 6.2.3. *All the signals $s_k(t)$, $k = 1, \dots, K$, are sampled from zero-mean, stationary complex Gaussian stochastic processes.*



Thus, the theoretical covariance matrix of the array received signal $\mathbf{z}(t)$ is

$$\mathbf{R}_{zz} = \mathbb{E} \{ \mathbf{z}(t) \mathbf{z}^H(t) \} = \mathbf{A}(\boldsymbol{\phi}, \boldsymbol{\theta}) \boldsymbol{\Sigma} \mathbf{A}^H(\boldsymbol{\phi}, \boldsymbol{\theta}) + \sigma_n^2 \mathbf{I}_M, \quad (6-2)$$

where

$$\boldsymbol{\Sigma} = \mathbb{E} \{ \mathbf{s}(t) \mathbf{s}^H(t) \} = \text{block diag} [\boldsymbol{\Sigma}_{\text{coh}}, \boldsymbol{\Sigma}_{\text{cor}}, \boldsymbol{\Sigma}_{\text{un}}] \quad (6-3)$$

is the covariance matrix of $\mathbf{s}(t)$. Here,

$$\boldsymbol{\Sigma}_{\text{coh}} = \boldsymbol{\beta} \boldsymbol{\beta}^H \sigma_1^2 \quad (6-4)$$

denotes the rank-one covariance matrix corresponding to the K_{coh} coherent sources with σ_1^2 denoting the power of the first source,

$$\boldsymbol{\Sigma}_{\text{cor}} = \mathbf{V}^{\frac{1}{2}} \mathbf{C} \mathbf{V}^{\frac{1}{2}} \quad (6-5)$$

is the full-rank and non-diagonal covariance matrix corresponding to the K_{cor} partially correlated sources with

$$\mathbf{V} = \text{diag} [\sigma_{K_{\text{coh}}+1}^2, \dots, \sigma_{K_{\text{coh}}+K_{\text{cor}}}^2] \quad (6-6)$$

containing the power of the K_{cor} correlated sources and $\mathbf{C} \in \mathbb{R}^{K_{\text{cor}} \times K_{\text{cor}}}$ denoting the correlation coefficient matrix, and

$$\boldsymbol{\Sigma}_{\text{un}} = \text{diag} [\sigma_{K_{\text{coh}}+K_{\text{cor}}+1}^2, \dots, \sigma_K^2] \quad (6-7)$$

represents the diagonal covariance matrix of the K_{un} uncorrelated sources consisting of the power of the K_{un} sources.

As a widely used metric to evaluate the parameter estimation accuracy, MSE in 2D DOA estimation is defined as

$$\begin{aligned} \text{MSE}_{\boldsymbol{\xi}} &= \frac{1}{2K} \sum_{k=1}^K \mathbb{E} \left\{ \left(\hat{\phi}_k - \phi_k \right)^2 + \left(\hat{\theta}_k - \theta_k \right)^2 \right\} \\ &= \frac{1}{2K} \text{Tr} \{ \mathbf{R}_{\boldsymbol{\epsilon}} \}, \end{aligned} \quad (6-8)$$



where $\hat{\phi}_k$ and $\hat{\theta}_k$ are respectively the estimates of ϕ_k and θ_k . Obviously, the MSE definition (6-8) implies:

Assumption 6.2.4. *All the parameters in ξ are equally weighted in MSE calculation.*

The classical CRB is a well known lower bound for evaluating the asymptotic MSE performance of any unbiased estimator. It is obtained from the inverse of the FIM. For T independent and identically distributed snapshots, the (m, n) -th entry of the FIM \mathbf{J} w.r.t. ξ under zero-mean Gaussian unconditional model is given by [2]

$$\mathbf{J}_{mn} = T \text{Tr} \left\{ \frac{\partial \mathbf{R}_{zz}}{\partial \xi_m} \mathbf{R}_{zz}^{-1} \frac{\partial \mathbf{R}_{zz}}{\partial \xi_n} \mathbf{R}_{zz}^{-1} \right\}. \quad (6-9)$$

Accordingly, \mathbf{J} can be partitioned into blocks as

$$\mathbf{J} = \begin{bmatrix} \mathbf{J}_{\phi\phi} & \mathbf{J}_{\phi\theta} \\ \mathbf{J}_{\theta\phi} & \mathbf{J}_{\theta\theta} \end{bmatrix}. \quad (6-10)$$

Here, the diagonal blocks $\mathbf{J}_{\phi\phi}$ and $\mathbf{J}_{\theta\theta}$ are respectively the FIM w.r.t. the azimuth ϕ and the elevation θ , and the off-diagonal blocks $\mathbf{J}_{\phi\theta}$ and $\mathbf{J}_{\theta\phi}$ reflect the coupling between azimuth ϕ and elevation θ .

6.3 ZZB Derivation for 2D DOAs Estimation

In this section, we derive the ZZB for 2D DOAs estimation, where the derived ZZB is formulated as the function of correlation coefficient matrix. In subsection 6.3.1, we extend the ZZB derivation from multi-source 1D DOA estimation [72] to multi-source 2D DOA estimation without considering the effect of the matching process between the estimated and the true DOAs on the ZZB derivation. Similar to 1D DOA estimation scenario, the effect of the matching process on the ZZB must be taken into account. However, in 2D DOA estimation problem, the matching process follows the minimum Euclidean distance criterion and cannot be extended from the 1D DOA scenario. Thus, we incorporate stochastic EBMP into ZZB derivation framework and provide the ZZB with closed-form solution in subsection 6.3.2. Besides the ZZB



for multi-source 2D DOA estimation, we also provides closed-form ZZB for azimuth/elevation separate estimation under 2D DOA estimation scenario.

In 2D DOA estimation problem, the general ZZB expression without valley filling function becomes

$$\mathbf{w}^T \mathbf{R}_\epsilon \mathbf{w} \geq \frac{1}{2} \int_0^\infty \max_{\delta: \mathbf{w}^T \delta = h} \left[\int_{\mathbb{R}^{2K}} (f_\xi(\boldsymbol{\psi}) + f_\xi(\boldsymbol{\psi} + \boldsymbol{\delta})) P_{\min}(\boldsymbol{\psi}, \boldsymbol{\psi} + \boldsymbol{\delta}) d\boldsymbol{\psi} \right] h dh,$$

According to Assumption 6.2.4, the weight vector \mathbf{w} for 2D DOA estimation becomes

$$\mathbf{w} = \frac{1}{\sqrt{2K}} \mathbf{1}_{2K}, \quad (6-11)$$

and (6-11) correspondingly becomes

$$\begin{aligned} & \frac{1}{2K} \mathbf{1}_{2K}^T \mathbf{R}_\epsilon \mathbf{1}_{2K} \\ & \geq \frac{1}{2} \int_0^\infty \max_{\delta: \mathbf{1}_{2K}^T \delta = \sqrt{2K}h} \left[\int_{\mathbb{R}^{2K}} (f_\xi(\boldsymbol{\psi}) + f_\xi(\boldsymbol{\psi} + \boldsymbol{\delta})) P_{\min}(\boldsymbol{\psi}, \boldsymbol{\psi} + \boldsymbol{\delta}) d\boldsymbol{\psi} \right] h dh. \end{aligned} \quad (6-12)$$

Different from the 1D DOA estimation in [72], the dimension of weight vector here equals the number of estimated parameters $2K$ rather than the number of sources K , since there are two parameters to be estimated simultaneously for each source.

When we estimate azimuth or elevation separately, the weight vector can be

$$\mathbf{w} = \left[\frac{1}{\sqrt{K}} \mathbf{1}_K^T, \mathbf{0}_K^T \right]^T \quad (6-13)$$

for azimuth estimation and

$$\mathbf{w} = \left[\mathbf{0}_K^T, \frac{1}{\sqrt{K}} \mathbf{1}_K^T \right]^T \quad (6-14)$$

for elevation estimation. Correspondingly, the general ZZB expressions can be obtained by substituting (6-13) and (6-14) into (6-11).

For single source case, the parameter vector is $\boldsymbol{\xi} = [\phi, \theta]^T$, and the corresponding ZZB has been derived in [58]. Although the expression in (6-12) is similar to the ZZB for 1D DOA



estimation [72], further investigation is necessary to derive explicit ZZB expression for multiple sources 2D DOA estimation. The reason is that, we cannot straightforwardly treat the ZZB for K -sources 2D DOA estimation as $2K$ -sources 1D DOA estimation problem, although the number of estimated parameters is the same. For 1D DOA estimation, all the DOAs are independent and homogenous, which allows us to introduce the order statistics into the ZZB derivation, to make it tight in the *a priori* performance region [72]. However, in the 2D case, the azimuth and elevation for the same source must be paired before MSE calculation, making the order statistics in [72] for ZZB derivation infeasible.

6.3.1 ZZB derivation for independent DOAs

Different from [72], here we provide the ZZB for hybrid coherent, correlated, and uncorrelated multiple sources under 2D DOA estimation scenario.

For the observation data matrix \mathbf{Z} , the lower bound for $P_{\min}(\boldsymbol{\varphi}, \boldsymbol{\varphi} + \boldsymbol{\delta})$ is given in [143]

$$P_{\min}(\boldsymbol{\psi}, \boldsymbol{\psi} + \boldsymbol{\delta}) \geq P(\boldsymbol{\delta}) = e^{\left[\mu(p; \boldsymbol{\delta}) + \frac{1}{8} \frac{\partial^2 \mu(p; \boldsymbol{\delta})}{\partial p^2} \right]} \mathcal{Q} \left(\frac{1}{2} \sqrt{\frac{\partial^2 \mu(p; \boldsymbol{\delta})}{\partial p^2}} \right) \Bigg|_{p=\frac{1}{2}}, \quad (6-15)$$

where

$$\mu(p; \boldsymbol{\delta}) = \ln \int f(\mathbf{Z}|\boldsymbol{\psi} + \boldsymbol{\delta})^p f(\mathbf{Z}|\boldsymbol{\psi})^{1-p} d\mathbf{Z} \quad (6-16)$$

is the semi-invariant moment generating function, where the explicit expression has been given in [143]

$$\mu(p; \boldsymbol{\delta}) = T \left[p \ln |\mathbf{R}_{zz|\mathcal{H}_0}| + (1-p) \ln |\mathbf{R}_{zz|\mathcal{H}_1}| - \ln |p\mathbf{R}_{zz|\mathcal{H}_0} + (1-p)\mathbf{R}_{zz|\mathcal{H}_1}| \right], \quad (6-17)$$

where $\mathbf{R}_{zz|\mathcal{H}_0}$ and $\mathbf{R}_{zz|\mathcal{H}_1}$ denote the covariance matrix \mathbf{R}_{zz} under the hypothesis \mathcal{H}_0 and \mathcal{H}_1 , respectively. Accordingly, given $p = \frac{1}{2}$, it is easy to derive that

$$\mu(p; \boldsymbol{\delta}) \Big|_{p=\frac{1}{2}} = T \left[\frac{\ln (|\mathbf{R}_{zz|\mathcal{H}_0}| |\mathbf{R}_{zz|\mathcal{H}_1}|)}{2} - \ln \left| \frac{\mathbf{R}_+}{2} \right| \right], \quad (6-18)$$



and

$$\left. \frac{\partial^2 \mu(p; \boldsymbol{\delta})}{\partial p^2} \right|_{p=\frac{1}{2}} = 4T \text{Tr} \left\{ (\mathbf{R}_+^{-1} \mathbf{R}_-)^2 \right\}, \quad (6-19)$$

where $\mathbf{R}_+ = \mathbf{R}_{zz|\mathcal{H}_0} + \mathbf{R}_{zz|\mathcal{H}_1}$ and $\mathbf{R}_- = \mathbf{R}_{zz|\mathcal{H}_0} - \mathbf{R}_{zz|\mathcal{H}_1}$.

By performing the second-order Taylor series expansion around the point $\boldsymbol{\delta} \approx \mathbf{0}_{2K}$, the $\mu(p; \boldsymbol{\delta})|_{p=\frac{1}{2}}$ and $\left. \frac{\partial^2 \mu(p; \boldsymbol{\delta})}{\partial p^2} \right|_{p=\frac{1}{2}}$ can be expressed with the FIM as

$$\mu(p; \boldsymbol{\delta})|_{p=\frac{1}{2}} \approx -\frac{1}{8} \boldsymbol{\delta}^T \mathbf{J} \boldsymbol{\delta}, \quad (6-20)$$

and

$$\left. \frac{\partial^2 \mu(p; \boldsymbol{\delta})}{\partial p^2} \right|_{p=\frac{1}{2}} \approx \boldsymbol{\delta}^T \mathbf{J} \boldsymbol{\delta}. \quad (6-21)$$

Thus, we have $P(\boldsymbol{\delta}) \approx P_S(\boldsymbol{\delta})$ around the point $\boldsymbol{\delta} \approx \mathbf{0}_{2K}$ by substituting (6-20) and (6-21) into (6-15), where

$$P_S(\boldsymbol{\delta}) = \mathcal{Q} \left(\frac{1}{2} \sqrt{\boldsymbol{\delta}^T \mathbf{J} \boldsymbol{\delta}} \right), \quad (6-22)$$

Obviously, $P(\boldsymbol{\delta}) \approx P_S(\boldsymbol{\delta})$ only occurs in a small region Δ around the point $\mathbf{0}_{2K}$ due to the Taylor expansion. When $\boldsymbol{\delta}$ is outside the region, (6-18) can be approximated as

$$\begin{aligned} \mu(p; \boldsymbol{\delta})|_{p=\frac{1}{2}} &\approx T \ln \frac{\left| \mathbf{I}_K + \frac{M}{\sigma_n^2} \boldsymbol{\Sigma} \right|}{\left| \mathbf{I}_{2K} + \frac{M}{2\sigma_n^2} \mathbf{D} \right|} \\ &= T (g_{\text{coh}} + g_{\text{cor}} + g_{\text{un}}) \end{aligned} \quad (6-23)$$

by adopting the Sylvester's determinant theorem and the approximations

$$\mathbf{A}^H(\boldsymbol{\psi}) \mathbf{A}(\boldsymbol{\psi}) \approx M \mathbf{I}_K \quad (6-24)$$

and

$$\mathbf{A}^H(\boldsymbol{\psi}) \mathbf{A}(\boldsymbol{\psi} + \boldsymbol{\delta}) \approx \mathbf{0}_K. \quad (6-25)$$

Here,

$$\mathbf{D} = \text{block diag}[\boldsymbol{\Sigma}, \boldsymbol{\Sigma}], \quad (6-26)$$



$$g_{\text{coh}} = \ln \frac{4(1 + M\|\boldsymbol{\beta}\|_2^2\eta_1)}{(2 + M\|\boldsymbol{\beta}\|_2^2\eta_1)^2}, \quad (6-27)$$

$$g_{\text{cor}} = \ln \frac{|\mathbf{I}_{K_{\text{cor}}} + M\mathbf{C}\bar{\mathbf{V}}|}{|\mathbf{I}_{K_{\text{cor}}} + \frac{M}{2}\mathbf{C}\bar{\mathbf{V}}|^2}, \quad (6-28)$$

and

$$g_{\text{un}} = \sum_{k=K_{\text{coh}}+K_{\text{cor}}+1}^K \ln \frac{4(1 + M\eta_k)}{(2 + M\eta_k)^2}, \quad (6-29)$$

where $\eta_k = \frac{\sigma_k^2}{\sigma_n^2}$ is the SNR of the k -th source, and

$$\bar{\mathbf{V}} = \text{diag} [\eta_{K_{\text{coh}}+1}, \dots, \eta_{K_{\text{coh}}+K_{\text{cor}}}] \quad (6-30)$$

contains the SNRs η_k ($k = K_{\text{coh}} + 1, \dots, K_{\text{coh}} + K_{\text{cor}}$) of the K_{cor} correlated sources.

Then, according to the approximation (6-24) and (6-25), \mathbf{R}_+^{-1} in (6-19) can be approximated as

$$\mathbf{R}_+^{-1} \approx \frac{1}{2\sigma_n^2}\mathbf{I}_M - \frac{1}{4\sigma_n^4}\mathbf{B}\mathbf{D}\mathbf{Y}\mathbf{B}^H, \quad (6-31)$$

where

$$\mathbf{Y} = \left(\mathbf{I}_{2K} + \frac{M}{2\sigma_n^2}\mathbf{D} \right)^{-1} = \text{block diag}[\mathbf{Y}_{\text{coh}}, \mathbf{Y}_{\text{cor}}, \mathbf{Y}_{\text{un}}, \mathbf{Y}_{\text{coh}}, \mathbf{Y}_{\text{cor}}, \mathbf{Y}_{\text{un}}]. \quad (6-32)$$

Here,

$$\mathbf{Y}_{\text{coh}} = \mathbf{I}_{\text{coh}} - \frac{M\eta_1}{2 + M\|\boldsymbol{\beta}\|_2^2\eta_1}\boldsymbol{\beta}\boldsymbol{\beta}^H, \quad (6-33)$$

$$\mathbf{Y}_{\text{cor}} = \left(\mathbf{I}_{K_{\text{cor}}} + \frac{M}{2}\bar{\mathbf{V}}^{\frac{1}{2}}\mathbf{C}\bar{\mathbf{V}}^{\frac{1}{2}} \right)^{-1} \quad (6-34)$$

$$\mathbf{Y}_{\text{un}} = \text{diag} \left[\left(1 + \frac{M\eta_{K_{\text{coh}}+K_{\text{cor}}+1}}{2} \right)^{-1}, \dots, \left(1 + \frac{M\eta_K}{2} \right)^{-1} \right]. \quad (6-35)$$



Accordingly, (6-19) is approximated as

$$\left. \frac{\partial^2 \mu(p; \boldsymbol{\delta})}{\partial p^2} \right|_{p=\frac{1}{2}} \approx \frac{TM^2}{\sigma_n^4} \text{Tr} \left\{ \mathbf{D}^2 - \frac{M}{\sigma_n^2} \mathbf{D}^3 \mathbf{Y} + \frac{M^2}{4\sigma_n^4} \mathbf{D}^4 \mathbf{Y}^2 \right\}, \quad (6-36)$$

where

$$\text{Tr}\{\mathbf{D}^2\} = 2\|\boldsymbol{\beta}\|_2^4 \sigma_1^4 + 2\text{Tr}\{(\mathbf{C}\mathbf{V})^2\} + \sum_{k=K_{\text{coh}}+K_{\text{cor}}+1}^K 2\sigma_k^4, \quad (6-37)$$

$$\text{Tr}\{\mathbf{D}^3 \mathbf{Y}\} = \frac{4\|\boldsymbol{\beta}\|_2^6 \sigma_1^6}{2 + M\|\boldsymbol{\beta}\|_2^2 \eta_1} + 4\text{Tr} \left\{ (\mathbf{C}\mathbf{V})^3 (2\mathbf{I}_{K_{\text{cor}}} + M\mathbf{C}\bar{\mathbf{V}})^{-1} \right\} + \sum_{k=K_{\text{coh}}+K_{\text{cor}}+1}^K \frac{4\sigma_k^6}{2 + M\eta_k}, \quad (6-38)$$

and

$$\text{Tr}\{\mathbf{D}^4 \mathbf{Y}^2\} = \frac{8\|\boldsymbol{\beta}\|_2^8 \sigma_1^8}{(2 + M\|\boldsymbol{\beta}\|_2^2 \eta_1)^2} + 8\text{Tr} \left\{ (\mathbf{C}\mathbf{V})^4 (2\mathbf{I}_{K_{\text{cor}}} + M\mathbf{C}\bar{\mathbf{V}})^{-2} \right\} + \sum_{k=L+1}^K \frac{8\sigma_k^8}{(2 + M\eta_k)^2}. \quad (6-39)$$

Thus, (6-36) becomes

$$\left. \frac{\partial^2 \mu(p; \boldsymbol{\delta})}{\partial p^2} \right|_{p=\frac{1}{2}} \approx 8T (l_{\text{coh}} + l_{\text{cor}} + l_{\text{un}}), \quad (6-40)$$

where

$$l_{\text{coh}} = \left(\frac{M\|\boldsymbol{\beta}\|_2^2 \eta_1}{2 + M\|\boldsymbol{\beta}\|_2^2 \eta_1} \right)^2, \quad (6-41)$$

$$l_{\text{cor}} = \text{Tr} \left\{ (M\mathbf{C}\bar{\mathbf{V}})^2 (2\mathbf{I}_{K_{\text{cor}}} + M\mathbf{C}\bar{\mathbf{V}})^{-2} \right\}, \quad (6-42)$$

and

$$l_{\text{un}} = \sum_{k=K_{\text{coh}}+K_{\text{cor}}+1}^K \left(\frac{M\eta_k}{2 + M\eta_k} \right)^2. \quad (6-43)$$

Here, $\left. \frac{\partial^2 \mu(p; \boldsymbol{\delta})}{\partial p^2} \right|_{p=\frac{1}{2}}$ is a function of the correlation coefficient matrix \mathbf{C} , in addition to the SNRs of the K sources, the number of snapshots T , the number of array elements M and the coherent coefficient $\boldsymbol{\beta}$ that has been considered in [72]. Accordingly, by substituting (6-23) and (6-40)



into (6-15), we have $P(\boldsymbol{\delta}) \approx P_L$ when $\boldsymbol{\delta}$ is far away from the point $\mathbf{0}_{2K}$, where

$$P_L = e^{T(g_{\text{coh}}+g_{\text{cor}}+g_{\text{un}}+l_{\text{coh}}+l_{\text{cor}}+l_{\text{un}})} \mathcal{Q}\left(\sqrt{2T(l_{\text{coh}}+l_{\text{cor}}+l_{\text{un}})}\right). \quad (6-44)$$

Accordingly, $P(\boldsymbol{\delta})$ in (6-15) becomes

$$P(\boldsymbol{\delta}) \approx \begin{cases} P_S(\boldsymbol{\delta}), & \boldsymbol{\delta} \in \Delta \\ P_L, & \boldsymbol{\delta} \notin \Delta \end{cases} \quad (6-45)$$

with

$$\Delta = \{\boldsymbol{\delta} : \boldsymbol{\delta}^T \mathbf{J} \boldsymbol{\delta} \leq 8T(l_{\text{coh}}+l_{\text{cor}}+l_{\text{un}})\} \quad (6-46)$$

denoting the region w.r.t. $\boldsymbol{\delta}$.

It should be noted that, here we introduce partially correlated signal model into the derivation, and formulate the ZZB as an explicit function of the correlation coefficient matrix. Besides, ZZB methodology successfully establishes the relationship between the minimum probability of error of the binary hypothesis testing problem (2-4) and the lower bound on MSE, i.e., the bound is obtained via integrating the $P_{\min}(\boldsymbol{\psi}, \boldsymbol{\psi} + \boldsymbol{\delta})$ over the whole parameter space. Thus, we can see from (6-45) that, the integration over the parameter space can be further partitioned as

$$\begin{aligned} & \int_{\mathbb{R}^{2K}} (f_{\xi}(\boldsymbol{\psi}) + f_{\xi}(\boldsymbol{\psi} + \boldsymbol{\delta})) P_{\min}(\boldsymbol{\psi}, \boldsymbol{\psi} + \boldsymbol{\delta}) d\boldsymbol{\psi} \\ & \geq \begin{cases} P_S(\boldsymbol{\delta}) \int_{\mathbb{R}^{2K}} (f_{\xi}(\boldsymbol{\psi}) + f_{\xi}(\boldsymbol{\psi} + \boldsymbol{\delta})) d\boldsymbol{\psi}, & \boldsymbol{\delta} \in \Delta \\ P_L \int_{\mathbb{R}^{2K}} (f_{\xi}(\boldsymbol{\psi}) + f_{\xi}(\boldsymbol{\psi} + \boldsymbol{\delta})) d\boldsymbol{\psi}, & \boldsymbol{\delta} \notin \Delta \end{cases}. \end{aligned} \quad (6-47)$$

Obviously, $P_S(\boldsymbol{\delta})$ corresponds to the probability of error for $\boldsymbol{\delta} \in \Delta$, where the difference between \mathcal{H}_0 and \mathcal{H}_1 is small. Correspondingly, the product of $P_S(\boldsymbol{\delta})$ and integration over the whole parameter space evaluates small estimation error bound (so-called local bound). By contrast, P_L describes the probability of error for $\boldsymbol{\delta}$ far away from $\mathbf{0}_{2K}$, and thus the product of P_L and integration over the whole parameter space evaluates the large estimation error bound. Hence, the ZZB takes both the small and large errors into account, which makes it a global bound.



Since $P(\boldsymbol{\delta})$ does not depend on $\boldsymbol{\psi}$, the integration w.r.t. $\boldsymbol{\psi}$ in (6-11) becomes

$$\begin{aligned} \frac{1}{2} \int_{\mathbb{R}^{2K}} (f_{\xi}(\boldsymbol{\psi}) + f_{\xi}(\boldsymbol{\psi} + \boldsymbol{\delta})) P_{\min}(\boldsymbol{\psi}, \boldsymbol{\psi} + \boldsymbol{\delta}) d\boldsymbol{\psi} &\geq \frac{P(\boldsymbol{\delta})}{\zeta^K \gamma^K} \int_{\Phi} d\boldsymbol{\psi} \\ &= \frac{P(\boldsymbol{\delta})}{\zeta^K \gamma^K} \prod_{k=1}^K (\zeta - \delta_k) \prod_{k=K+1}^{2K} (\gamma - \delta_k) \end{aligned} \quad (6-48)$$

according to Assumption 6.2.2, where Φ denotes a $2K$ -dimensional hyperrectangle determined by the constraints

$$\boldsymbol{\xi}_{\min} \preceq \boldsymbol{\psi} \preceq \boldsymbol{\xi}_{\max} \quad (6-49)$$

and

$$\boldsymbol{\xi}_{\min} \preceq \boldsymbol{\psi} + \boldsymbol{\delta} \preceq \boldsymbol{\xi}_{\max} \quad (6-50)$$

with $\boldsymbol{\xi}_{\min} = [\varphi_{\min} \mathbf{1}_K^T, \vartheta_{\min} \mathbf{1}_K^T]^T$, $\boldsymbol{\xi}_{\max} = [\varphi_{\max} \mathbf{1}_K^T, \vartheta_{\max} \mathbf{1}_K^T]^T$. $\zeta = \varphi_{\max} - \varphi_{\min}$ and $\gamma = \vartheta_{\max} - \vartheta_{\min}$ denote the length of the intervals for azimuth and elevation, respectively.

By substituting $P(\boldsymbol{\delta})$ (6-45) into (6-48), we have

$$\frac{P(\boldsymbol{\delta})}{\zeta^K \gamma^K} \prod_{k=1}^K (\zeta - \delta_k) \prod_{k=K+1}^{2K} (\gamma - \delta_k) \approx \frac{P_L}{\zeta^K \gamma^K} \prod_{k=1}^K (\zeta - \delta_k) \prod_{k=K+1}^{2K} (\gamma - \delta_k) + \begin{cases} P_S(\boldsymbol{\delta}) - P_L & \boldsymbol{\delta} \in \Delta \\ 0 & \boldsymbol{\delta} \notin \Delta \end{cases}, \quad (6-51)$$

such that the optimization problem in (6-11) becomes

$$\begin{aligned} &\max_{\boldsymbol{\delta}: \mathbf{w}^T \boldsymbol{\delta} = h} \frac{P(\boldsymbol{\delta})}{\zeta^K \gamma^K} \prod_{k=1}^K (\zeta - \delta_k) \prod_{k=K+1}^{2K} (\gamma - \delta_k) \\ &\approx \max_{\boldsymbol{\delta}: \mathbf{w}^T \boldsymbol{\delta} = h} \frac{P_L}{\zeta^K \gamma^K} \prod_{k=1}^K (\zeta - \delta_k) \prod_{k=K+1}^{2K} (\gamma - \delta_k) + \max_{\boldsymbol{\delta} \in \Delta: \mathbf{w}^T \boldsymbol{\delta} = h} P_S(\boldsymbol{\delta}) - P_L. \end{aligned} \quad (6-52)$$

In joint 2D DOAs estimation scenario, the constraint becomes $\mathbf{1}_{2K}^T \boldsymbol{\delta} = \sqrt{2K}h$ due to (6-11). As such, the first term in (6-52) becomes

$$\max_{\boldsymbol{\delta}: \mathbf{1}_{2K}^T \boldsymbol{\delta} = \sqrt{2K}h} \frac{P_L}{\zeta^K \gamma^K} \prod_{k=1}^K (\zeta - \delta_k) \prod_{k=K+1}^{2K} (\gamma - \delta_k) = \frac{P_L}{\zeta^K \gamma^K} \left(\frac{\zeta + \gamma}{2} - \frac{h}{\sqrt{2K}} \right)^{2K} \quad (6-53)$$



according to the Property 1 in [72]. Specifically, when the length of the intervals for the azimuth and elevation are equal, (6-53) is further simplified as

$$\max_{\delta: \mathbf{1}_{2K}^T \delta = \sqrt{2K}h} \frac{P_L}{\varrho^{2K}} \prod_{k=1}^{2K} (\varrho - \delta_k) = P_L \left(1 - \frac{h}{\sqrt{2K}\varrho}\right)^{2K}. \quad (6-54)$$

Then, the second term in (6-52) becomes

$$\max_{\delta \in \Delta: \mathbf{1}_{2K}^T \delta = \sqrt{2K}h} P_S(\delta) = \mathcal{Q} \left(\frac{\sqrt{K}h}{\sqrt{2\mathbf{1}_{2K}^T \mathbf{J}^{-1} \mathbf{1}_{2K}}} \right), \quad (6-55)$$

since the maximum occurs at the point [58]¹

$$\delta = \sqrt{2K}h \frac{\mathbf{J}^{-1} \mathbf{1}_{2K}}{\mathbf{1}_{2K}^T \mathbf{J}^{-1} \mathbf{1}_{2K}}. \quad (6-56)$$

Correspondingly, (6-52) becomes

$$\begin{aligned} & \max_{\delta: \mathbf{1}_{2K}^T \delta = \sqrt{2K}h} \frac{P(\delta)}{\zeta^K \gamma^K} \prod_{k=1}^K (\zeta - \delta_k) \prod_{k=K+1}^{2K} (\gamma - \delta_k) \\ & \approx \frac{P_L}{\zeta^K \gamma^K} \left(\frac{\zeta + \gamma}{2} - \frac{h}{\sqrt{2K}} \right)^{2K} + \begin{cases} \mathcal{Q} \left(\frac{\sqrt{K}h}{\sqrt{2\mathbf{1}_{2K}^T \mathbf{J}^{-1} \mathbf{1}_{2K}}} \right) - P_L & 0 \leq h \leq \tilde{h}_\xi, \\ 0 & h > \tilde{h}_\xi. \end{cases} \end{aligned} \quad (6-57)$$

Hence, the ZZB (6-12) becomes

$$\begin{aligned} \frac{1}{2K} \mathbf{1}_{2K}^T \mathbf{R}_\epsilon \mathbf{1}_{2K} & \geq \frac{P_L}{\zeta^K \gamma^K} \int_0^{\sqrt{\frac{K}{2}}(\zeta+\gamma)} \left(\frac{\zeta + \gamma}{2} - \frac{h}{\sqrt{2K}} \right)^{2K} h dh \\ & + \int_0^{\tilde{h}} \left[\mathcal{Q} \left(\frac{\sqrt{K}h}{\sqrt{2\mathbf{1}_{2K}^T \mathbf{J}^{-1} \mathbf{1}_{2K}}} \right) - P_L \right] h dh. \end{aligned} \quad (6-58)$$

By solving the two integration, the ZZB for joint 2D DOAs estimation is given in

$$\frac{1}{2K} \mathbf{1}_{2K}^T \mathbf{R}_\epsilon \mathbf{1}_{2K} \geq \frac{2P_L K}{(2K+1)(2K+2)\zeta^K \gamma^K} \left(\frac{\zeta + \gamma}{2} \right)^{2K+2} + \Gamma_{\frac{3}{2}}(\tilde{u}_\xi) \frac{\mathbf{1}_{2K}^T \mathbf{J}^{-1} \mathbf{1}_{2K}}{2K}, \quad (6-59)$$

¹Although only DOAs are of interest in our problem, the calculation of \mathbf{J}^{-1} here needs to take unwanted parameters into account, see [2], [7].



where

$$\Gamma_{\frac{3}{2}}(\tilde{u}_{\xi}) = \frac{1}{\Gamma(\frac{3}{2})} \int_0^{\tilde{u}_{\xi}} e^{-\iota} \iota^{\frac{1}{2}} d\iota \quad (6-60)$$

is the normalized incomplete Gamma function with $\Gamma(\frac{3}{2}) = \frac{\sqrt{\pi}}{2}$ and

$$\tilde{u}_{\xi} = \frac{K \tilde{h}_{\xi}^2}{4 \mathbf{1}_{2K}^T \mathbf{J}^{-1} \mathbf{1}_{2K}}, \quad (6-61)$$

with

$$\tilde{h}_{\xi} \approx \min \left[\sqrt{\frac{4T \mathbf{1}_{2K}^T \mathbf{J}^{-1} \mathbf{1}_{2K}}{K}} (l_{\text{coh}} + l_{\text{cor}} + l_{\text{un}}), \sqrt{\frac{K}{2}} (\zeta + \gamma) \right]. \quad (6-62)$$

Specifically, when the length of the intervals for azimuth and elevation are the same, i.e., $\zeta = \gamma \triangleq \varrho$, the ZZB is simplified to

$$\frac{1}{2K} \mathbf{1}_{2K}^T \mathbf{R}_{\epsilon} \mathbf{1}_{2K} \geq \frac{12P_L \mathbf{1}_{2K}^T \mathbf{R}_{\xi} \mathbf{1}_{2K}}{(2K+1)(2K+2)} + \Gamma_{\frac{3}{2}}(\tilde{u}_{\xi}) \frac{\mathbf{1}_{2K}^T \mathbf{J}^{-1} \mathbf{1}_{2K}}{2K}, \quad (6-63)$$

where

$$\mathbf{R}_{\xi} = \frac{\varrho^2}{12} \mathbf{I}_{2K} \quad (6-64)$$

is the *a priori* covariance matrix of ξ .

Actually, the MSE of the $2K$ sources can be obtained by extracting the diagonal elements in the error correlation matrix, which is also lower bounded by the diagonal elements in the *a priori* covariance matrix \mathbf{R}_{ξ} and the inverse of the FIM \mathbf{J}^{-1} . Thus, the MSE of joint azimuth and elevation estimation can be lower bounded by the ZZB as

$$\text{MSE}_{\xi} \geq \frac{12P_L \text{Tr}\{\mathbf{R}_{\xi}\}}{(2K+1)(2K+2)} + \Gamma_{\frac{3}{2}}(\tilde{u}_{\xi}) \frac{\text{Tr}\{\mathbf{J}^{-1}\}}{2K}, \quad (6-65)$$

which is the linear combination between the APB

$$\text{APB}_{\xi} = \frac{6 \text{Tr}\{\mathbf{R}_{\xi}\}}{(2K+1)(2K+2)} \quad (6-66)$$

and the CRB.



In 2D DOA estimation, we often evaluate the MSE of azimuth estimation and elevation estimation separately, rather than the overall MSE of joint 2D DOAs estimation. In this case, there are different approaches to derive the corresponding ZZB. For example, when we evaluate the ZZB for azimuth estimation², one approach is to derive it by partitioning the ZZB for joint estimation (6-65) as

$$\text{MSE}_\phi \geq \frac{24P_L \text{Tr}\{\mathbf{R}_\phi\}}{(2K+1)(2K+2)} + \Gamma_{\frac{3}{2}}(\tilde{u}_\xi) \frac{\text{Tr}\{\mathbf{J}_\phi^{-1}\}}{K}, \quad (6-67)$$

where the APB is

$$\text{APB}_{\phi,1} = \frac{12\text{Tr}\{\mathbf{R}_\phi\}}{(2K+1)(2K+2)} \quad (6-68)$$

with

$$\mathbf{R}_\phi = \frac{\zeta^2}{12} \mathbf{I}_K \quad (6-69)$$

denoting the *a priori* covariance matrix of ϕ , and \mathbf{J}_ϕ^{-1} is obtained from the (1,1) block of \mathbf{J}^{-1} . The other approach is to derive it by adopting the weight vector (6-13) and following the framework in [72]. To be more specific, when we only estimate the azimuth, the constraint becomes $\mathbf{1}_K^T \boldsymbol{\delta}_\phi = \sqrt{K}h$ and the $\boldsymbol{\delta}_\theta$ becomes a free variable, where $\boldsymbol{\delta} = [\boldsymbol{\delta}_\phi^T, \boldsymbol{\delta}_\theta^T]^T$ with $\boldsymbol{\delta}_\phi^T$ and $\boldsymbol{\delta}_\theta^T$ respectively corresponding to the azimuth ϕ and the elevation θ . Since all the parameters in $\boldsymbol{\psi}$ and $\boldsymbol{\psi} + \boldsymbol{\delta}$ obey the constraints (6-49)-(6-50) and $\mathbf{0}_{2K} \preceq \boldsymbol{\delta}$ [57], it is easy to observe that the maximum occurs if and only if $\boldsymbol{\delta}_\phi = \mathbf{0}_K$. Hence, the first term in (6-52) becomes

$$\max_{\boldsymbol{\delta}_\phi: \mathbf{1}_K^T \boldsymbol{\delta}_\phi = \sqrt{K}h} \frac{P_L}{\zeta^K} \prod_{k=1}^K (\zeta - \delta_k) = P_L \left(1 - \frac{h}{\sqrt{K}\zeta}\right)^K, \quad (6-70)$$

which degrades to the 1D case given in the Eq. (94) in [72]. The maximum of the second term in (6-52) occurs at the point

$$\boldsymbol{\delta}_\phi = \sqrt{K}h \frac{\mathbf{J}_\phi^{-1} \mathbf{1}_K}{\mathbf{1}_K^T \mathbf{J}_\phi^{-1} \mathbf{1}_K} \quad (6-71)$$

²The ZZB for elevation estimation can be derived in a similar way.



and $\delta_\theta = \mathbf{0}_K$, such that

$$\max_{\delta \in \Delta: \mathbf{1}_K^T \delta_\phi = \sqrt{K}h, \delta_\theta} P_S(\delta) = \mathcal{Q} \left(\frac{\sqrt{K}h}{2\sqrt{\mathbf{1}_K^T \mathbf{J}_\phi^{-1} \mathbf{1}_K}} \right). \quad (6-72)$$

Then, the ZZB for azimuth estimation from 2D DOA scenario can be obtained by following the derivation in [72], which leads to

$$\text{MSE}_\phi \geq \frac{12P_L \text{Tr}\{\mathbf{R}_\phi\}}{(K+1)(K+2)} + \Gamma_{\frac{3}{2}}(\tilde{u}_\phi) \frac{\text{Tr}\{\mathbf{J}_\phi^{-1}\}}{K}, \quad (6-73)$$

where the APB correspondingly becomes

$$\text{APB}_{\phi,2} = \frac{6\text{Tr}\{\mathbf{R}_\phi\}}{(K+1)(K+2)}. \quad (6-74)$$

Here,

$$\tilde{u}_\phi = \frac{K\tilde{h}_\phi^2}{8\mathbf{1}_K^T \mathbf{J}_\phi^{-1} \mathbf{1}_K} \quad (6-75)$$

with

$$\tilde{h}_\phi \approx \min \left[\sqrt{\frac{8T\mathbf{1}_K^T \mathbf{J}_\phi^{-1} \mathbf{1}_K}{K} (l_{\text{coh}} + l_{\text{cor}} + l_{\text{un}})}, \sqrt{K}\zeta \right]. \quad (6-76)$$

The reason why we can obtain two ZZB expressions here is that, according to [57], the ZZB expression depends on specific weight vector \mathbf{w} . That means, by adopting two different weight vectors (6-11) and (6-13), we can obtain different ZZB expressions for azimuth estimation. It is noted that, although these two ZZBs have similar expressions to the Eq. (32) in [72], the FIM \mathbf{J}_ϕ^{-1} involves the coupling between the azimuth and elevation from the same source, which does not appear in 1D DOA estimation problem.

6.3.2 ZZB for estimation after matching process according to minimum Euclidean distance criterion

Obviously, before we perform estimation, we do not have the *a priori* knowledge about the DOA, such that we assume uniform distributions (see, Assumption 6.2.2) for the azimuth/eleva-

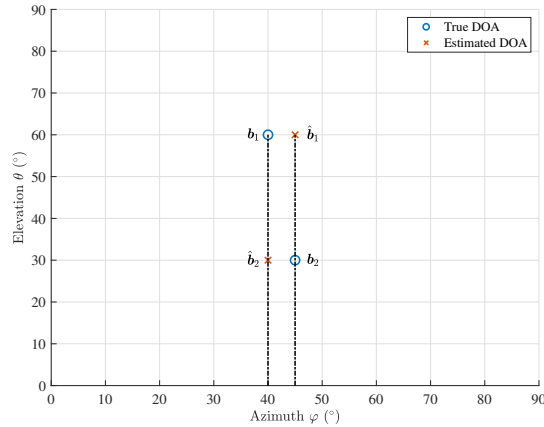


Figure 6.1 Illustration of the reason why we need to adopt minimum Euclidean distance criterion for 2D matching between the estimated and the true DOAs.

tion of each source. That means, each signal impinges on the array from any azimuth/elevation with the same probability, and the azimuth/elevation of different sources are independent of each other. However, for multi-source DOA estimators, the estimated DOAs are output in a disordered manner (e.g., MUSIC algorithm). Hence, we have to perform a matching process between the estimated and the true DOAs in the MSE calculation. Unfortunately, there is no index to directly indicate the matching relationship between the estimated and the true DOAs. Thus, an extra criterion have to be introduced for MSE calculation. Specifically, in 1D DOA estimation, an ordering process for both the estimated and the true DOAs is usually performed to realize a good matching and guarantee the correct MSE result, and its effect on the ZZB has been investigated in [72] by exploiting ordering statistics. However, in 2D DOA estimation, such an ordering process on the azimuth or elevation does not guarantee the correct MSE result. Here is an example.

Example 1: Consider there are two signals impinging on the array from $\mathbf{b}_1 = [\phi_1, \theta_1] = [40^\circ, 60^\circ]$ and $\mathbf{b}_2 = [\phi_2, \theta_2] = [45^\circ, 30^\circ]$, while two estimates are obtained $\hat{\mathbf{b}}_1 = [\hat{\phi}_1, \hat{\theta}_1] = [45^\circ, 60^\circ]$ and $\hat{\mathbf{b}}_2 = [\hat{\phi}_2, \hat{\theta}_2] = [40^\circ, 30^\circ]$, respectively (see Fig. 6.1). Now, we consider how to match the estimated DOA to the corresponding true DOA for MSE calculation. If we adopt an ordering process along the azimuth, the estimate $\hat{\mathbf{b}}_2$ is matched to \mathbf{b}_1 while the estimate $\hat{\mathbf{b}}_1$ is matched to \mathbf{b}_2 respectively (as shown in the dash dot lines in Fig. 6.1), such that the RMSE is

calculated as

$$\text{RMSE}_2 = \sqrt{\frac{1}{4} \left(\|\hat{\mathbf{b}}_2 - \mathbf{b}_1\|_2^2 + \|\hat{\mathbf{b}}_1 - \mathbf{b}_2\|_2^2 \right)} \approx 21.21^\circ. \quad (6-77)$$

Thus, it is not a correct MSE result because the estimate $\hat{\mathbf{b}}_1$ and $\hat{\mathbf{b}}_2$ are close to \mathbf{b}_1 and \mathbf{b}_2 , respectively. In other words, the estimate $\hat{\mathbf{b}}_1$ is preferred to be matched to \mathbf{b}_1 while $\hat{\mathbf{b}}_2$ is preferred to be matched to \mathbf{b}_2 , to lead to a smaller RMSE

$$\text{RMSE}_2 = \sqrt{\frac{1}{4} \left(\|\hat{\mathbf{b}}_1 - \mathbf{b}_1\|_2^2 + \|\hat{\mathbf{b}}_2 - \mathbf{b}_2\|_2^2 \right)} \approx 3.54^\circ. \quad (6-78)$$

Obviously, in 2D DOA estimation, we prefer to adopt minimum Euclidean distance criterion to realize the matching between the estimated and the true DOAs. Then, its effect on the ZZB cannot be analyzed with the order statistics as [72] and still remains to be investigated.

Mathematically, such a matching process with minimum Euclidean distance criterion can be formulated as an EBMP with minimum total Euclidean distance. To be more specific, we define an undirected complete bipartite graph $\mathcal{G} = (\mathbb{U}, \mathbb{V}, \mathcal{E})$ with $\mathbb{U} = \{\mathbf{b}_i = [\phi_i, \theta_i] | i = 1, \dots, K\}$ and $\mathbb{V} = \{\hat{\mathbf{b}}_j = [\hat{\phi}_j, \hat{\theta}_j] | j = 1, \dots, K\}$ denoting the set containing the true and the estimated DOAs respectively, $\mathcal{E} = \{d_{i,j} | i, j = 1, \dots, K\}$ denoting the set containing the weighted undirected edges connecting vertices of \mathbb{U} and \mathbb{V} . The weight $d_{i,j}$ here represents the squared Euclidean distance between $\hat{\mathbf{b}}_j$ and \mathbf{b}_i , i.e.,

$$d_{i,j} = \|\hat{\mathbf{b}}_j - \mathbf{b}_i\|_2^2. \quad (6-79)$$

Thus, the matching between the estimated and the true DOAs according to the minimum Euclidean distance criterion can be formulated as finding the perfect matching with minimum total weights in the bipartite graph \mathcal{G} . Here, matching and perfect matching are defined as:

Definition 1 (Matching). *A matching in an undirected graph \mathcal{G} is a set of edges without common vertices.*

Definition 2 (Perfect Matching). *A perfect matching in the undirected graph \mathcal{G} is a matching that covers every vertex.*

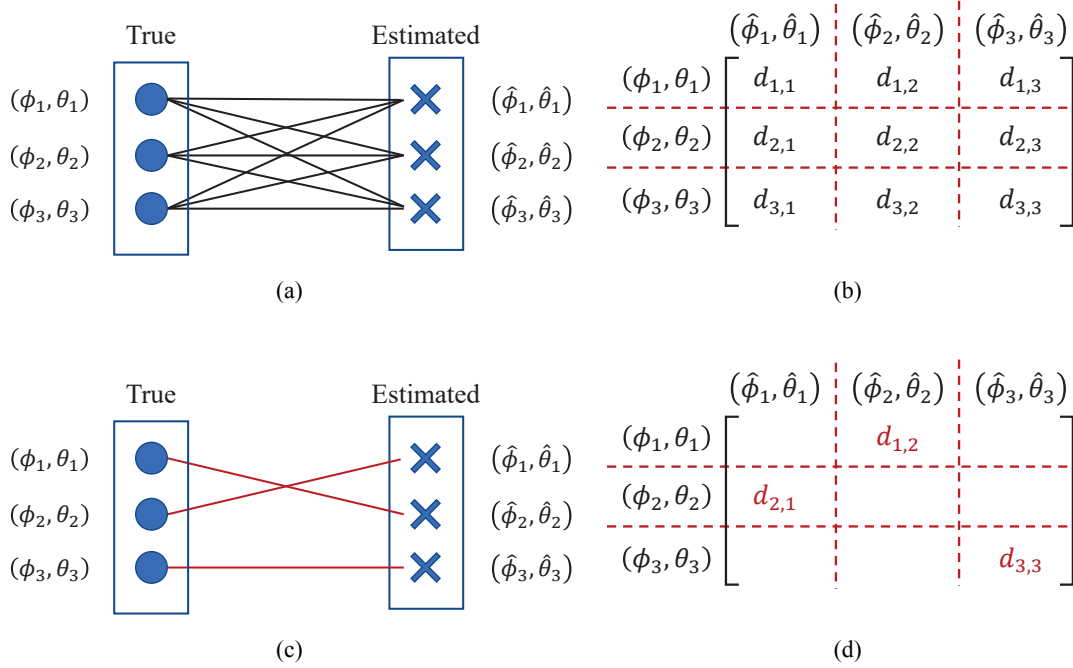


Figure 6.2 Illustration of EBMP. (a) A complete bipartite graph \mathcal{G} between the sets of the true and the estimated DOAs. (b) The weighted matrix with the elements denoting the Euclidean distance. (c) One of the perfect matchings of the complete bipartite graph. (d) The elements in the weighted matrix corresponding to the perfect matching.

For better illustration, we consider an intuitive example with $K = 3$ sources shown in Fig. 6.2. The formulated undirected complete bipartite graph \mathcal{G} and the weight of each edge are shown in Fig. 6.2a and Fig. 6.2b respectively. One of a perfect matchings of the graph \mathcal{G} and the corresponding weights are shown in Fig. 6.2c and Fig. 6.2d. Since there are different perfect matchings in \mathcal{G} , we need to find the one with minimum total weight among all the perfect matchings. The minimum total weight is expressed as [154]

$$\mathcal{D}_{\text{opt}} = \min_{\alpha} \mathcal{D}(\alpha) = \min_{\alpha} \sum_{i=1}^K \|e_{\alpha(i)}\|_2^2, \quad \alpha \in \mathcal{S}_{\mathbb{V}}, \quad (6-80)$$

where

$$e_{\alpha(i)} = \hat{\mathbf{b}}_{\alpha(i)} - \mathbf{b}_i \quad (6-81)$$

is the difference between the estimate $\hat{\mathbf{b}}_{\alpha(i)}$ and the i -th true DOA \mathbf{b}_i , $\alpha(i)$ denotes the i -th element after the permutation α over the K elements in the set \mathbb{V} , and $\mathcal{S}_{\mathbb{V}}$ denotes the finite



symmetric group consisting of all the permutations over the K elements in \mathbb{V} . Since \mathcal{D}_{opt} is the minimum total squared Euclidean distance, the optimal matching relationship between the K estimated DOAs and true DOAs is determined from the permutation α that leads to \mathcal{D}_{opt} .

According to (6-80), the minimum Euclidean distance criterion always prefers to match the estimated DOA with the true DOA nearby to realize overall minimum MSE result. Actually, in the asymptotic region, such a matching process does lead to the correct MSE result. The reason is that, only small estimation error occurs in the asymptotic region, i.e., the estimated DOA always appears near to the corresponding true DOA. However, in the non-asymptotic region, large estimation errors that are distributed throughout the *a priori* interval of the parameters [58] start to occur. In this case, the matching process with minimum Euclidean distance criterion still matches the estimated DOA with the true DOA nearby, which implicitly reduces the effect of large estimation errors on the MSE result. To this end, after the matching process adopting minimum Euclidean distance criterion, the MSE of estimators will converge to a smaller value in the *a priori* performance region. Obviously, the ZZB (6-59) derived in subsection 6.3.1 does not consider this extra effect of the matching process and is not appropriate for lower bounding the MSE in the non-asymptotic region after the matching process.

To be more specific, the MSE convergence for multi-source 2D DOA estimation is obtained by the expectation of \mathcal{D}_{opt} over the parameter vector ξ , i.e.,

$$\bar{\mathcal{D}}_{\text{opt}} = \mathbb{E}\{\mathcal{D}_{\text{opt}}\}. \quad (6-82)$$

On the other hand, without the effect of the matching process, the estimation error of each azimuth/elevation naturally tends to its *a priori* variance in the *a priori* performance region, because all the DOAs are randomly and independently estimated from the throughout *a priori* interval. Since the *a priori* variances of the azimuth and elevation only depend on the length of the *a priori* interval ζ and γ in the ZZB (6-59), the effect of the matching process on the ZZB can be formulated as the ratio between $\bar{\mathcal{D}}_{\text{opt}}$ and the trace of *a priori* covariance matrix \mathbf{R}_{ξ} , i.e.,

$$\kappa = \frac{\bar{\mathcal{D}}_{\text{opt}}}{\text{Tr}\{\mathbf{R}_{\xi}\}}. \quad (6-83)$$



According to Assumption 6.2.2, all the azimuths and elevations are random variables following uniform distributions. Thus, the solution of $\bar{\mathcal{D}}_{\text{opt}}$ can be solved by the stochastic EBMP [154], which is defined as

Definition 3 (Stochastic EBMP). *The two sets of K elements in EBMP, i.e., \mathbb{U} and \mathbb{V} , are obtained by extracting $2K$ points independently with a given PDF on a certain domain Ω .*

Obviously, in the *a priori* performance region, all of the K estimated DOAs and K true DOAs are random variables following uniform distributions in the domain $\Omega = [\varphi_{\min}, \varphi_{\max}] \times [\vartheta_{\min}, \vartheta_{\max}]$. Unfortunately, the exact solution of $\bar{\mathcal{D}}_{\text{opt}}$ in such a general rectangle domain is still an open problem mathematically. Here, we only consider a special case of the square domain, i.e., length of the *a priori* intervals for azimuth and elevation are the same ($\zeta = \gamma = \varrho$). In this case, the ZZB degrades to (6-65) and the length of the *a priori* intervals ζ and γ in (6-59) are compactly expressed in the trace of *a priori* covariance matrix \mathbf{R}_ξ (6-64).

The solution of $\bar{\mathcal{D}}_{\text{opt}}$ is given by generalizing the solution [154, Eq. (26)] for unit square $\bar{\Omega} = [0, 1] \times [0, 1]$ with to a square $\tilde{\Omega}$ with edge length ϱ^3 as

$$\lim_{K \rightarrow +\infty} \bar{\mathcal{D}}_{\text{opt}} = \varrho^2 \left(\frac{\ln K}{2\pi} + \varepsilon \right), \quad (6-84)$$

where $\varepsilon = 0.677$ is obtained from a fit procedure. However, it is unrealistic to perform such a fit procedure to obtain the bound with numerical Monte-Carlo trials, then we ignore the second term obtained from fit procedure and make a relaxation

$$\bar{\mathcal{D}}_{\text{opt}} \geq \frac{\varrho^2 \ln K}{2\pi}. \quad (6-85)$$

Accordingly, the ratio κ is lower bounded by

$$\kappa \geq \frac{\varrho^2 \ln K}{2\pi \text{Tr}\{\mathbf{R}_\xi\}}. \quad (6-86)$$

³The edge length ϱ means that the length of the intervals for azimuth and elevation should be equal, instead of the beginning and the end of the interval.

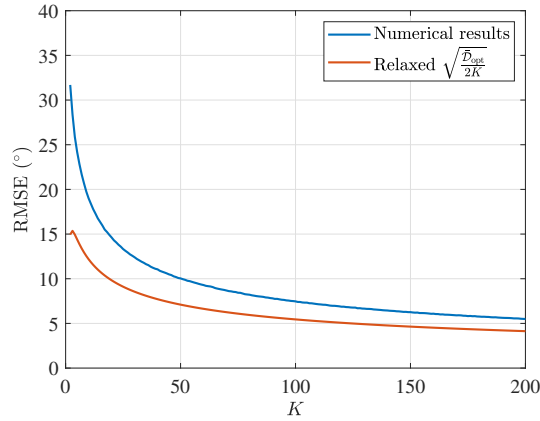


Figure 6.3 Effectiveness of the relaxation.

Here, we demonstrate the effectiveness of the relaxation (6-85) in Fig. 6.3, where the RMSE of 2D DOA w.r.t. different number of sources K is plotted. For each K , we randomly generate $\mathcal{L} = 10,000$ true 2D DOAs and estimated DOAs respectively according to the uniform distribution $\mathcal{U}[0^\circ, 90^\circ]$ and calculate the numerical RMSE

$$\text{RMSE}_K = \sqrt{\frac{1}{2K\mathcal{L}} \sum_{\ell=1}^{\mathcal{L}} \|\hat{\xi}_\ell - \xi_\ell\|_2^2}, \quad (6-87)$$

where $\hat{\xi}_\ell$ denotes the estimate of ξ_ℓ in the ℓ -th Monte-Carlo trial after the matching process according to minimum Euclidean distance criterion. Then, we plot the relaxed analytic RMSE $\sqrt{\frac{\bar{D}_{opt}}{2K}}$ according to (6-85). It is noted that, the length of the interval $\varrho = 90^\circ$ here means that, both the azimuth and elevation are located within the interval with length 90° , but ϑ_{\min} can be different from φ_{\min} . Obviously, (6-85) is an effective relaxation for the lower bound. When the number of sources K increases, both the numerical results and the relaxation decreases, which indicates that, the MSE converges to a smaller value due to the effect of the matching process.

Thus, the ZZB considering matching process with minimum Euclidean distance criterion is obtained by incorporating the ratio κ into (6-65) as

$$\text{MSE}_\xi \geq 2P_L \frac{3\varrho^2 \ln K}{\pi(2K+1)(2K+2)} + \Gamma_{\frac{3}{2}}(\tilde{u}_\xi) \frac{\text{Tr}\{\mathbf{J}^{-1}\}}{2K}, \quad (6-88)$$



where the APB (6-66) becomes

$$\text{APB}_\xi = \frac{3\varrho^2 \ln K}{\pi(2K+1)(2K+2)}. \quad (6-89)$$

When $K = 1$, there is no matching process between the estimated and the true DOA, then the ZZB given in (6-65) is valid for evaluating the MSE performance.

When we only estimate azimuth from 2D DOA model, we also need to adopt the minimum Euclidean distance criterion to realize the matching process for MSE calculation. Thus, the ZZB for azimuth estimation with such a matching process can be derived from (6-67) and (6-73) as

$$\text{MSE}_\phi \geq 2P_L \frac{3\varrho^2 \ln K}{\pi(2K+1)(2K+2)} + \Gamma_{\frac{3}{2}}(\tilde{u}_\xi) \frac{\text{Tr}\{\mathbf{J}_\phi^{-1}\}}{K} \quad (6-90)$$

with

$$\text{APB}_{\phi,1} = \frac{3\varrho^2 \ln K}{\pi(2K+1)(2K+2)}, \quad (6-91)$$

and

$$\text{MSE}_\phi \geq 2P_L \frac{3\varrho^2 \ln K}{2\pi(K+1)(K+2)} + \Gamma_{\frac{3}{2}}(\tilde{u}_\phi) \frac{\text{Tr}\{\mathbf{J}_\phi^{-1}\}}{K} \quad (6-92)$$

with

$$\text{APB}_{\phi,2} = \frac{3\varrho^2 \ln K}{2\pi(K+1)(K+2)}. \quad (6-93)$$

Note that, the ZZB for azimuth estimation is different from the one for 1D DOA estimation [72]. The reason is that, we consider the matching process with minimum Euclidean distance criterion over a 2D plane rather than an ordering process along the azimuth. Besides, the FIM for 2D estimation successfully captures the coupling between the azimuth and elevation of the same source, which leads to a different CRB compared to that for 1D DOA estimation.

Finally, in our ZZB derivation, we assume that the estimates of the azimuth and elevation



for the same source are well paired together, which, however, is not always valid for specific 2D DOA estimation problem depending on the array configuration and the estimation algorithm. Hence, it is promising to provide a tighter bound considering the extra estimation error brought from the azimuth-elevation pairing. Furthermore, it remains further study to be performed for the case when the azimuth and elevation do not share the same *a priori* interval.

6.4 Numerical Analysis

In this section, we evaluate the derived ZZB for multi-source 2D DOA estimation, where a URA comprises $M = M_Z \times M_{\mathcal{X}} = 10 \times 10 = 100$ sensors with half-wavelength inter-sensor spacing along \mathcal{Z}, \mathcal{X} -axes, respectively⁴. Thus, the steering vectors along \mathcal{Z}, \mathcal{X} -axes are

$$\mathbf{a}_{\mathcal{Z}}(\theta_k) = [1, e^{-j\pi \cos \theta_k}, \dots, e^{-j(M_Z-1)\pi \cos \theta_k}]^T, \quad (6-94)$$

and

$$\mathbf{a}_{\mathcal{X}}(\phi_k, \theta_k) = [1, e^{-j\pi \sin \theta_k \cos \phi_k}, \dots, e^{-j(M_{\mathcal{X}}-1) \sin \theta_k \cos \phi_k}]^T, \quad (6-95)$$

such that the steering vector $\mathbf{a}(\phi_k, \theta_k)$ in steering matrix $\mathbf{A}(\boldsymbol{\phi}, \boldsymbol{\theta})$ becomes

$$\mathbf{a}(\phi_k, \theta_k) = \mathbf{a}_{\mathcal{Z}}(\theta_k) \otimes \mathbf{a}_{\mathcal{X}}(\phi_k, \theta_k), k = 1, \dots, K. \quad (6-96)$$

We assume that each azimuth and elevation follow a uniform distribution $\mathcal{U}[45^\circ, 135^\circ]$ and run $\mathcal{L} = 500$ Monte-Carlo trials for each SNR point to obtain the curves in our simulation. In each Monte-Carlo trial, all the true azimuths and elevations for K sources are randomly sampled according to the assumed uniform distribution. To keep the sources resolvable, we assume that there is a least 10° separation among different azimuths and elevations, i.e.,

$$|\phi_i - \phi_j| \geq 10^\circ, |\theta_i - \theta_j| \geq 10^\circ, \forall i, j \in 1, \dots, K, i \neq j. \quad (6-97)$$

⁴It is worth noting that the derived ZZB is appropriate for arbitrary 2D array configuration. The URA in the simulations is only adopted as an example.

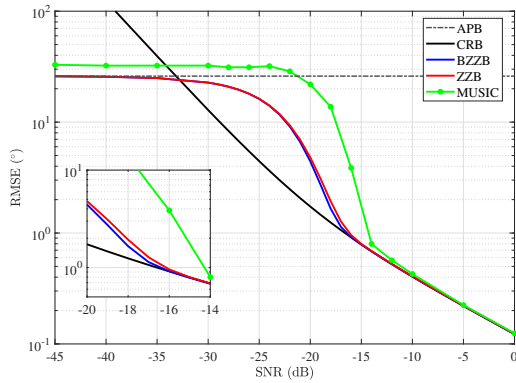


Figure 6.4 Comparison of bounds for single source 2D DOA estimation.

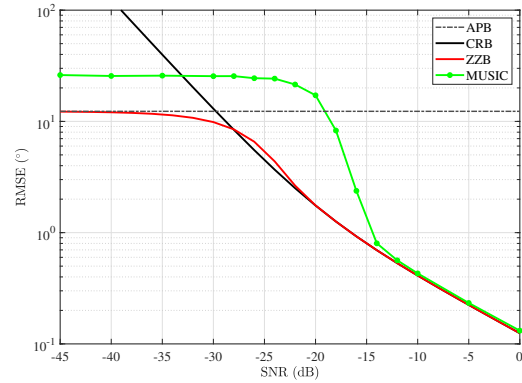


Figure 6.5 Comparison of bounds for multi-source estimation ($K = 3$).

Unless otherwise specified, the number of snapshots is fixed to $T = 20$ in each simulation.

Considering that the ZZB for single source 2D estimation only has been given in [58] (BZZB), we first compare the ZZB in this chapter with the existing ZZB [58] in Fig. 6.4. Obviously, there is no matching process between the estimated and the true DOA in single source case, such that the ZZB (6-65) can be utilized to evaluate the MSE performance. The APB (6-66), the CRB derived from the inverse of FIM (6-10), and the RMSE of the 2D MUSIC algorithm are plotted for reference. It is observed that, the ZZB coincides with the ZZB in [58] from the *a priori* performance region to the asymptotic region, provides a tight bound for the MUSIC algorithm, and converges to the APB in the *a priori* performance region and to the CRB in the asymptotic region, respectively. Here, the APB is determined by the mean between the *a priori* variances of the azimuth and elevation, which means that, the MSE converges to the *a priori* variance of the parameters in the *a priori* performance region, as correctly predicted by the ZZB. On the contrary, the CRB grows divergently in the non-asymptotic region when SNR decreases. When the SNR increases, the BZZB reaches the CRB (about -17 dB) slightly earlier than the derived ZZB (about -16 dB), because the BZZB used an extra approximation in the Eq. (C.14) in [58].

We then plot the ZZB for multi-source 2D DOA estimation in Fig. 6.5, where $K = 3$ uncorrelated sources are assumed to have the same SNRs. Different from the single source DOA estimation, it is essential to the perform matching process during the MSE calculation as discussed in subsection 6.3.2, such that we compare the ZZB (6-88) with the APB (6-89), the

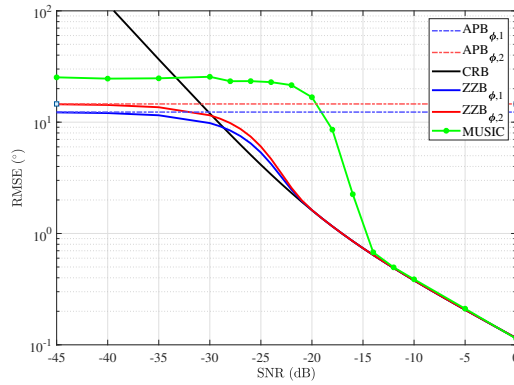


Figure 6.6 Comparison of bounds for multi-source azimuth estimation ($K = 3$).

CRB, and the RMSE of the 2D MUSIC algorithm. We can observe that, similar to the single source case, the derived ZZB converges to the APB and the CRB in the *a priori* performance region and the asymptotic region, respectively, and effectively lower bounds the RMSE of 2D MUSIC algorithm in all SNR regions. It is noted that, although the ZZB does not provide a tight bound in the *a priori* performance region due to the relaxation in (6-85), it still outperforms the CRB and provides a global bound. When the estimator works in the non-asymptotic region, the large errors distributed throughout the whole *a priori* interval of the parameters gradually dominate the estimation, which prevent the CRB providing valid lower bound. By contrast, the ZZB successfully captures both the small estimation error and the large error, as discussed in subsection 6.3.1. Compared with the single source case, the ZZB reaches the CRB at a lower SNR, because the linear combination coefficients $2P_L$ and $\Gamma_{\frac{3}{2}}(\tilde{u}_\xi)$ reach to 0 and 1 more rapidly, respectively.

Also, there is a common situation where we need to just estimate azimuth/elevation from the 2D DOA model. Hence, we further investigate the ZZB on azimuth estimation in Fig. 6.6. Here, we investigate the two ZZB expressions (6-90) and (6-92) derived from different approaches, where the corresponding two APBs (6-91) and (6-93), the CRB and the RMSE of the 2D MUSIC algorithm are also plotted for reference. It is observed that, each ZZB converges to the corresponding APB in the *a priori* performance region and provides global valid bound for the RMSE of the azimuth estimated by MUSIC algorithm, where the $APB_{\phi,2}$ (6-93) is greater than the $APB_{\phi,1}$ (6-91). On the other hand, both the two ZZBs converge to the same CRB at the



same threshold SNR. Obviously, the ZZB derived from the weight vector specifically aiming at azimuth estimation (6-14) is tighter than that partitioned from the joint estimation bound with the weight vector (6-11), such that we prefer to adopt the weight vectors (6-13) and (6-14) to derive the ZZB for azimuth estimation and elevation estimation, respectively, while adopt the (6-11) to derive the ZZB for joint 2D DOAs estimation.

Since the derived ZZB provides an explicit expression for all the coherent, correlated, and uncorrelated sources, we evaluate the derived ZZB considering different sources coherence in Fig. 6.7. Here, we assume there are $K = 3$ sources with the same SNR and 1) partially correlated with the correlation coefficient matrix

$$\mathbf{C} = \begin{bmatrix} 1 & 0.5 & 0.25 \\ 0.5 & 1 & 0.5 \\ 0.25 & 0.5 & 1 \end{bmatrix}; \quad (6-98)$$

2) fully coherent with coefficient $\beta = [1, e^{j\lambda_1}, e^{j\lambda_2}]^T$; and 3) uncorrelated. λ_1 and λ_2 here are independent and identically distributed random phases following a uniform distribution $\mathcal{U}[-\pi, \pi]$. It is observed from Fig. 6.7 that, in the *a priori* performance region, all the ZZBs converges to the same APB regardless of the coherence among sources, since the APB does not depend on neither the coherent coefficient nor the correlation coefficient matrix. When SNR increases, the more the correlation between the sources is, the more rapidly the ZZB decreases. Thus, outside the *a priori* performance region, the coherent ZZB is below the correlated ZZB and the uncorrelated ZZB. The reason is that, there is least stochasticity for the fully coherent sources among all the three cases, which makes the fully coherent signal model closer to the deterministic signal model that leads to lower MSE bound than stochastic model. That is to say, although the coherence among sources usually requires extra operation to avoid the decrease of estimation accuracy, the coherence may allow to achieve higher estimation accuracy.

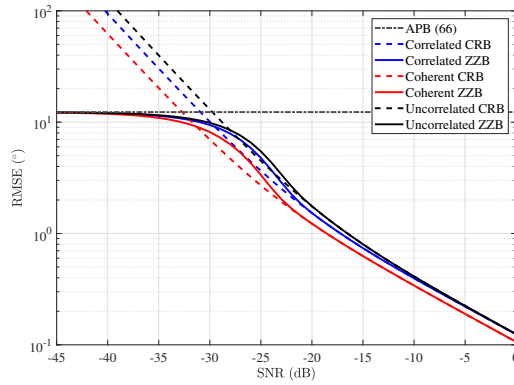


Figure 6.7 Comparison of coherent, correlated and uncorrelated bounds.

6.5 Summary

In this chapter, we derived an explicit ZZB for 2D multi-source DOA estimation. Benefiting from the general signal model, the ZZB is for the first time appropriate for partially correlated sources, and does not depend on the specific 2D array manifold. Different from the 1D DOA estimation case, in 2D DOA estimation, the matching process between the estimated and the true DOAs must be implemented according to the minimum Euclidean distance criterion. Hence, we analyzed the effect of such matching process on the ZZB with the formulated stochastic EBMP and we provided the global valid ZZB for evaluating multi-source DOA estimation. In addition to the joint 2D DOAs estimation, we also provided two approaches to derive ZZB for azimuth/elevation estimation by utilizing different weight vectors. The results show that the ZZB derived by the weight vector aiming at the azimuth/elevation estimation is tighter than that obtained by the vector for joint 2D DOAs estimation. Simulation results demonstrate the advantage of the derived ZZB over the CRB. It is noted that, the derived ZZB provides globally valid bound, but not tight in the non-asymptotic region, since there is only an asymptotic solution for stochastic EBMP under the assumption of azimuth and elevation sharing the same *a priori* interval. Hence, the derivation of tighter ZZB for 2D DOA estimation under more general conditions is still remains to be studied, such as azimuth and elevation with different *a priori* distributions or different *a priori* interval. Besides, although the derived ZZB provides a general expression regardless of the specific array manifold, we believe that it is also promising



to provide improved ZZB considering the characteristic of the array configuration. Finally, we remark that, the basic ideas of this chapter are valid for other multi-source multi-parameter estimation problems, including multi-source joint parameters estimation among velocity, range, and angle.



Chapter 7. Conclusions and Future work

7.1 Conclusions

This dissertation systematically reviews the lower bounds on the MSE for nonlinear parameter estimation problems. Based on the literature review, the ZZB is selected as the research subject. The basic theory and analytical framework of the ZZB for scalar and vector parameter estimation problems are introduced in detail, and a generalized expression of the ZZB for these two types of parameter estimation problems is provided.

Subsequently, addressing the challenges posed by the limitations of existing research on the ZZB, which is confined to simple assumptions such as Gaussian white noise and single target scenarios, this dissertation focused on typical parameter estimation problems in target localization, such as distance and angle. This dissertation extends to the ZZB for distance and angle estimation in complex scenarios involving non-white noise and multiple targets.

Specifically, we investigate the ZZB for time delay estimation based on CS, discussing the impact of arbitrary CS kernels and Gaussian colored noise under single source case. We studies the ZZB for 1D DOA estimation with multiple sources, focusing on the ZZB for single-type vector parameter estimation composed of 1D DOA angles, achieving a theoretical breakthrough from single-source to multi-source. We examines the ZZB for 2D DOA estimation with multiple sources, addressing complex vector parameter estimation problems composed of elevation and azimuth angles, achieving a theoretical breakthrough for more generalized parameter estimation problems under the ZZB.

For the above issues, this dissertation provides reliable and easy-to-use explicit/closed-form expressions of the ZZB, offering better estimation error evaluation tools for these parameter estimation problems. The main contributions and innovations of this dissertation are as follows:

1. This dissertation presents an explicit ZZB for time delay parameter estimation based on CS, making the ZZB applicable to any CS kernel and any Gaussian colored noise. This



overcomes the theoretical limitations of existing work that relies on Gaussian white noise and random CS kernels, thereby broadening the applicability of the ZZB. Compared to the commonly used BCRB, the ZZB provided in this dissertation offers a globally tight performance lower bound across all SNR ranges and provides accurate predictions of the asymptotic region threshold SNR for MMSE estimator.

2. A closed-form ZZB for multi-source 1D DOA estimation is provided, which is a unified expression for underdetermined/overdetermined estimation. By introducing a coherent/incoherent mixed multi-source DOA estimation signal model, this dissertation formulates the ZZB as a function of the coherence coefficients among different sources. Besides, this dissertation introduces order statistics to systematically discuss the impact of the necessary sorting process on the MSE results in the low SNR prior region. The relationship between the convergence of the MSE in the low SNR prior region and the number of sources is revealed.
3. A closed-form ZZB for multi-source 2D DOA estimation is derived. This dissertation also incorporates partially correlated source signals into the ZZB analysis, resulting in a closed-form expression of the ZZB related to the correlation coefficient matrix. This dissertation introduces the random Euclidean bipartite matching problem to quantitatively analyze the impact of this criterion on the convergence of MSE in the low SNR prior region. Additionally, the dissertation provides ZZB expressions for only elevation/azimuth angle estimation under the multi-source 2D DOA estimation model and intuitively demonstrates the tightness of the ZZB expressions brought by different weight vectors.

7.2 Future work

This dissertation conducts research on the ZZB for typical nonlinear parameter estimation problems such as distance and angle. It is worth noting that there are remaining challenges that require further research, such as:

1. How to provide reliable and easy-to-use expressions for the ZZB in more complex signal



models, such as Gaussian mixture distributions.

2. How to provide closed-form ZZB expressions when the vector parameter follows a non-uniform *a priori* distribution.
3. How to provide a closed-form ZZB for multi-source 2D DOA estimation when the *a priori* ranges of elevation and azimuth angles are different
4. How to derive tighter closed-form ZZB that accounts for specific array manifolds.



References

- [1] S. M. Kay, *Fundamentals of Statistical Signal Processing, Volume II: Detection Theory*. Upper Saddle River, NJ: Prentice Hall PTR, 1993.
- [2] H. L. Van Trees, *Detection, Estimation, and Modulation Theory, Part IV: Optimum Array Processing*. Wiley, 2002.
- [3] H. L. V. Trees and K. L. Bell, *Bayesian Bounds for Parameter Estimation and Nonlinear Filtering/Tracking*. New York, NY, USA: Wiley, 2007.
- [4] C. R. Rao, "Information and the accuracy attainable in the estimation of several parameters," *Bulletin of Cal. Math. Soc.*, vol. 37, no. 3, pp. 89–91, 1945.
- [5] H. Cramér, *Mathematical Methods of Statistics*. Princeton University Press, 1946.
- [6] P. Stoica and A. Nehorai, "MUSIC, maximum likelihood and Cramér-Rao bound," *IEEE Trans. Acoust. Speech Signal Process.*, vol. 37, no. 5, pp. 720–741, May 1989.
- [7] ———, "Performance study of conditional and unconditional direction-of-arrival estimation," *IEEE Trans. Acoust. Speech, Signal Process.*, vol. 38, no. 10, pp. 1783–1795, Oct. 1990.
- [8] M. Wang and A. Nehorai, "Coarrays, MUSIC, and the Cramér-Rao bound," *IEEE Trans. Signal Process.*, vol. 65, no. 4, pp. 933–946, Feb. 2017.
- [9] C.-L. Liu and P. P. Vaidyanathan, "Cramér-Rao bounds for coprime and other sparse arrays, which find more sources than sensors," *Digit. Signal Process.*, vol. 61, pp. 43–61, Feb. 2017.
- [10] A. N. D'Andrea, U. Mengali, and R. Reggiannini, "The modified Cramér-Rao bound and its application to synchronization problems," *IEEE Trans. Commun.*, vol. 42, no. 234, pp. 1391–1399, Feb. 1994.
- [11] F. Gini, R. Reggiannini, and U. Mengali, "The modified Cramér-Rao bound in vector parameter estimation," *IEEE Trans. on Commun.*, vol. 46, no. 1, pp. 52–60, Jan. 1998.
- [12] S. Fortunati, F. Gini, and M. S. Greco, "The misspecified Cramér-Rao bound and its application to scatter matrix estimation in complex elliptically symmetric distributions," *IEEE Trans. Signal Process.*, vol. 64, no. 9, pp. 2387–2399, May 2016.
- [13] S. Fortunati, F. Gini, M. S. Greco, and C. D. Richmond, "Performance bounds for parameter estimation under misspecified models: Fundamental findings and applications," *IEEE Signal Process. Mag.*, vol. 34, no. 6, pp. 142–157, Nov. 2017.
- [14] S. Fortunati, F. Gini, M. S. Greco, A. M. Zoubir, and M. Rangaswamy, "Semiparametric inference and lower bounds for real elliptically symmetric distributions," *IEEE Trans. Signal Process.*, vol. 67, no. 1, pp. 164–177, Jan. 2019.
- [15] H. V. Habi, H. Messer, and Y. Bresler, "Learning to bound: A generative Cramér-Rao bound," *IEEE Trans. Signal Process.*, vol. 71, pp. 1216–1231, Mar. 2023.
- [16] F. Liu, Y.-F. Liu, A. Li, C. Masouros, and Y. C. Eldar, "Cramér-Rao bound optimization for joint radar-communication beamforming," *IEEE Trans. on Signal Process.*, vol. 70, pp. 240–253, 2022.
- [17] X. Wang, Z. Fei, J. Huang, and H. Yu, "Joint waveform and discrete phase shift design for RIS-assisted integrated sensing and communication system under Cramér-Rao bound constraint," *IEEE Trans. Veh. Technol.*, vol. 71, no. 1, pp. 1004–1009, Jan. 2022.
- [18] A. Bhattacharyya, "On some analogues of the amount of information and their use in statistical estimation," *Sankhya*, vol. 8, no. 3, pp. 201–218, 1947.
- [19] K. Todros and J. Tabrikian, "General classes of performance lower bounds for parameter estimation—part I: Non-bayesian bounds for unbiased estimators," *IEEE Trans. Info. Theory*, vol. 56, no. 10, pp. 5045–5063, Oct. 2010.
- [20] B. J. N. Blight and P. V. Rao, "The convergence of Bhattacharyya bounds," *Biometrika*, vol. 61, no. 1, pp. 137–142, Apr. 1974.
- [21] H. Tanaka and M. Akahira, "On a family of distributions attaining the Bhattacharyya bound," *Ann. Inst. Stat. Math.*, vol. 55, pp. 137–142, Jun. 2003.
- [22] G. R. Mohtashami Borzadaran, A. H. Rezaei Roknabadi, and M. Khorashadizadeh, "A view on Bhattacharyya bounds for inverse Gaussian distributions," *Metrika*, vol. 72, pp. 151–161, Sep. 2010.



- [23] C. D. Richmond and L. L. Horowitz, "Parameter bounds under misspecified models," in *Proc. 2013 Asilomar Conf. Signals Syst. Comput.*, Pacific Grove, CA, USA, Nov. 2013, pp. 176–180.
- [24] F. Lu and J. V. Krogmeier, "Modified Bhattacharyya bounds and their application to timing estimation," in *Proc. IEEE Wireless Commun. Netw. Conf.*, vol. 1, Orlando, FL, USA, Mar. 2002, 244–248 vol.1.
- [25] E. W. Barankin, "Locally best unbiased estimates," *Ann. Math. Stat.*, vol. 20, no. 4, pp. 477–501, Dec. 1949.
- [26] J. M. Hammersley, "On estimating restricted parameters," *J. Roy. Stat. Soc.*, vol. 12, no. 2, pp. 192–240, 1950.
- [27] R. J. McAulay and L. P. Seidman, "A useful form of the Barankin lower bound and its application to PPM threshold analysis," *IEEE Trans. Info. Theory*, vol. 15, no. 2, pp. 273–279, Mar. 1969.
- [28] R. J. McAulay and E. M. Hofstetter, "Barankin bounds on parameter estimation," *IEEE Trans. Info. Theory*, vol. 17, no. 6, pp. 669–676, Nov. 1971.
- [29] J. S. Abel, "A bound on mean-square-estimate error," *IEEE Trans. Info. Theory*, vol. 39, no. 5, pp. 1675–1680, Sep. 1993.
- [30] A. Quinlan, E. Chaumette, and P. Larzabal, "A direct method to generate approximations of the Barankin bound," in *Proc. IEEE Int. Conf. Acoust. Speech Signal Process.*, vol. 3, Toulouse, France, May 2006, pp. 808–811.
- [31] T. L. Marzetta, "Computing the Barankin bound, by solving an unconstrained quadratic optimization problem," in *Proc. IEEE Int. Conf. Acoust. Speech Signal Process.*, vol. 5, Munich, Germany, Apr. 1997, pp. 3829–3832.
- [32] A. B. Baggeroer, "Barankin bound on the variance of estimates of Gaussian random process," MIT Lincoln Lab., Lexington, MA, Tech. Rep., Jan. 1969.
- [33] J. Tabrikian and J. L. Krolik, "Barankin bound for source localization in shallow water," in *Proc. IEEE Int. Conf. Acoust. Speech Signal Process.*, vol. 1, Munich, Germany, Apr. 1997, pp. 499–502.
- [34] ———, "Barankin bounds for source localization in an uncertain ocean environment," *IEEE Trans. Signal Process.*, vol. 47, no. 11, pp. 2917–2927, Nov. 1999.
- [35] J. Tabrikian, "Barankin bounds for target localization by MIMO radars," in *Proc. IEEE Workshop Sens. Array Multichannel Process.*, Waltham, MA, USA, Jul. 2006, pp. 278–281.
- [36] A. Pinkus and J. Tabrikian, "Barankin bound for range and doppler estimation using orthogonal signal transmission," in *Proc. IEEE Conf. Radar*, Verona, NY, USA, Apr. 2006, pp. 94–99.
- [37] T. Li, J. Tabrikian, and A. Nehorai, "A Barankin-type bound on direction estimation using acoustic sensor arrays," *IEEE Trans. Signal Process.*, vol. 59, no. 1, pp. 431–435, Jan. 2011.
- [38] A. J. Weiss and E. Weinstein, "A lower bound on the mean-square error in random parameter estimation," *IEEE Trans. Inf. Theory*, vol. 31, no. 5, pp. 680–682, Sep. 1985.
- [39] A. Renaux, P. Forster, P. Larzabal, C. D. Richmond, and A. Nehorai, "A fresh look at the Bayesian bounds of the Weiss-Weinstein family," *IEEE Trans. Signal Process.*, vol. 56, no. 11, pp. 5334–5352, Jun. 2008.
- [40] K. Todros and J. Tabrikian, "General classes of performance lower bounds for parameter estimation—part II: Bayesian bounds," *IEEE Trans. Info. Theory*, vol. 56, no. 10, pp. 5064–5082, Oct. 2010.
- [41] H. L. Van Trees, *Detection, Estimation, and Modulation Theory, Part I: Detection, Estimation, and Linear Modulation Theory*. Wiley, 2004.
- [42] A. Renaux, P. Forster, P. Larzabal, and C. D. Richmond, "The Bayesian Abel bound on the mean square error," in *Proc. IEEE Int. Conf. Acoust. Speech Signal Process.*, vol. 3, Toulouse, France, May 2006, pp. III–III.
- [43] B. Z. Bobrovsky, E. Mayer-Wolf, and M. Zakai, "Some classes of global Cramér-Rao bounds," *Ann. Statist.*, vol. 15, no. 4, pp. 1421–1438, Dec. 1987.
- [44] B. Z. Bobrovsky and M. Zakai, "A lower bound on the estimation error for certain diffusion processes," *IEEE Trans. Inf. Theory*, vol. 22, no. 1, pp. 45–52, Jan. 1976.
- [45] I. Reuven and H. Messer, "A Barankin-type lower bound on the estimation error of a hybrid parameter vector," *IEEE Trans. Inf. Theory*, vol. 43, no. 3, pp. 1084–1093, 1997.
- [46] T. J. Nohara and S. Haykin, "Application of the Weiss-Weinstein bound to a two-dimensional antenna array," *IEEE Trans. Acoust. Speech Signal Process.*, vol. 36, no. 9, pp. 1533–1534, Sep. 1988.



- [47] W. Xu and A. B. Baggeroer, "Weiss-Weinstein bound for matched-field parameter estimation," *J. Acoust. Soc. Am.*, vol. 107, pp. 2858–2859, May 2000.
- [48] D. T. Vu, A. Renaux, R. Boyer, and S. Marcos, "Closed-form expression of the Weiss-Weinstein bound for 3D source localization: The conditional case," in *Proc. IEEE Sens. Array Multichannel Signal Process. Workshop*, Jerusalem, Israel, Oct. 2010, pp. 125–128.
- [49] —, "Weiss-Weinstein bound and SNR threshold analysis for doa estimation with a cold array," in *Proc. IEEE Statist. Signal Process. Workshop (SSP)*, Nice, France, Jun. 2011, pp. 13–16.
- [50] —, "Some results on the Weiss-Weinstein bound for conditional and unconditional signal models in array processing," *Signal Process.*, vol. 95, pp. 126–148, 2014.
- [51] A. Renaux, "Weiss-Weinstein bound for data-aided carrier estimation," *IEEE Signal Process. Lett.*, vol. 14, no. 4, pp. 283–286, Apr. 2007.
- [52] N. D. Tran, A. Renaux, R. Boyer, S. Marcos, and P. Larzabal, "Weiss-Weinstein bound for MIMO radar with colocated linear arrays for SNR threshold prediction," *Signal Process.*, vol. 92, no. 5, pp. 1353–1358, May 2012.
- [53] L. Bacharach, A. Renaux, M. N. E. Korso, and É. Chaumette, "Weiss-Weinstein bound on multiple change-points estimation," *IEEE Trans. Signal Process.*, vol. 65, no. 10, pp. 2686–2700, May 2017.
- [54] J. Ziv and M. Zakai, "Some lower bounds on signal parameter estimation," *IEEE Trans. Inf. Theory*, vol. 15, no. 3, pp. 386–391, May 1969.
- [55] L. P. Seidman, "Performance limitations and error calculations for parameter estimation," *Proc. IEEE*, vol. 58, no. 5, pp. 644–652, May 1970.
- [56] D. Chazan, M. Zakai, and J. Ziv, "Improved lower bounds on signal parameter estimation," *IEEE Trans. Inf. Theory*, vol. 21, no. 1, pp. 90–93, Jan. 1975.
- [57] K. L. Bell, Y. Steinberg, Y. Ephraim, and H. L. Van Trees, "Extended Ziv-Zakai lower bound for vector parameter estimation," *IEEE Trans. Inf. Theory*, vol. 43, no. 2, pp. 624–637, Mar. 1997.
- [58] K. L. Bell, Y. Ephraim, and H. L. Van Trees, "Explicit Ziv-Zakai lower bound for bearing estimation," *IEEE Trans. Signal Process.*, vol. 44, no. 11, pp. 2810–2824, Nov. 1996.
- [59] B. M. Sadler, L. Huang, and Z. Xu, "Ziv-Zakai time delay estimation bound for ultra-wideband signals," in *Proc. IEEE Int. Conf. Acoust. Speech Signal Process.*, Honolulu, HI, USA, Apr. 2007, pp. 549–552.
- [60] N. Liu, Z. Xu, and B. M. Sadler, "Ziv-Zakai time-delay estimation bounds for frequency-hopping waveforms under frequency-selective fading," *IEEE Trans. Signal Process.*, vol. 58, no. 12, pp. 6400–6406, Dec. 2010.
- [61] B. M. Sadler, N. Liu, and Z. Xu, "Ziv-Zakai bounds on time delay estimation in unknown convolutive random channels," *IEEE Trans. Signal Process.*, vol. 58, no. 5, pp. 2729–2745, May 2010.
- [62] N. Decarli and D. Dardari, "Ziv-Zakai bound for time delay estimation of unknown deterministic signals," in *Proc. IEEE Int. Conf. Acoust. Speech Signal Process.*, Florence, Italy, May 2014, pp. 4673–4677.
- [63] D. Ramasamy, S. Venkateswaran, and U. Madhow, "Compressive parameter estimation in AWGN," *IEEE Trans. Signal Process.*, vol. 62, no. 8, pp. 2012–2027, Apr. 2014.
- [64] Z. Zhang, Z. Shi, C. Zhou, C. Yan, and Y. Gu, "Ziv-Zakai bound for compressive time delay estimation," *IEEE Trans. Signal Process.*, vol. 70, pp. 4006–4019, Jun. 2022.
- [65] Z. Zhang, C. Zhou, C. Yan, and Z. Shi, "Deterministic Ziv-Zakai bound for compressive time delay estimation," in *Proc. IEEE Radar Conf.*, New York, NY, Mar. 2022, pp. 1–5.
- [66] Z. Zhang, Z. Shi, Y. Gu, M. S. Greco, and F. Gini, "Ziv-Zakai bound for compressive time delay estimation from zero-mean Gaussian signal," *IEEE Signal Process. Lett.*, vol. 30, pp. 1112–1116, 2023.
- [67] K. V. Mishra and Y. C. Eldar, "Performance of time delay estimation in a cognitive radar," in *Proc. IEEE Int. Conf. Acoust. Speech Signal Process.*, New Orleans, LA, Mar. 2017, pp. 3141–3145.
- [68] X. Gu and M. Wong, "A modified Ziv-Zakai lower bound and its application in array processing," in *Proc. Int. Conf. Acoust. Speech Signal Process.*, vol. 2, Toronto, ON, Canada, Apr. 1991, pp. 1477–1480.
- [69] D. Khan and K. L. Bell, "Explicit Ziv-Zakai bound for analysis of DOA estimation performance of sparse linear arrays," *Signal Process.*, vol. 93, no. 12, pp. 3449–3458, Dec. 2013.



- [70] D. B. Alexander, R. M. Narayanan, and B. Himed, "Lower bounds for wideband direction-finding with mutual coupling," in *Proc. IEEE Radar Conf.*, Boston, MA, USA, Apr. 2019, pp. 1–6.
- [71] A. Gupta, U. Madhow, A. Arbabian, and A. Sadri, "Design of large effective apertures for millimeter wave systems using a sparse array of subarrays," *IEEE Trans. Signal Process.*, vol. 67, no. 24, pp. 6483–6497, Dec. 2019.
- [72] Z. Zhang, Z. Shi, and Y. Gu, "Ziv-Zakai bound for DOAs estimation," *IEEE Trans. Signal Process.*, vol. 71, pp. 136–149, 2023.
- [73] D. Dardari and M. Z. Win, "Ziv-Zakai bound on time-of-arrival estimation with statistical channel knowledge at the receiver," in *Proc. IEEE Int. Conf. Ultra-Wideband*, Vancouver, BC, Canada, Sep. 2009, pp. 624–629.
- [74] P. Wang and Y. T. Jade Morton, "Impact analysis of intercell interference in cellular networks for navigation applications," *IEEE Trans. Aerosp. Electron. Syst.*, vol. 59, no. 1, pp. 685–694, Feb. 2023.
- [75] M. Driusso, M. Comisso, F. Babich, and C. Marshall, "Performance analysis of time of arrival estimation on OFDM signals," *IEEE Signal Process. Lett.*, vol. 22, no. 7, pp. 983–987, Jul. 2015.
- [76] M. Tsang, "Ziv-Zakai error bounds for quantum parameter estimation," *Phys. Rev. Lett.*, vol. 108, p. 230401, 23 Jun. 2012.
- [77] Y. Gao and H. Lee, "Generalized limits for parameter sensitivity via quantum Ziv-Zakai bound," *J. Phys. A Math. Theor.*, vol. 45, no. 41, p. 415306, Sep. 2012.
- [78] D. W. Berry, M. Tsang, M. J. W. Hall, and H. M. Wiseman, "Quantum Bell-Ziv-Zakai bounds and Heisenberg limits for waveform estimation," *Phys. Rev. X*, vol. 5, p. 031018, 3 Aug. 2015.
- [79] M. F. Keskin, E. Gonendik, and S. Gezici, "Improved lower bounds for ranging in synchronous visible light positioning systems," *J. Light. Technol.*, vol. 34, no. 23, pp. 5496–5504, Dec. 2016.
- [80] M. Xu, H. Chen, and P. K. Varshney, "Ziv-Zakai bounds on image registration," *IEEE Trans. Signal Process.*, vol. 57, no. 5, pp. 1745–1755, May 2009.
- [81] J. Sun, S. Ma, G. Xu, and S. Li, "Trade-off between positioning and communication for millimeter wave systems with Ziv-Zakai bound," *IEEE Trans. Commun.*, vol. 71, no. 6, pp. 3752–3762, Jun. 2023.
- [82] Y. Xiong and F. Liu, "SNR-adaptive ranging waveform design based on Ziv-Zakai bound optimization," *IEEE Signal Process. Lett.*, pp. 1–5, 2023.
- [83] A. Dytso, M. Cardone, and I. Zieder, "High-noise asymptotics of the Ziv-Zakai bound," *IEEE Signal Process. Lett.*, vol. 29, pp. 1933–1937, 2022.
- [84] E. Cinlar, *Introduction to Stochastic Processes*. Englewood Cliffs, NJ: Prentice-Hall, 1975.
- [85] A. Quazi, "An overview on the time delay estimate in active and passive systems for target localization," *IEEE Trans. Acoust. Speech Signal Process.*, vol. 29, no. 3, pp. 527–533, Jun. 1981.
- [86] A. Dogandžić and A. Nehorai, "Cramér-Rao bounds for estimating range, velocity, and direction with an active array," *IEEE Trans. Signal Process.*, vol. 49, no. 6, pp. 1122–1137, Jun. 2001.
- [87] M. Wax and A. Leshem, "Joint estimation of time delays and directions of arrival of multiple reflections of a known signal," *IEEE Trans. Signal Process.*, vol. 45, no. 10, pp. 2477–2484, Oct. 1997.
- [88] J. Riba, J. Sala, and G. Vázquez, "Conditional maximum likelihood timing recovery: Estimators and bounds," *IEEE Trans. Signal Process.*, vol. 49, no. 4, pp. 835–850, Apr. 2001.
- [89] K. Gedalyahu and Y. C. Eldar, "Time-delay estimation from low-rate samples: A union of subspaces approach," *IEEE Trans. Signal Process.*, vol. 58, no. 6, pp. 3017–3031, Jun. 2010.
- [90] D. L. Donoho, "Compressed sensing," *IEEE Trans. Inf. Theory*, vol. 52, no. 4, pp. 1289–1306, Apr. 2006.
- [91] E. J. Candès and M. B. Wakin, "An introduction to compressive sampling," *IEEE Signal Process. Mag.*, vol. 25, no. 2, pp. 21–30, Mar. 2008.
- [92] R. Baraniuk and P. Steeghs, "Compressive radar imaging," in *Proc. IEEE Radar Conf.*, Waltham, USA, MA, Apr. 2007, pp. 128–133.
- [93] J. H. G. Ender, "On compressive sensing applied to radar," *Signal Process.*, vol. 90, no. 5, pp. 1402–1414, May 2010.
- [94] Y. Yu, A. P. Petropulu, and H. V. Poor, "Measurement matrix design for compressive sensing-based MIMO radar," *IEEE Trans. Signal Process.*, vol. 59, no. 11, pp. 5338–5352, Nov. 2011.



- [95] ———, “CSSF MIMO RADAR: Compressive-sensing and step-frequency based MIMO radar,” *IEEE Trans. Aerosp. Electron. Syst.*, vol. 48, no. 2, pp. 1490–1504, Apr. 2012.
- [96] Y. Gu and N. A. Goodman, “Compressed sensing kernel design for radar range profiling,” in *Proc. IEEE Radar Conf.*, Ottawa, On, Canada, May 2013, pp. 1–5.
- [97] ———, “Compressive sensing kernel optimization for time delay estimation,” in *Proc. IEEE Radar Conf.*, Cincinnati, OH, USA, May 2014, pp. 1209–1213.
- [98] M. G. Amin, *Compressive Sensing for Urban Radar*. Boca Raton, FL: CRC Press, 2014.
- [99] Y. Gu, N. A. Goodman, and A. Ashok, “Radar target profiling and recognition based on TSI-optimized compressive sensing kernel,” *IEEE Trans. Signal Process.*, vol. 62, no. 12, pp. 3194–3207, May 2014.
- [100] M. Rossi, A. M. Haimovich, and Y. C. Eldar, “Spatial compressive sensing for MIMO radar,” *IEEE Trans. Signal Process.*, vol. 62, no. 2, pp. 419–430, Jan. 2014.
- [101] Y. Gu and N. A. Goodman, “Information-theoretic compressive sensing kernel optimization and Bayesian Cramér-Rao bound for time delay estimation,” *IEEE Trans. Signal Process.*, vol. 65, no. 17, pp. 4525–4537, Sep. 2017.
- [102] A. De Maio, Y. C. Eldar, and A. M. Haimovich, *Compressed Sensing in Radar Signal Processing*. Cambridge University Press, 2019.
- [103] Y. Park, W. Seong, and Y. Choo, “Compressive time delay estimation off the grid,” *J. Acoust. Soc. Am.*, vol. 141, no. 6, pp. 585–591, May 2017.
- [104] C. Ekanadham, D. Tranchina, and E. P. Simoncelli, “Recovery of sparse translation-invariant signals with continuous basis pursuit,” *IEEE Trans. Signal Process.*, vol. 59, no. 10, pp. 4735–4744, Jun. 2011.
- [105] W. Zhang and F. Yu, “Off-the-grid compressive time delay estimation via manifold-based optimization,” *IEEE Comm. Lett.*, vol. 21, no. 5, pp. 983–986, May 2017.
- [106] Y. Noam and H. Messer, “Notes on the tightness of the hybrid Cramér-Rao lower bound,” *IEEE Trans. Signal Process.*, vol. 57, no. 6, pp. 2074–2084, Jun. 2009.
- [107] S. Bar and J. Tabrikian, “Bayesian estimation in the presence of deterministic nuisance parameters—Part I: Performance bounds,” *IEEE Trans. Signal Process.*, vol. 63, no. 24, pp. 6632–6646, Dec. 2015.
- [108] B. Babadi, N. Kalouptsidis, and V. Tarokh, “Asymptotic achievability of the Cramér-Rao bound for noisy compressive sampling,” *IEEE Trans. Signal Process.*, vol. 57, no. 3, pp. 1233–1236, Mar. 2009.
- [109] R. Niazadeh, M. Babaie-Zadeh, and C. Jutten, “On the achievability of Cramér-Rao bound in noisy compressed sensing,” *IEEE Trans. Signal Process.*, vol. 60, no. 1, pp. 518–526, Jan. 2012.
- [110] P. Pakrooh, A. Pezeshki, L. L. Scharf, D. Cochran, and S. D. Howard, “Analysis of Fisher information and the Cramér-Rao bound for nonlinear parameter estimation after random compression,” *IEEE Trans. Signal Process.*, vol. 63, no. 23, pp. 6423–6428, Dec. 2015.
- [111] W. Xu, A. B. Gaggeroer, and C. D. Richmond, “Bayesian bounds for matched-field parameter estimation,” *IEEE Trans. Signal Process.*, vol. 52, no. 12, pp. 3293–3305, Dec. 2004.
- [112] T. Routtenberg and J. Tabrikian, “A general class of outage error probability lower bounds in Bayesian parameter estimation,” *IEEE Trans. Signal Process.*, vol. 60, no. 5, pp. 2152–2166, May 2012.
- [113] S. Bellini and G. Tartara, “Bounds on error in signal parameter estimation,” *IEEE Trans. Commun.*, vol. 22, no. 3, pp. 340–342, Mar. 1974.
- [114] A. J. Weiss and E. Weinstein, “Fundamental limitations in passive time delay estimation—Part I: Narrow-band systems,” *IEEE Trans. Acoust. Speech Signal Process.*, vol. 31, no. 2, pp. 472–486, Apr. 1983.
- [115] V. M. Chiriach, Q. He, A. M. Haimovich, and R. S. Blum, “Ziv-Zakai bound for joint parameter estimation in MIMO radar systems,” *IEEE Trans. Signal Process.*, vol. 63, no. 18, pp. 4956–4968, Jun. 2015.
- [116] A. Eftekhari and M. B. Wakin, “New analysis of manifold embeddings and signal recovery from compressive measurements,” *Appl. Comput. Harmon. Anal.*, vol. 39, no. 1, pp. 67–109, Jul. 2015.
- [117] Y. Gu, Y. D. Zhang, and N. A. Goodman, “Optimized compressive sensing-based direction-of-arrival estimation in massive MIMO,” in *Proc. IEEE Int. Conf. Acoust. Speech Signal Process.*, New Orleans, LA, USA, Jun. 2017, pp. 3181–3185.



- [118] C. Zhou, Y. Gu, Y. D. Zhang, Z. Shi, T. Jin, and X. Wu, "Compressive sensing based coprime array direction-of-arrival estimation," *IET Commun.*, vol. 11, no. 11, pp. 1719–1724, Aug. 2017.
- [119] Y. Gu and Y. D. Zhang, "Compressive sampling optimization for user signal parameter estimation in massive MIMO systems," *Digital Signal Process.*, vol. 94, pp. 105–113, Nov. 2019.
- [120] Y. Gu, N. A. Goodman, S. Hong, and Y. Li, "Robust adaptive beamforming based on interference covariance matrix sparse reconstruction," *Signal Process.*, vol. 96, pp. 375–381, Mar. 2014.
- [121] A. De Maio, Y. C. Eldar, and A. M. Haimovich, *Compressed Sensing in Radar Signal Processing*. Cambridge University Press, 2019.
- [122] F. Gini, R. Reggiannini, and U. Mengali, "The modified Cramér-Rao bound in vector parameter estimation," *IEEE Trans. Commun.*, vol. 46, no. 1, pp. 52–60, Jan. 1998.
- [123] F. Gini and R. Reggiannini, "On the use of Cramér-Rao-like bounds in the presence of random nuisance parameters," *IEEE Trans. Commun.*, vol. 48, no. 12, pp. 2120–2126, Dec. 2000.
- [124] M. Pardini, F. Lombardini, and F. Gini, "The hybrid Cramér-Rao bound on broadside DOA estimation of extended sources in presence of array errors," *IEEE Trans. Signal Process.*, vol. 56, no. 4, pp. 1726–1730, Apr. 2008.
- [125] A. Bekker, D.-G. Chen, and J. T. Ferreira, *Computational and Methodological Statistics and Biostatistics: Contemporary Essays in Advancement*. Springer International Publishing, 2020.
- [126] E. Chaumette, A. Renaux, and M. N. El Korso, "A class of Weiss–Weinstein bounds and its relationship with the Bobrovsky–Mayer–Wolf–Zakai bounds," *IEEE Trans. Info. Theory*, vol. 63, no. 4, pp. 2226–2240, Apr. 2017.
- [127] R. O. Schmidt, "Multiple emitter location and signal parameter estimation," *IEEE Trans. Antennas Propag.*, vol. 34, no. 3, pp. 276–280, Mar. 1986.
- [128] B. D. Rao and K. V. S. Hari, "Performance analysis of root-MUSIC," *IEEE Trans. Acoust. Speech Signal Process.*, vol. 37, no. 12, pp. 1939–1949, Dec. 1989.
- [129] C.-L. Liu and P. P. Vaidyanathan, "Remarks on the spatial smoothing step in coarray MUSIC," *IEEE Signal Process. Lett.*, vol. 22, no. 9, pp. 1438–1442, Sep. 2015.
- [130] R. Roy and T. Kailath, "ESPRIT-estimation of signal parameters via rotational invariance techniques," *IEEE Trans. Acoust. Speech Signal Process.*, vol. 37, no. 7, pp. 984–995, Jul. 1989.
- [131] F.-M. Han and X.-D. Zhang, "An ESPRIT-like algorithm for coherent DOA estimation," *IEEE Antennas Wirel. Propag. Lett.*, vol. 4, pp. 443–446, Dec. 2005.
- [132] F.-J. Chen, S. Kwong, and C.-W. Kok, "ESPRIT-like two-dimensional DOA estimation for coherent signals," *IEEE Trans. Aerosp. Electron. Syst.*, vol. 46, no. 3, pp. 1477–1484, Jul. 2010.
- [133] D. Malioutov, M. Çetin, and A. S. Willsky, "A sparse signal reconstruction perspective for source localization with sensor arrays," *IEEE Trans. Signal Process.*, vol. 53, no. 8, pp. 3010–3022, Aug. 2005.
- [134] C. Zhou, Y. Gu, X. Fan, Z. Shi, G. Mao, and Y. D. Zhang, "Direction-of-arrival estimation for coprime array via virtual array interpolation," *IEEE Trans. Signal Process.*, vol. 66, no. 22, pp. 5956–5971, Nov. 2018.
- [135] C. Zhou, Y. Gu, Z. Shi, and Y. D. Zhang, "Off-grid direction-of-arrival estimation using coprime array interpolation," *IEEE Signal Process. Lett.*, vol. 25, no. 11, pp. 1710–1714, Sep. 2018.
- [136] A. M. Elbir, "DeepMUSIC: Multiple signal classification via deep learning," *IEEE Sens. Lett.*, vol. 4, no. 4, pp. 1–4, Apr. 2020.
- [137] A. Barthelme and W. Utschick, "A machine learning approach to DoA estimation and model order selection for antenna arrays with subarray sampling," *IEEE Trans. Signal Process.*, vol. 69, pp. 3075–3087, May 2021.
- [138] G. K. Papageorgiou, M. Sellathurai, and Y. C. Eldar, "Deep networks for direction-of-arrival estimation in low SNR," *IEEE Trans. Signal Process.*, vol. 69, pp. 3714–3729, Jun. 2021.
- [139] T. Laas and W. Xu, "On the Ziv-Zakai bound for time difference of arrival estimation in CP-OFDM systems," in *Proc. IEEE Wirel. Commun. Netw. Conf. (WCNC)*, Nanjing, China, Mar. 2021, pp. 1–5.
- [140] Z. Yang, P. Stoica, and J. Tang, "Source resolvability of spatial-smoothing-based subspace methods: A hadamard product perspective," *IEEE Trans. Signal Process.*, vol. 67, no. 10, pp. 2543–2553, May 2019.



- [141] Z. Zheng, Y. Huang, W.-Q. Wang, and H. C. So, “Direction-of-arrival estimation of coherent signals via coprime array interpolation,” *IEEE Signal Process. Lett.*, vol. 27, pp. 585–589, Mar. 2020.
- [142] H. Zheng, C. Zhou, Z. Shi, and Y. Gu, “Structured tensor reconstruction for coherent DOA estimation,” *IEEE Signal Process. Lett.*, vol. 29, pp. 1634–1638, Jul. 2022.
- [143] H. L. Van Trees, *Detection, Estimation, and Modulation Theory, Part III: Radar-Sonar Signal Processing and Gaussian Signal in Noise*. Wiley, 2001.
- [144] S. M. Kay, *Fundamentals of Statistical Signal Processing, Volume I: Estimation Theory*. Prentice Hall PTR, 1993.
- [145] G. Casella and R. L. Berger, *Statistical Inference*. Thomson Learning, 2002.
- [146] P. Pal and P. P. Vaidyanathan, “Coprime sampling and the MUSIC algorithm,” in *Proc. IEEE Digit. Signal Process. Workshop / IEEE Singal Process. Educ. Workshop (DSP/SPE)*, Sedona, AZ, Jan. 2011, pp. 289–294.
- [147] Z. Zhang, C. Zhou, Y. Gu, J. Zhou, and Z. Shi, “An IDFT approach for coprime array direction-of-arrival estimation,” *Digit. Signal Process.*, vol. 94, pp. 45–55, Nov. 2019.
- [148] Y. Gu and Y. D. Zhang, *Information-Theoretic Radar Signal Processing*. Wiley-IEEE Press, 2024.
- [149] F. Yan, X. Meng, M. S. Greco, F. Gini, and Y. Zhang, “Half-dimension subspace decomposition for fast direction finding with arbitrary linear arrays,” *IEEE Signal Process. Lett.*, vol. 29, pp. 1482–1486, 2022.
- [150] X. Meng, B. Cao, F. Yan, M. S. Greco, F. Gini, and Y. Zhang, “Real-valued MUSIC for efficient direction of arrival estimation with arbitrary arrays: Mirror suppression and resolution improvement,” *Signal Process.*, vol. 202, p. 108 766, Jan. 2023.
- [151] M. Xue, L. Xu, and J. Li, “IAA spectral estimation: Fast implementation using the gohberg–semencul factorization,” *IEEE Trans. Signal Process.*, vol. 59, no. 7, pp. 3251–3261, Jul. 2011.
- [152] H. Zheng, C. Zhou, Z. Shi, Y. Gu, and Y. D. Zhang, “Coarray tensor direction-of-arrival estimation,” *IEEE Trans. Signal Process.*, vol. 71, pp. 1128–1142, 2023.
- [153] C. Zhou, Y. Gu, Z. Shi, and M. Haardt, “Structured nyquist correlation reconstruction for doa estimation with sparse arrays,” *IEEE Trans. Signal Process.*, vol. 71, pp. 1849–1862, 2023.
- [154] S. Caracciolo and G. Sicuro, “Quadratic stochastic Euclidean bipartite matching problem,” *Phys. Rev. Lett.*, vol. 115, no. 23, p. 230 601, Dec. 2015.